MPP-2010-22
TKK-10-14
TPP10-15
SFB/CPP-10-18

Phase Space Matching and Finite Lifetime Effects for Top-Pair Production Close to Threshold

André H. Hoang

Max-Planck-Institut für Physik (Werner-Heisenberg-Institut)
Föhringer Ring 6, D-80805 München, Germany *

Christoph J. Reißer

Institut für Theoretische Teilchenphysik
Karlsruhe Institute of Technology (KIT),
D-76128 Karlsruhe, Germany †

Pedro Ruiz-Femenía

Institut für Theoretische Teilchenphysik und Kosmologie
RWTH Aachen University
D-52056 Aachen, Germany ‡

* Electronic address: ahoang@mppmu.mpg.de
† Electronic address: reisser@kit.edu
‡ Electronic address: ruiz@physik.rwth-aachen.de

Abstract

The top-pair $t\bar{t}$ production cross section close to threshold in e^+e^- collisions is strongly affected by the small lifetime of the top quark. Since the cross section is defined through final states containing the top decay products, a consistent definition of the cross section depends on prescriptions how these final states are accounted for the cross section. Experimentally, these prescriptions are implemented for example through cuts on kinematic quantities such as the reconstructed top quark invariant masses. As long as these cuts do not reject final states that can arise from the decay of a top and an anti-top quark with a small off-shellness compatible with the nonrelativistic power-counting, they can be implemented through imaginary phase space matching conditions in NRQCD. The prescription-dependent cross section can then be determined from the optical theorem using the e^+e^- forward scattering amplitude. We compute the phase space matching conditions associated to cuts on the top and anti-top invariant masses at next-to-next-to-leading logarithmic (NNLL) order and partially at next-to-next-to-next-to-leading logarithmic (N^{3}LL) order in the nonrelativistic expansion and, together with finite lifetime and electroweak effects known from previous work, analyze their numerical impact on the $t\bar{t}$ cross section. We show that the phase space matching contributions are essential to make reliable NRQCD predictions, particularly for energies below the peak region, where the cross section is small. We find that irreducible background contributions associated to final states that do not come from top decays are strongly suppressed and can be neglected for the theoretical predictions.

I. INTRODUCTION

The measurement of the line shape of the total cross section $\sigma(e^+e^- \to t\bar{t})$ for top quark pair production at energies around the top-antitop threshold ($\sqrt{q^2} \sim 350\,\mathrm{GeV}$) constitutes a major part of the top physics program at a future linear collider (LC). The rise and the form of the cross section allow for precise measurements of the top quark mass m_t in a threshold mass scheme [1], the top quark width Γ_t, the top-Yukawa coupling y_t and the strong coupling α_s. In view of the expected experimental precision at the LC [2], theoretical uncertainties for the predictions at the level of $\mathrm{d}\sigma/\sigma \sim 2-3\%$ in the peak and the continuum region are desired [3]. In the energy region below the peak where the cross section is becoming tiny the theory error should not exceed the level of around 5 fb [2].

From the theoretical perspective the QCD dynamics of the top quark pair for threshold energies is quite nontrivial since the small relative velocity of the top-antitop pair $v \ll 1$ leads to a proliferation of physical scales that need to be accounted for: the top mass m_t, the relative three-momentum $\mathbf{p} \sim m_t v$ and the nonrelativistic kinetic energy $E \sim m_t v^2$ of the top quark pair. In the standard QCD perturbative expansion singular terms $\propto (\alpha_s/v)^n$ and $\propto (\alpha_s \ln v)^n$ arise from the ratios of these scales. Since the Coulomb-like dynamics enforces the power-counting $v \sim \alpha_s(m_t v)$ the proper treatment of these terms requires resummations within a power-counting framework with a simultaneous expansion in $v \sim \alpha_s \ll 1$. This can be achieved with nonrelativistic QCD (NRQCD), a low-energy effective field theory (EFT) of QCD that separates the different quantum fluctuations that are relevant for the kinematic situation of heavy nonrelativistic quark pairs. Within the fixed-order approach, which achieves a systematic summation of terms $\propto \alpha_s^n v^m$, complete NNLO predictions (i.e. $n+m \leq 3$) have been made [1]. For available NNNLO results we refer to Refs. [4–12]. Using a proper low-scale short-distance threshold mass scheme with cut-off scale $R \sim m_t\alpha_s$ [13–16] (which avoids the pole mass renormalon) the energy where the cross section rises is stable in perturbation theory. However, the fixed-order predictions suffer from large normalization uncertainties at the level of 10-20 % which indicate potentially large logarithmic terms. These normalization uncertainties are particularly problematic for measurements of the top width and the Yukawa coupling y_t. This problem of potentially large logarithmic terms is addressed in renormalization group improved NRQCD calculations of the cross section, which account for a systematic summation of terms $\propto \alpha_s^n v^m \ln^k v$. Renormalization group improved QCD results are fully known at NLL order (i.e. $n+m-k \leq 2$). At NNLL order (i.e. $n+m-k \leq 3$) all ingredients are known except for the NNLL renormalization group evolution of the Wilson coefficient of the leading order top pair current [17–19]. Partial results for the NNLL order anomalous dimension of the current have been computed in Ref. [4, 20]. At the present stage renormalization group improved results have a normalization uncertainty of 6-10 % [19, 21].

Electroweak effects and in particular the top quark decay play an equally important role. Already at leading order it is important to account for the top decay width since it widens the top-antitop bound state resonances and turns the threshold cross section into a smooth lineshape. Despite this fact the determination of subleading electroweak and finite lifetime effects have received somewhat less attention in the literature in the past. Theoretically, for predictions of an inclusive cross section the top width acts as an infrared cutoff for the top energy and thus allows for a perturbative computation for all threshold energies. We have $\Gamma_t \approx (G_F/8\sqrt{2}\pi)m_t^3 \approx 1.5$ GeV, which scales like $g_2^2 m_t \sim g_1^2 m_t$ where g_1 and g_2 are the U(1) and SU(2) couplings, and we also find numerically that $\Gamma_t \sim m_t\alpha_s^2$. With $g_1^2 \sim g_2^2 \sim \alpha_s$ it is therefore natural to adopt the power-counting

$$v \sim \alpha_s \sim \alpha_{\rm qed}^{1/2} \ll 1 \tag{1}$$

when making perturbative theoretical predictions.

Electroweak interactions are responsible for various effects that can be categorized into four classes: (a) "Hard" electroweak effects, which includes hard, point-like corrections related to the $t\bar{t}$ production mechanism by virtual photons and Z exchange, as well as electroweak corrections to the hard matching conditions of the NRQCD operators and potentials, (b) electromagnetic effects for the luminosity spectrum of the e^+e^- initial state, (c) electromagnetic corrections to the low-energy nonrelativistic dynamics of the $t\bar{t}$ pair and its decay products and (d) effects related to the finite top quark lifetime. The corrections from class (a) can be determined by standard methods through matching for top quarks in the on-shell limit and are real numbers. Up to NNLL order they have been discussed and implemented in Ref. [22]. Earlier work can be found in Refs. [23, 24]. The QED beam effects from class (b) are taken into account by a convolution of the "partonic" cross section with an on-shell e^+e^- pair in the initial state with the collider's luminosity spectrum. The luminosity spectrum accounts for initial state radiation, the accelerator-dependent beam energy spread and the beam-strahlung, and effects coming from beam-beam interactions. Since the luminosity spectrum is for the most part determined either experimentally or from experimental simulations we do not consider it any further in this work. The photon interactions of the $t\bar{t}$ pair belonging to class (c) are quite similar to the gluonic corrections and can be incorporated in the same way into NRQCD through potentials and ultrasoft interactions. The most important of these effects are the QED corrections to the Coulomb potential contributing at NLL order.

The finite lifetime effects of class (d) are the main purpose of this work. A proper treatment of instability effects entails that for the definition of the cross section, final states compatible with the top decay chains are accounted for. Since this necessarily also includes final states that do not arise from top decays, but are experimentally indistinguishable, the cross section - and potentially also the theoretical methods to compute it - are dependent on what selection prescriptions are employed. In general, as long as selection cuts do not reject final states that can arise from the decay of a top and an anti-top quark with a small off-shellness compatible with the power counting of a nonrelativistic (anti-)top quark propagator[1], they can be implemented through imaginary contributions to the Wilson coefficients of the NRQCD operators. This means that the top decay products are integrated out together with the information on the selection cuts. The resulting NRQCD Lagrangian is formally non-Hermitian. The cross section can then be obtained via the optical theorem, i.e. from the imaginary part of the $e^+e^- \to e^+e^-$ forward scattering amplitude [25–27]. In this work we adopt this inclusive approach.

One can distinguish two different types of imaginary contributions to the NRQCD Wilson coefficients: (1) contributions arising from cuts of full theory diagrams through top decay final states and (2) contributions describing the selection prescriptions, which we will also frequently refer to as cuts in the following. [2] The type-1 contributions describe decays of (anti)top quark modes that are propagating in NRQCD. In the matching procedure they

[1] We call such selection prescriptions "inclusive" throughout our work.

[2] The different meanings of the word "cut" used frequently in this work should be clear from the context.

arise from cuts of full theory diagrams through (anti)top decay final states. The leading type-1 NRQCD term is the well known on-shell width contribution,

$$\delta\mathcal{L} = \sum_{\mathbf{p}} \psi_{\mathbf{p}}^\dagger \, \frac{i}{2}\Gamma_t \, \psi_{\mathbf{p}} + \sum_{\mathbf{p}} \chi_{\mathbf{p}}^\dagger \, \frac{i}{2}\Gamma_t \, \chi_{\mathbf{p}} \,, \tag{2}$$

which in the matching procedure comes from the bW cut of the full theory top quark on-shell self-energy, and which contributes at leading-log (LL) order in NRQCD. Here Γ_t is the top quark on-shell width, and $\psi_{\mathbf{p}}$ and $\chi_{\mathbf{p}}$ represent Pauli spinor field operators that destroy top and antitop quarks, respectively. This term leads to the NRQCD (anti)top propagator of the form

$$\frac{i}{p_0 - \frac{\mathbf{p}^2}{2m_t} + i\frac{\Gamma_t}{2}} \tag{3}$$

and can be readily implemented into computations for stable top quarks supplemented by the replacement rule $E \to E + i\Gamma_t$, where $E = \sqrt{s} - 2m_t$ is the c.m. energy with respect to the two-particle threshold [25, 26]. The type-1 contributions to the Wilson coefficients up to NNLL order and neglecting the width of the W-boson were determined in Ref. [27]. As a new higher order feature these include interference contributions from double-resonant ($e^+e^- \to t\bar{t} \to b\bar{b}W^+W^-$) and single-resonant ($e^+e^- \to t\bar{b}W^- , \bar{t}bW^+ \to b\bar{b}W^+W^-$) amplitudes as illustrated in Fig. 1. Electroweak gauge-invariance is maintained during the matching procedure by the inclusion of the imaginary contribution of the top quark wave function renormalization Z-factor arising from the bW intermediate state in the top self-energy of the full theory.

An important new theoretical aspect is the emergence of imaginary anomalous dimensions caused by UV-divergences in the NRQCD $t\bar{t}$ phase space integrations [27]. These UV-divergences originate from the Breit-Wigner behavior of the top and antitop propagators of Eq. (3) which, upon being cut, lift the on-shell dispersion relation $p_0 = \mathbf{p}^2/2m_t$. In the forward scattering amplitude these propagators allow (anti)top intermediate states contributing to the NRQCD cross sections which have arbitrarily large invariant mass. Once v^2-suppressed NNLL order operators are inserted, this behavior causes UV-divergences which are compensated by imaginary counter-terms associated with $(e^+e^-)(e^+e^-)$ forward-scattering operators. The resulting NLL order imaginary anomalous dimensions of the Wilson coefficients of the $(e^+e^-)(e^+e^-)$ forward-scattering operators sum $\ln v$ terms from the top decay phase space. It was shown in Ref. [27] that the type-1 contributions to the imaginary parts of the NRQCD Wilson coefficients are numerically important for the normalization of the cross section and for the correct prediction of the c.m. energy of the $t\bar{t}$ quasi-resonance peak. The existence of phase space divergences in NRQCD inclusive cross section computations for top pair production at threshold indicates that - due to the finite lifetime - predictions beyond the leading order approximation need additional short-distance information to be defined unambiguously. This short-distance information is provided by the experimental selection criteria for the final states that are accounted for the cross section determination, and also incorporate background contributions related to diagrams without an intermediate $t\bar{t}$ pair.[3] In NRQCD this phase-space short-distance information is incorporated in the imaginary contributions to the Wilson coefficients of type-2 we have already

[3] Also outside the framework of effective theories such selection criteria are in general necessary, and

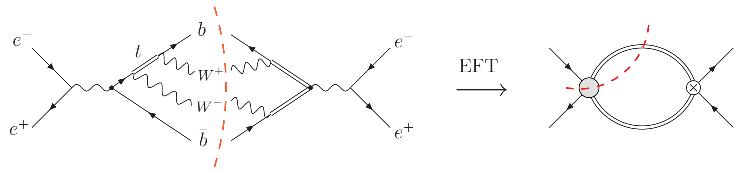

FIG. 1: Interference of the double-resonant diagram with a single-resonant one, as described in the full and effective theories. The (grey) blob in the $t\bar{t}$ production vertex in the EFT diagram represents the NNLL matching condition which results from integrating out the lower $\bar{b}W^-$ loop. The cut through this vertex represents the contribution of the absorptive part of the matching condition in the optical theorem. The (red) dashed line means we extract the imaginary part of the forward scattering amplitude or, equivalently, that we perform the phase space integration over the particles in the cut. Note that we use double lines for representing the top quarks.

mentioned above. We call the computation of these contributions the "phase space matching" procedure. Many different feasible inclusive cross section definitions can be devised.

In this work we determine and analyze the type-2 imaginary contributions to the NRQCD Wilson coefficients at NNLL and N^{3}LL order for cuts on the invariant masses of the reconstructed top and antitop quarks, M_t and $M_{\bar{t}}$, respectively. For simplicity we neglect the width of the W bosons and combinatorial background in the reconstruction. The combinatorial background can be estimated from Monte-Carlo simulations. We demonstrate that for moderate top invariant mass cuts

$$|M_{t,\bar{t}} - m_t| \,\leq\, \Delta M_t \tag{4}$$

with $\Delta M_t \sim 15 - 35$ GeV, the phase space matching conditions are dominated by the NRQCD phase space contributions, i.e. they can be computed from the difference between the (potentially) divergent NRQCD phase space integrations without any cuts and the ones with the cuts in Eq. (4) being imposed. This is because using the $\overline{\text{MS}}$ scheme in NRQCD diagrams involving the unstable top propagator of Eq. (3) largely overestimates the contributions from unphysical phase space regions that are parametrically away from the potential, soft and ultrasoft regions that can be described by NRQCD.[4] Thus the main numerical effect of the phase space matching procedure is to remove these unphysical contributions and the phase space matching procedure can be carried out within NRQCD itself. The remaining hard contributions, which require the evaluation of multi-leg full theory diagrams, are smaller than 5 fb and can be neglected in view of the expected experimental precision. This simplifies the computations substantially and makes the determination of higher order QCD corrections feasible. Since one can assume that the situation is similar for the threshold production of other heavy unstable colored particles in new physics models, it is straightforward to generalize our results for such processes, also for the hadron collider environment.

---

prescription-free cross section definitions for unstable particle production do no exist. The numerical impact of the selection prescriptions can, however, be frequently neglected if the width of the involved particles is much smaller than other relevant kinematic scales.

[4] A similar feature arises also for the computation matching conditions within NRQCD for a stable quark, see Ref. [28] for a comparison of a cutoff scheme with $\overline{\text{MS}}$.

An important conceptual aspect of the invariant mass cuts defined in Eq. (4) is that already for moderate cuts $\Delta M_t \sim 15-35$ GeV the cut $\Delta\mathbf{p}$ on the nonrelativistic (anti)top three-momentum $\mathbf{p}$ is $\Delta\mathbf{p} \sim \sqrt{2m_t\Delta M_t} \sim 100$ GeV, and thus represents a hard scale of the order m_t. This justifies the implementation of the phase space effects into the matching conditions of the Wilson coefficients. From a technical point of view, the method of computating the phase space matching conditions within NRQCD is quite similar to using a cutoff scheme to regularize ultraviolet (UV) divergences in loop diagrams for the renormalization. The procedure therefore leads to power-counting breaking effects which could spoil the nonrelativistic expansion. We find that this is not the case partly because the momentum cutoff $\Delta\mathbf{p}$ is still sufficiently smaller than the top mass m_t. In analogy to the usual renormalization and matching computations beyond the one-loop level, the phase space matching procedure also requires the determination of phase space matching coefficients of subdiagrams at higher orders in the loop expansion. Many technical details of the calculations carried out in this work are given in Ref. [29].

The outline of this paper is as follows: In Section II we review the NRQCD framework which we use to describe the top-antitop resonance region, and collect previous results on electroweak and finite lifetime effects in the cross section. In Section III A we discuss the main concepts of the NRQCD phase space matching procedure with special emphasis on the definition of the inclusive cross section. In Section III B we compute the imaginary type-2 matching conditions for the Wilson coefficients of the $(e^+e^-)(e^+e^-)$ forward scattering operators with $\alpha_s = 0$ and a cut ΔM_t on the reconstructed invariant masses of the top and antitop quarks, including also $\mathcal{O}(v^2)$ relativistic corrections. The structure of the nonrelativistic expansion of the phase space matching contributions for the inclusive NRQCD cross section is examined in Sec. III C by a comparison with the full Standard Model tree-level predictions for the processes $e^+e^- \to t\bar{t} \to b\bar{b}W^+W^-$ and $e^+e^- \to b\bar{b}W^+W^-$ obtained from Madgraph [30]. The $\mathcal{O}(\alpha_s)$ QCD corrections to the phase space matching conditions arising from ultrasoft gluon exchange and potential interactions are computed in Sec. IV. The calculations allow to determine the complete set of NNLL phase space matching contributions and of a part of the N^{3}LL corrections. The results are discussed in detail and analyzed specifically with respect to the convergence of the α_s-expansion, and we also discuss nonperturbative effects. Details on the computation of the $\mathcal{O}(\alpha_s)$ ultrasoft corrections to the phase space matching coefficients are relegated to Appendix A. Finally, in Sec. V, we analyze the numerical impact of the phase space matching contributions to the inclusive NRQCD cross section and compare their size to the other types of electroweak and finite lifetime corrections. Readers only interested in the main concepts of the phase space matching and the numerics of the final results might jump from here directly to Sec. III A and then to Sec. V.

II. NRQCD FORMALISM AND PREVIOUS RESULTS

For the work in this paper we use the vNRQCD effective field theory formalism [31–33] to describe the nonrelativistic top-antitop dynamics relevant for the inclusive threshold cross section. In this section we briefly review the basic vNRQCD notation and ingredients with special emphasis on electroweak and finite lifetime effects in the cross section. We also outline the previous results concerning the type-1 imaginary contributions to the vNRQCD Wilson coefficients determined in Ref. [27]. We note that the results are general and can in principle also be implemented with minimal notational modifications within other formalisms such as pNRQCD [34].

Basics:

The vNRQCD Lagrangian contains heavy quark bilinear, potential, soft and ultrasoft operator terms. Up to the NNLL order the bilinear terms read

$$\mathcal{L}_{\text{bilinear}}(x) = \sum_{\mathbf{p}} \psi_{\mathbf{p}}^{\dagger}(x)\Big\{ iD^0 - \frac{(\mathbf{p}-i\mathbf{D})^2}{2m_t} + \frac{\mathbf{p}^4}{8m_t^3} + \frac{i}{2}\Gamma_t\Big(1-\frac{\mathbf{p}^2}{2m_t^2}\Big) - \delta m_t \Big\}\psi_{\mathbf{p}}(x) + (\psi_{\mathbf{p}} \to \chi_{\mathbf{p}})\,, \tag{5}$$

where the fields $\psi_{\mathbf{p}}$ and $\chi_{\mathbf{p}}$ destroy top and antitop quarks with label momentum $\mathbf{p}$, and Γ_t is the top quark width defined at the top quark pole. The velocity counting of the (anti)top quark fields for $d = 4$ is $\psi_{\mathbf{p}} \sim \chi_{\mathbf{p}} \sim v^{3/2}$. The term $\propto \Gamma_t \frac{\mathbf{p}^2}{2m_t}$ is the top lifetime dilation correction. We also included the ultrasoft gauge covariant derivative $D^\mu = (D^0, -\mathbf{D}) = \partial^\mu + igA^\mu$ where A^μ is the ultrasoft gauge field. The dependence on D^μ is directly tied to the (anti)top three-momentum label $\mathbf{p}$ to all orders of perturbation theory through reparametrization invariance [35]. We use the v-counting $D^0 \sim m_t v^2 \sim \Gamma_t$, and the ultrasoft interactions start contributing in matrix elements at N^{3}LL order. The term δm_t is a residual mass term which is of order v^2 in a short-distance threshold mass scheme [1]. The LL order terms in Eq. (5) lead to the top/antitop propagator in Eq. (3).

The leading order potential term contains the well known Coulomb interaction,

$$\mathcal{L}_{\text{pot}} = -\sum_{\mathbf{p},\mathbf{p}'} \frac{\mathcal{V}_c^{(s)}(\nu)}{(\mathbf{p}-\mathbf{p}')^2}\, \psi_{\mathbf{p}'}^{\dagger}\psi_{\mathbf{p}}\chi_{-\mathbf{p}'}^{\dagger}\chi_{-\mathbf{p}}\,, \tag{6}$$

where

$$\mathcal{V}_c^{(s)}(\nu) = -4\pi C_F \alpha_s(m_t\nu) \tag{7}$$

is the Coulomb Wilson coefficient for a color singlet heavy quark pair and ν is the vNRQCD velocity renormalization scale. The velocity renormalization scale ν is introduced to conveniently describe the correlated renormalization group evolution of soft ($\sim m_t v$) and ultrasoft ($\sim m_t v^2$) effects, and its natural scaling to sum large logarithmic terms is $\nu \sim v \sim \alpha_s$. The evolution of the Coulomb Wilson coefficient differs from the running of the strong coupling starting at NNLL order due to ultrasoft gluon corrections. There are also radiative corrections to the Coulomb interaction arising from soft gluon loops. In vNRQCD they contribute through matrix elements involving T-products of soft gluon operators. These QCD corrections to the Coulomb potential are known at $\mathcal{O}(\alpha_s)$ [36] and $\mathcal{O}(\alpha_s^2)$ [37–39], and have recently been determined even at $\mathcal{O}(\alpha_s^3)$ [10–12]. A discussion on the v^2-suppressed vNRQCD potentials is given in Refs. [32, 33]. We note that there are also potentials generated by the electroweak interactions. The dominant one is the QED contribution to the Coulomb potential which can be easily implemented by writing $\mathcal{V}_c^{(s)}(\nu) = -4\pi C_F\alpha_s(m_t\nu) - 4\pi\alpha(m_t\nu)$. According to Eq. (1) this QED effect contributes at NLL order. There are no $\mathcal{O}(\alpha\alpha_s)$ QED NNLL corrections that contribute to the Coulomb potential. There are also higher order electroweak potentials initiated e.g. by the exchange of the Higgs [6, 40, 41] or the Z-boson.

Eqs. (5) and (6) yield the LL nonrelativistic top-antitop dynamics. For predictions of the inclusive cross section one important ingredient is the zero-distance Green function. At LL order and using dimensional regularization with $d = 4-2\epsilon$, the unrenormalized zero-distance Green function has the form ($a = C_F\alpha_s$)

$$G^0(a, v, m_t, \nu) \;=\; \frac{m_t^2}{4\pi}\left\{ i\,v - a\left[\ln\left(\frac{-i\,v}{\nu}\right) - \frac{1}{2} + \ln 2 + \gamma_E + \psi\left(1-\frac{i\,a}{2\,v}\right)\right]\right\} + \frac{m_t^2\,a}{4\pi}\,\frac{1}{4\,\epsilon}\,, \tag{8}$$

where

$$v \;=\; \sqrt{\frac{\sqrt{s} - 2(m_t + \delta m_t) + i\Gamma_t}{m_t}}\,, \tag{9}$$

$\psi(x) \equiv d/dx \ln\Gamma(x)$ is the digamma function, and $\sqrt{s}$ is the e^+e^- c.m. energy. The divergent $1/\epsilon$ term in Eq. (8) is a UV-divergence in the real part of the LL order Green function and does not play any role for the production of stable particles.

Top pair production currents:

Top-antitop pair production and annihilation is described by currents involving the top and antitop fields. For cross section predictions up to NNLL order one needs the leading and subleading ${}^3S_1$ currents $\mathcal{O}^j_{\mathbf{p},1}$ and $\mathcal{O}^j_{\mathbf{p},2}$, respectively, and the ${}^3P_1$ current $\mathcal{O}^j_{\mathbf{p},3}$, which is $\mathbf{p}/m_t$-suppressed compared to the leading S-wave current. These currents have the form [17, 18]

$$\begin{aligned}
\mathcal{O}^j_{\mathbf{p},1} \;&=\; \psi_{\mathbf{p}}^\dagger\,\sigma^j(i\sigma^2)\chi^*_{-\mathbf{p}}\,, \qquad \mathcal{O}^j_{\mathbf{p},2} = \frac{1}{m_t^2}\,\psi_{\mathbf{p}}^\dagger\,\mathbf{p}^2\,\sigma^j(i\sigma^2)\chi^*_{-\mathbf{p}}\,,\\
\mathcal{O}^j_{\mathbf{p},3} \;&=\; \frac{-i}{2m_t}\,\psi_{\mathbf{p}}^\dagger\,[\sigma^j, \boldsymbol{\sigma}\cdot\mathbf{p}]\,(i\sigma^2)\chi^*_{-\mathbf{p}}\,.
\end{aligned} \tag{10}$$

To ensure electroweak gauge invariance at subleading order it is necessary to include the initial electron and positron fields, which leads to the $t\bar{t}$ production operators

$$\mathcal{O}_{V,\mathbf{p},\sigma} \;=\; \left[\,\bar{e}_+\,\gamma_j\,e_-\,\right]\mathcal{O}^j_{\mathbf{p},\sigma}\,, \qquad \mathcal{O}_{A,\mathbf{p},\sigma} \;=\; \left[\,\bar{e}_+\,\gamma_j\,\gamma_5\,e_-\,\right]\mathcal{O}^j_{\mathbf{p},\sigma}\,, \tag{11}$$

where the index $j = 1, 2, 3$ is summed and the index $\sigma = 1, 2, 3$ distinguishes between the different currents. The current $\mathcal{O}_{V,\mathbf{p},1}$ contributes at LL order for the inclusive cross section, and $\mathcal{O}_{V,\mathbf{p},2}$ and $\mathcal{O}_{V,\mathbf{p},3}$ contribute at NNLL order. Because the effective theory is constructed such that it describes $t\bar{t}$ production only in the threshold region and in the c. m. frame, only those initial e^+e^- states[5] $a^{c\dagger}_{\tau'}(\mathbf{k}')a^{s}_{\tau}\dagger(\mathbf{k})|0\rangle$ are allowed that fulfill $s \equiv (k + k')^2 \approx 4m_t^2$ and $\mathbf{k} = -\mathbf{k}'$. For simplicity we assume electron and positron to travel along the z-direction, therefore the explicit form of their 4-momenta is

$$k^\mu \;=\; \left(\frac{\sqrt{s}}{2}, \frac{\sqrt{s}}{2}\,\hat{\mathbf{e}}_z\right)\,, \qquad k'^\mu \;=\; \left(\frac{\sqrt{s}}{2}, -\frac{\sqrt{s}}{2}\,\hat{\mathbf{e}}_z\right)\,, \tag{12}$$

[5] Here, $a_\tau(\mathbf{k})$ and $a^c_{\tau'}(\mathbf{k}')$ are operators for the annihilation of an electron and a positron with spin τ, τ' and 3-momentum $\mathbf{k}$, $\mathbf{k}'$, respectively, and $|0\rangle$ is the vacuum state.

$\hat{\mathbf{e}}_z$ being the unit vector in z-direction. The fields e_- and e_+ in Eqs. (11) are now defined as

$$e_-(x) \;=\; \sum_{\tau,\sqrt{s}} a_\tau(\mathbf{k})\, u_\tau(\mathbf{k})\, e^{-i\hat{k}\cdot x}\,, \qquad e_+(x) \;=\; \sum_{\tau,\sqrt{s}} a^{c\dagger}_\tau(\mathbf{k}')\, v_\tau(\mathbf{k}')\, e^{i\hat{k}'\cdot x}\,, \tag{13}$$

where $u_\tau(\mathbf{k})$ and $v_\tau(\mathbf{k}')$ denote Dirac spinors for electron and positron, respectively, and the momenta $\mathbf{k}$ and $\mathbf{k}'$ refer to Eqs. (12). The sum over the c. m. energy $\sqrt{s}$ is restricted to the threshold region. For simplicity we do not sum over the angles of the electron and positron momenta. The phase factors in Eqs. (13) are defined such that they describe only the $t\bar{t}$ low-energy fluctuations,

$$\hat{k}^\mu \;=\; \left(\frac{\sqrt{s}}{2} - m_t, \frac{\sqrt{s}}{2}\,\hat{\mathbf{e}}_z\right)\,, \qquad \hat{k}'^\mu \;=\; \left(\frac{\sqrt{s}}{2} - m_t, -\frac{\sqrt{s}}{2}\,\hat{\mathbf{e}}_z\right)\,. \tag{14}$$

The dependence on 3-momenta in Eq. (14) vanishes after the operators $\mathcal{O}_{V/A,\mathbf{p},\sigma}$ have been applied to the initial e^+e^- state. The operators for $t\bar{t}$ annihilation are obtained from $\mathcal{O}_{V/A,\mathbf{p},\sigma}$ by Hermitian conjugation.

Due to the dependence of the intermediate photon and Z boson propagator on the c.m. energy in the process $e^+e^- \to \gamma^*, Z^* \to t\bar{t}$, we also introduce the $t\bar{t}$ production operators

$$\mathcal{O}^{(1)}_{V,\mathbf{p},1} \;=\; \left[\,\bar{e}_+\,\gamma_j\,(\hat{E}/m_t)\,e_-\,\right]\mathcal{O}^j_{\mathbf{p},1}\,, \qquad \mathcal{O}^{(1)}_{A,\mathbf{p},1} \;=\; \left[\,\bar{e}_+\,\gamma_j\,\gamma_5\,(\hat{E}/m_t)\,e_-\,\right]\mathcal{O}^j_{\mathbf{p},1}\,. \tag{15}$$

Here, $\hat{E}$ denotes the operator $\hat{E} = i\partial_0$ acting on the fields to the right and to the left and thus picks up the kinetic energy $E \equiv \sqrt{s} - 2m_t \sim m_t v^2$ from the initial e^+e^- state. So these operators contribute a NNLL order. Concerning QCD effects, the operators $\mathcal{O}^{(1)}_{V/A,\mathbf{p},1}$ have the same matching conditions and renormalization group evolution as $\mathcal{O}_{V/A,\mathbf{p},1}$ of Eqs. (11) but their Wilson coefficients differ in the electroweak contributions. Similar additional operators related to $\mathcal{O}_{V/A,\mathbf{p},2}$ and $\mathcal{O}_{V/A,\mathbf{p},3}$ do not need to be introduced since they would give contributions beyond N^{3}LL order.

The contribution of the currents to the Lagrangian reads

$$\begin{aligned}\mathcal{L}_{\rm cur} = \sum_{\mathbf{p}} \Big[& C_{V,1}\,\mathcal{O}_{V,\mathbf{p},1} + C_{A,1}\,\mathcal{O}_{A,\mathbf{p},1} + C^{(1)}_{V,1}\,\mathcal{O}^{(1)}_{V,\mathbf{p},1} + C^{(1)}_{A,1}\,\mathcal{O}^{(1)}_{A,\mathbf{p},1} \\ & + C_{V,2}\,\mathcal{O}_{V,\mathbf{p},2} + C_{A,2}\,\mathcal{O}_{A,\mathbf{p},2} + C_{V,3}\,\mathcal{O}_{V,\mathbf{p},3} + C_{A,3}\,\mathcal{O}_{A,\mathbf{p},3} \Big] + \text{H. c.}\,.\end{aligned} \tag{16}$$

If QED radiative corrections are neglected, the electron and positron fields in the current operators act like classic fields and do not contribute to the nonrelativistic $t\bar{t}$ dynamics. The Hermitian conjugation (H. c.) acts on the operators in the usual way and on possible CP-violating phases in the Wilson coefficients as complex conjugation. It does, however, *not* act on imaginary contributions in the Wilson coefficients that are related to finite-lifetime contributions. Since we do not consider CP-phases in this work, the Wilson coefficients of operators and their conjugated counterparts are equal. At NNLL order the currents run only due to QCD effects. Their matching conditions, which we will generally parameterize at the hard matching velocity scale $\nu = 1$, contain electroweak contributions already at LL order. Including QCD, electroweak and finite lifetime effects up to NNLL order the Wilson coefficients can be written in the form

$$
\begin{aligned}
C_{V/A,1}(\Lambda,\nu) &= C^{\rm Born}_{V/A,1}\, c_1(\nu)\,(1+i\,\delta\tilde c_1(\Lambda)) + i\,C^{\rm int}_{V/A,1}(1+\delta\tilde c^{\rm int}_1(\Lambda)) + C^{\rm 1loop}_{V/A,1}\,,\\
C^{(1)}_{V/A,1}(\nu) &= C^{(1),\rm Born}_{V/A,1}\, c_1(\nu)\,,\\
C_{V/A,2}(\nu) &= C^{\rm Born}_{V/A,1}\, c_2(\nu)\,,\\
C_{V/A,3}(\nu) &= C^{\rm Born}_{V/A,3}\, c_3(\nu)\,.
\end{aligned}
\tag{17}
$$

In Eqs. (17) all imaginary contributions are indicated by an explicit factor of the imaginary i. The terms $c_i(\nu)$ parameterize the QCD evolution and the hard matching conditions. Their explicit form at NLL order can be found in Refs. [33, 42, 43]. Note that for the NNLL running of $c_1(\nu)$ currently only the non-mixing contributions [4] are fully known. Partial results for the NNLL mixing contributions have been determined in Refs. [20, 44]. For our numerical analysis of the phase space matching contributions to the inclusive NRQCD cross section we need the NNLL order corrections to the matching coefficient $c_1(\nu=1)$,

$$
c_1(\nu=1) = 1 + h_1^{(1)} + h_1^{(2)} + \ldots\,,
\tag{18}
$$

where

$$
\begin{aligned}
h_1^{(1)} &= -\frac{2\,C_F}{\pi}\,\alpha_s(m_t)\,,\\
h_1^{(2)} &= \alpha_s^2(m_t)\bigg[C_F^2\bigg(\frac{\ln 2}{3}-\frac{31}{24}-\frac{2}{\pi^2}\bigg)+C_AC_F\bigg(\frac{\ln 2}{2}-\frac{5}{8}\bigg)+\frac{\kappa}{2}\bigg]-\frac{2\,Q_t^2}{\pi}\alpha_{\rm qed}(m_t)\,,
\end{aligned}
\tag{19}
$$

and the constant κ was given in Refs. [45, 46]. The last term in Eq. (19) is the one-loop QED matching correction to $c_1(\nu=1)$, which contributes at NNLL order according to the power-counting $\alpha_{\rm qed}\sim\alpha_s^2$. In Eqs. (17) the terms $C^{\rm Born}_{V/A,i}$ denote electroweak matching contributions from the tree level amplitude for the $e^+e^-\to\gamma,Z\to t\bar t$ production process and $C^{\rm 1loop}_{V/A,1}$ refers to the hard one-loop electroweak corrections. The results for $C^{\rm 1loop}_{V/A,1}$ are elaborate and can be found in Ref. [22] (see also Refs. [23, 24]). The imaginary terms with $C^{\rm int}_{V/A,1}$ contain finite lifetime effects arising from the interference of the dominant double resonant process $e^+e^-\to t\bar t\to W^+W^-b\bar b$ with single resonant processes leading to the same final state, but having only one top or one antitop at the intermediate stage, see Fig. 1. The terms $C^{\rm 1loop}_{V/A,1}$ and $iC^{\rm int}_{V/A,1}$ are obtained from one-loop full theory diagrams and contribute at NNLL order in the counting scheme of Eq. (1) due to an additional factor of $\alpha\sim v^2$. Thus at the order we are working they are only accounted for in the leading order current $\mathcal{O}_{A/V,\mathbf{p},1}$. The terms $i\delta\tilde c_1(\Lambda)$ and $i\delta\tilde c_1^{\rm int}(\Lambda)$ indicate imaginary matching contributions related to the experimental selection cuts generically denoted by the argument Λ. As we show in Sec. IV B they are required to account for a phase space matching correction of $t\bar t$ vertex subdiagrams that arise at $\mathcal{O}(\alpha_s)$. For inclusive selection cuts such as the invariant mass prescription of Eq. (4) this term contributes at N^{3}LL order. To shorten the notation we frequently drop the matching scale ($\nu=1$) dependence of the electroweak matching conditions displayed in Eqs. (17). It is implied that the electroweak couplings are evaluated at the same hard matching scale as the QCD matching conditions.

The electroweak matching contributions from the tree level amplitude of the $e^+e^- \to \gamma, Z \to t\bar{t}$ production process read [27] ($\alpha \equiv \alpha_{\rm qed}(m_t)$)

$$\begin{aligned}
C_V^{\rm Born} &= -4\pi\alpha\left[\frac{Q_t}{4m_t^2} - \frac{v_e v_t}{4m_t^2 - M_Z^2}\right], & C_{A,1}^{\rm Born} &= -4\pi\alpha\frac{a_e v_t}{4m_t^2 - M_Z^2}, \\
C_{V,1}^{(1),\rm Born} &= \pi\alpha\left[\frac{Q_t}{m_t^2} - \frac{16 v_e v_t m_t^2}{(4m_t^2 - M_Z^2)^2}\right], & C_{A,1}^{(1),\rm Born} &= 16\pi\alpha\frac{a_e v_t m_t^2}{(4m_t^2 - M_Z^2)^2}, \\
C_{V,2}^{\rm Born} &= -1/6\, C_{V,1}^{\rm Born}, & C_{A,2}^{\rm Born} &= -1/6\, C_{A,1}^{\rm Born}, \\
C_{V,3}^{\rm Born} &= 4\pi\alpha\frac{v_e a_t}{4m_t^2 - M_Z^2}, & C_{A,3}^{\rm Born} &= -4\pi\alpha\frac{a_e a_t}{4m_t^2 - M_Z^2},
\end{aligned} \tag{20}$$

where

$$v_f = \frac{t_3^f - 2Q_f s_w^2}{2 s_w c_w}, \qquad a_f = \frac{t_3^f}{2 s_w c_w},$$

the symbol Q_f is the electric charge, and t_3^f is the third component of the weak isospin of the fermion f. The abbreviations s_w and c_w denote the sine and cosine of the weak mixing angle, respectively. The coefficients $C_{V/A,1}^{(1),\rm Born}$ arise from the $\mathcal{O}(v^2)$ terms in the expansion of the photon and Z boson propagators near threshold using $s = 4m_t^2(1 + E/m_t + \ldots)$, where the dots represent terms of order E^2 and higher. An alternative approach is to keep the exact relativistic form for the photon and Z propagators. This leads to the expressions

$$\begin{aligned}
C_{V,1}^{\rm Born} &= -4\pi\alpha\left[\frac{Q_t}{s} - \frac{v_e v_t}{s - M_Z^2}\right], & C_{A,1}^{\rm Born} &= -4\pi\alpha\frac{a_e v_t}{s - M_Z^2}, \\
C_{V,1}^{(1),\rm Born} &= 0, & C_{A,1}^{(1),\rm Born} &= 0 \\
C_{V,2}^{\rm Born} &= -1/6\, C_{V,1}^{\rm Born}, & C_{A,2}^{\rm Born} &= -1/6\, C_{A,1}^{\rm Born}, \\
C_{V,3}^{\rm Born} &= 4\pi\alpha\frac{v_e a_t}{s - M_Z^2}, & C_{A,3}^{\rm Born} &= -4\pi\alpha\frac{a_e a_t}{s - M_Z^2}.
\end{aligned} \tag{21}$$

For our numerical examinations we use these alternative definitions for $C_{V/A,i}^{\rm Born}$ and $C_{V/A,i}^{(1),\rm Born}$ ($i = 1, 2, 3$) unless noted otherwise.

The imaginary interference coefficients $C_{V/A,1}^{\rm int}$ are determined from the bW cuts in the one-loop electroweak corrections to the $e^+e^- \to t\bar{t}$ amplitude with on-shell stable external (anti)top quarks. They also contain the imaginary contribution of the (anti)top wave function renormalization Z-factor, and this term is essential to maintain gauge-invariance. They have the form [27]

$$\begin{aligned}
iC_{V,1}^{\rm int} = -i\,&\frac{\alpha^2\pi|V_{tb}|^2}{12 m_t^2 s_w^2 x(4c_w^2 - x)(1+x)}\left[\frac{3x(1+x)}{(1-x)}\left(1 + \frac{x-4}{4s_w^2}\right)\ln\left(\frac{2-x}{x}\right)\right. \\
&+ Q_e Q_t(1-x)(4-x)(1+2x)(1+x+x^2) \\
&+ Q_e(x-1)(1+4x+2x^2+2x^3) + Q_t(1-x)(1+2x)(1+x+x^2) \\
&\left.- \frac{1}{2}(1+12x+9x^2+2x^3) + \frac{1}{8s_w^2}(2+41x+28x^2-x^3+2x^4)\right],
\end{aligned} \tag{22}$$

$$
\begin{aligned}
iC_{A,1}^{\rm int} = \; & i\,\frac{\alpha^2\pi|V_{tb}|^2}{12m_t^2 s_w^2 x(4c_w^2-x)(1+x)}\,\bigg[\,\frac{3x(1+x)}{(1-x)}\bigg(1+\frac{x-4}{4s_w^2}\bigg)\,\ln\Big(\frac{2-x}{x}\Big) \\
& + Q_t(1-x)(1+2x)(1+x+x^2) \\
& - \frac{1}{2}(1+12x+9x^2+2x^3) + \frac{1}{8s_w^2}(2+41x+28x^2-x^3+2x^4)\bigg]\,,
\end{aligned}
\tag{23}
$$

where $x \equiv M_W^2/m_t^2$.

Forward scattering operators:

The $(e^+e^-)(e^+e^-)$ forward scattering operators are required to renormalize the phase space divergences. Their evolution accounts for the summation of $\ln v$ terms that arise specifically from finite-lifetime effects. The matching conditions for their Wilson coefficients account for selection prescriptions applied on the observed final states to define the inclusive cross section. These phase space matching conditions depend on the c.m. energy, and we therefore need to define a set of operators capable to reproduce this energy-dependence within NRQCD. The forward scattering operators are defined as

$$
\begin{aligned}
\tilde{\mathcal{O}}_V^{(n)} &= -\big[\,\bar{e}_-\,\gamma^\mu\,e_+\big]\,\big[\,\bar{e}_+\,\gamma_\mu\,(\hat{E}/m_t)^n\,e_-\,\big]\,, \\
\tilde{\mathcal{O}}_A^{(n)} &= -\big[\,\bar{e}_-\,\gamma^\mu\,\gamma_5\,e_+\big]\,\big[\,\bar{e}_+\,\gamma_\mu\,\gamma_5\,(\hat{E}/m_t)^n\,e_-\,\big]\,,
\end{aligned}
\tag{24}
$$

and thus the $\tilde{\mathcal{O}}_{V/A}^{(n)}$ pick up n powers of the $t\bar{t}$ kinetic energy $E=\sqrt{s}-2m_t$ from the initial e^+e^- state. The normalization of the electron and positron fields ensures that we have

$$
\frac{1}{4}\sum_{\tau,\tau'}\Big\langle\,0\,\Big|\,a_\tau(\mathbf{k})\,a_{\tau'}^c(\mathbf{k}')\,\tilde{\mathcal{O}}_{V/A}^{(n)}\,a_{\tau'}^{c\dagger}(\mathbf{k}')\,a_\tau^\dagger(\mathbf{k})\,\Big|\,0\,\Big\rangle = s\,\bigg(\frac{E}{m_t}\bigg)^n
$$

for the spin-averaged forward scattering amplitude.

The contribution of the forward scattering operators to the Lagrangian reads

$$
\mathcal{L}_{\rm fsc} = \sum_n \tilde{C}_V^{(n)}\tilde{\mathcal{O}}_V^{(n)} + \tilde{C}_A^{(n)}\tilde{\mathcal{O}}_A^{(n)}\,,
\tag{25}
$$

where the $\tilde{C}_{V/A}^{(n)}(\Lambda,\nu)$ are the Wilson coefficients. They depend on the renormalization velocity scale ν, and they have a dependence on the selection cuts, generically denoted by Λ. Frequently we will use the shorter notation $\tilde{C}_{V/A}\equiv\tilde{C}_{V/A}^{(0)}$ for the coefficients of the dominant energy-independent forward scattering operators $\tilde{\mathcal{O}}_{V/A}$. For the examinations in this work we consider the operators $\tilde{\mathcal{O}}_{V/A}$ and $\tilde{\mathcal{O}}_{V/A}^{(1)}$.

QCD factorization formula:

For the inclusive cross section of $t\bar{t}$ production close to threshold accounting for the phase space matching contributions up to N^{3}LL order and for the QCD and other electroweak and finite lifetime effects at NNLL order we have the factorization formula [18, 22, 27]

$$
\begin{aligned}
\sigma_{\rm incl}(\Lambda) \;=\; & \frac{1}{s} L^{lk}\,\mathrm{Im}\Bigg[\Big(C_{V,1}(\Lambda,\nu)^2 + C_{A,1}(\Lambda,\nu)^2\Big)\mathcal{A}_1^{lk} \\
& \qquad + \Big(2C_{V,1}(\Lambda,\nu)C_{V,1}^{(1)}(\nu) + 2C_{A,1}(\Lambda,\nu)C_{A,1}^{(1)}(\nu)\Big)(E/m_t)\mathcal{A}_1^{lk} \\
& \qquad + \Big(2C_{V,1}(\Lambda,\nu)C_{V,2}(\nu) + 2C_{A,1}(\Lambda,\nu)C_{A,2}(\nu)\Big)\mathcal{A}_2^{lk} \\
& \qquad + \Big(C_{V,3}(\nu)^2 + C_{A,3}(\nu)^2\Big)\mathcal{A}_3^{lk}\Bigg] \\
& + \sum_{n=0}^{1}(E/m_t)^n\,\mathrm{Im}\Big[\tilde{C}_V^{(n)}(\Lambda,\nu) + \tilde{C}_A^{(n)}(\Lambda,\nu)\Big]\,. \qquad (26)
\end{aligned}
$$

The spin-averaged lepton tensor reads

$$
\begin{aligned}
L^{lk} \;&=\; \frac{1}{4}\sum_{\tau,\tau'}\Big[\bar{v}_{\tau'}(\mathbf{k}')\,\gamma^l\,(\gamma_5)\,u_\tau(\mathbf{k})\Big]\Big[\bar{u}_\tau(\mathbf{k})\,\gamma^k\,(\gamma_5)\,v_{\tau'}(\mathbf{k}')\Big] \\
&=\; \frac{1}{2}\,(k+k')^2\,(\delta^{lk} - \hat{e}_z^l\hat{e}_z^k)\,, \qquad (27)
\end{aligned}
$$

with the definitions of electron/positron momenta given in Eqs. (12). The quantities $\mathcal{A}_i^{lk}$ are time-ordered products of the $t\bar{t}$ production and annihilation currents defined in Eq. (10). Note that the electron and positron field operators, from which the operators in Eqs. (11), (15) and (24) are composed, only pick out the initial and final e^+e^- states and do not affect the correlators $\mathcal{A}_i^{lk}$ in any way. The explicit expressions for the $\mathcal{A}_i^{lk}$ are

$$
\begin{aligned}
\mathcal{A}_1^{lk} \;&=\; i\sum_{\mathbf{p},\mathbf{p}'}\int d^4x\, e^{-i\hat{q}\cdot x}\Big\langle 0\Big|\,T\,\mathcal{O}_{\mathbf{p},1}^{l\,\dagger}(0)\,\mathcal{O}_{\mathbf{p}',1}^{k}(x)\Big|\,0\Big\rangle\,, \\
\mathcal{A}_2^{lk} \;&=\; \frac{i}{2}\sum_{\mathbf{p},\mathbf{p}'}\int d^4x\, e^{-i\hat{q}\cdot x}\Big\langle 0\Big|\,T\,\Big[\mathcal{O}_{\mathbf{p},1}^{l\,\dagger}(0)\,\mathcal{O}_{\mathbf{p}',2}^{k}(x) + \mathcal{O}_{\mathbf{p},2}^{l\,\dagger}(0)\,\mathcal{O}_{\mathbf{p}',1}^{k}(x)\Big]\Big|\,0\Big\rangle\,, \\
\mathcal{A}_3^{lk} \;&=\; i\sum_{\mathbf{p},\mathbf{p}'}\int d^4x\, e^{-i\hat{q}\cdot x}\Big\langle 0\Big|\,T\,\mathcal{O}_{\mathbf{p},3}^{l\,\dagger}(0)\,\mathcal{O}_{\mathbf{p}',3}^{k}(x)\Big|\,0\Big\rangle\,, \qquad (28)
\end{aligned}
$$

where $\hat{q} \equiv (\sqrt{s} - 2m_t, 0)$. For the v^2-suppressed electroweak and finite lifetime matching coefficients $C_{V/A,1}^{\rm 1loop}$ and $iC_{V/A,1}^{\rm int}$ contained in $C_{V/A,1}$ it is sufficient to use the LL current correlator $\mathcal{A}_{1,\rm LL}$. All terms in the second, third and fourth lines of Eq. (26) are v^2-suppressed and therefore contribute at NNLL order. This suppression originates from factors E/m_t, $\mathbf{p}^2/m_t^2$ appearing in $\mathcal{O}_{\mathbf{p},2}^k$ and two factors of $\boldsymbol{\sigma}\cdot\mathbf{p}/m_t$ appearing in $\mathcal{O}_{\mathbf{p},3}^k$, respectively. The terms in the first four lines also appear in pure QCD for stable heavy quarks see e.g. Refs. [17–19]. The fifth line contains the phase space matching corrections related to the $(e^+e^-)(e^+e^-)$ forward scattering operators. As shown in Sec. III B the coefficients $\tilde{C}_{V/A}^{(0)} = \tilde{C}_{V/A}$ start contributing at NLL, and the terms $E/m_t\tilde{C}^{(1)}_{V/A}$ are N^{3}LL corrections. We note that all terms shown in Eq. (26) are understood as finite $\overline{\text{MS}}$-renormalized quantities.

We can write $\mathcal{A}_i^{lk} = \delta^{lk}/3\mathcal{A}_i$ after tracing the sigma matrices of the currents in 3 dimensions. The correlators $\mathcal{A}_i$ can then be expressed in terms of contributions to the zero-distance S-wave and P-wave Green functions of the two-body Schrödinger equation:

$$\begin{aligned}
\mathcal{A}_1(v, m_t, \nu) \;&=\; 6N_c\Big[G^c(a, v, m_t, \nu) + \Big(\mathcal{V}_2^{(s)}(\nu) + 2\mathcal{V}_s^{(s)}(\nu)\Big)\, G^\delta(a, v, m_t, \nu) \\
&\qquad + \mathcal{V}_r^{(s)}(\nu) G^r(a, v, m_t, \nu) + \mathcal{V}_k^{(s)}(\nu) G^k(a, v, m_t, \nu) \\
&\qquad + G^{\text{kin}}(a, v, m_t, \nu) + G^{\text{dil}}(a, v, m_t, \nu)\Big]\,, \\
\mathcal{A}_3(v, m_t, \nu) \;&=\; \frac{4N_c}{m_t^2} G^1(a, v, m_t, \nu)\,. \qquad (29)
\end{aligned}$$

Here, the terms $\mathcal{V}_i^{(s)}(\nu)$ $(i = 2, s, r, k)$ are the Wilson coefficients of the v^2-suppressed potentials [33]. The correlator $\mathcal{A}_2$ can be related to $\mathcal{A}_1$ by the heavy quark equation of motion giving $\mathcal{A}_2(v, m_t, \nu) = v^2\mathcal{A}_1(v, m_t, \nu)$. Thus only the LL terms in $\mathcal{A}_1$ are necessary to obtain the NNLL order contributions of $\mathcal{A}_2$. The function G^c is the Coulomb Green function. The LL approximation for G^c is known analytically and has been displayed in Eq. (8). At NLL and NNLL order, related to the $\mathcal{O}(\alpha_s)$ [36] and $\mathcal{O}(\alpha_s^2)$ [37–39] corrections to the Coulomb potential, we use the numerical results obtained in Refs. [17, 18]. They are based on an exact solution of the corresponding Schrödinger equation using computational techniques developed in Refs. [47, 48]. For the analytic formula for G^1, see Ref. [18]. All the relativistic corrections to the Green function, $G^{\delta,r,k,\text{kin}}$, are available in analytic form, see Refs. [4, 18]. They are computed from insertions of the v^2-suppressed potentials and the kinetic energy corrections. The Green function correction G^{dil} arises from an insertion of the lifetime dilation correction to the bilinear quark field operators shown in Eq. (5). The expressions for G^{dil} reads [27]

$$G^{\text{dil}} \;=\; -i\,\frac{\Gamma_t}{2m_t}\left[1 + \frac{v}{2}\frac{\partial}{\partial v} + a\frac{\partial}{\partial a}\right] G^0(a, v, m_t, \nu)\,. \qquad (30)$$

Phase space divergences and renormalization group evolution:

Using the unrenormalized current correlators $\mathcal{A}_i^{lk}$ in the factorization formula (26) leads to the ultraviolet $1/\epsilon$ phase space divergences either from insertions of v^2-suppressed operators or insertions of Wilson coefficient corrections describing finite lifetime corrections. The divergences are absorbed by the counterterms associated to the $(e^+e^-)(e^+e^-)$ forward scattering operators $\tilde{O}_{V/A}$ given in Eq. (24) and are treated with the usual renormalization techniques known from effective theories. However, it is a novel feature that the phase space divergences and the anomalous dimension of the operators $\tilde{\mathcal{O}}_{V/A}$ are purely imaginary. In the

$\overline{\rm MS}$ scheme the NNLL counterterms of the renormalized $\tilde{\mathcal{O}}_{V/A}$ operators have the form [27]

$$\begin{aligned}
\delta\tilde{C}_{V/A} &= i\,\frac{N_c m_t^2}{32\pi^2\epsilon}\left[(C^{\rm Born}_{V/A,1})^2\frac{\Gamma_t}{m_t}+2C^{\rm Born}_{V/A,1}C^{\rm int}_{V/A,1}\right]\mathcal{V}_c^{(s)}(\nu)\\
&\quad+i\,\frac{N_c m_t^2}{32\pi^2\epsilon}\,(C^{\rm Born}_{V/A,1})^2\frac{\Gamma_t}{m_t}\left[\Big(2c_2(\nu)-1\Big)\mathcal{V}_c^{(s)}(\nu)+\mathcal{V}_r^{(s)}(\nu)\right]\\
&\quad+i\,\frac{N_c m_t^2}{48\pi^2\epsilon}\,(C^{\rm Born}_{V/A,3})^2\frac{\Gamma_t}{m_t}\,\mathcal{V}_c^{(s)}(\nu)\,.
\end{aligned}$$

Solving the resulting renormalization group equations for the $\tilde{C}_{V/A}$ one obtains

$$\begin{aligned}
\tilde{C}_{V/A}(\Lambda,\nu) &= \tilde{C}_{V/A}(\Lambda,1)+i\,\frac{2N_c m_t^2 C_F}{3\beta_0}\left\{\left[\Big((C^{\rm Born}_{V/A,1})^2+(C^{\rm Born}_{V/A,3})^2\Big)\frac{\Gamma_t}{m_t}\right.\right.\\
&\quad\left.+3C^{\rm Born}_{V/A,1}C^{\rm int}_{V/A,1}\right]\ln(z)-\frac{4C_F}{\beta_0}\,\frac{\Gamma_t}{m_t}\,(C^{\rm Born}_{V/A,1})^2\ln^2(z)\\
&\quad\left.+\frac{4(C_A+2C_F)}{\beta_0}\,\frac{\Gamma_t}{m_t}\,(C^{\rm Born}_{V/A,1})^2\rho(z)\right\}, \qquad (31)
\end{aligned}$$

where

$$\begin{aligned}
\rho(z) &= \frac{\pi^2}{12}-\frac{1}{2}\ln^2 2+\ln 2\ln(z)-{\rm Li}_2\left(\frac{z}{2}\right)\,,\\
z &\equiv \frac{\alpha_s(m_t\nu)}{\alpha_s(m_t)}\,. \qquad (32)
\end{aligned}$$

Here we have introduced the Λ-dependent hard scale ($\nu=1$) matching conditions $\tilde{C}_{V/A}(\Lambda,1)$.[6] They are determined by the phase space matching procedure as described in the following sections and incorporate the information on the experimental selection cuts as well as the contributions from background diagrams. The phase space logarithms resummed in Eq. (31) correspond to logarithmic terms involving ratios of the hard scales m_t,Λ and nonrelativistic kinematic scales. They contribute at order $\alpha^3\sim v^6$ in the inclusive cross section. So compared to the LL cross section, which counts as $\alpha^2 v\sim v^5$, the phase space logs constitute NLL contributions. This is expected since the phase space divergences arise from matrix elements contributing at NNLL order. In the following sections we determine the matching conditions $\tilde{C}_{V/A}(\Lambda,1)$, which contain the details of the selection cuts that are applied for the definition of the cross section. As explained in the introduction, for inclusive cross section definitions the information on these selection cuts represents hard effects within the NRQCD framework.

III. CONCEPTS OF PHASE SPACE MATCHING

In this section we discuss the main concepts that go into the phase space matching on the basis of an explicit computation of the phase space matching conditions for a cut on the

[6] Frequently we drop the argument '$\nu=1$' in the coefficients $\tilde{C}_{V/A}(\Lambda,1)$ to simplify the notation.

invariant masses of the reconstructed top and antitop quarks. For simplicity we neglect in this section the effects of the strong interactions, i.e. we set $\alpha_s = 0$. A number of additional issues arise if QCD effects are included. QCD corrections to the phase space matching conditions are computed and discussed in Sec. IV.

A. Basic Setup

We define what we call the invariant masses of the top and antitop quarks through the reconstructed masses of the bW^+ and $\bar{b}W^-$ systems coming from the top and antitop decays:

$$M_t^2 = p_t^2 = (p_b + p_{W^+})^2\,, \qquad\qquad M_{\bar{t}}^2 = p_{\bar{t}}^2 = (p_{\bar{b}} + p_{W^-})^2\,. \tag{33}$$

Without QCD effects related to jet and soft particle emission this definition is unambiguous, and we neglect combinatorial background in the following. The latter would have to be determined from Monte-Carlo studies in addition to the examinations carried out in this work. We consider selection cuts on the top and antitop invariant masses of the form

$$(m_t - \Delta M_t) \le M_{t,\bar{t}} \le (m_t + \Delta M_t)\,. \tag{34}$$

We note that to keep Eq. (34) ambiguity-free once QCD effects are accounted for, it is necessary to employ a short-distance top quark mass definition for m_t that is suitable for reconstruction. Such mass definitions have a low infrared cutoff scale $R \sim \Gamma_t$ to avoid the pole mass $\mathcal{O}(\Lambda_{\rm QCD})$ renormalon [15]. An example is the jet mass introduced in Refs. [49, 50]. The $\overline{\rm MS}$ mass does not belong to this class of short-distance masses since it has $R \sim m_t$.

The constraint on the top and antitop invariant masses $M_{t,\bar{t}}$ can be translated into a condition on the off-shellness $p_{t,\bar{t}}^2 - m_t^2$ appearing in the top and antitop propagators, see Eq. (3). At LL order in the nonrelativistic expansion the constraint on the nonrelativistic off-shellness in the NRQCD propagator has the form

$$-\Delta M_t \,\le\, p_{t,\bar{t},0} - m_t - \frac{\mathbf{p}_{t,\bar{t}}^2}{2m_t} \,\le\, \Delta M_t\,. \tag{35}$$

The relativistic NNLL order corrections to these constraints are given in the second part of Sec. III B. Through momentum conservation Eq. (35) leads to a constraint on the phase space integrations for the cross section as illustrated in Fig. 2. From Eq. (35) we see that the ultrasoft and the soft phase space momentum integrations are limited by the scales ΔM_t and $\sqrt{2m_t\Delta M_t}$, respectively. In this work we consider moderate invariant mass cuts with $\Delta M_t \sim 15 - 35$ GeV. Thus we have

$$m_t v^2 \,\lesssim\, \Delta M_t \sim 15 - 35 \text{ GeV}\,, \qquad m_t v \,\lesssim\, \sqrt{2m_t\Delta M_t} \sim 70 - 110 \text{ GeV}\,, \tag{36}$$

and the upper bounds of integration are substantially above the generic v-scaling of the soft and ultrasoft momentum components. Since $\sqrt{2m_t\Delta M_t}$ is parametrically of order m_t we use for our bookkeeping the counting $\sqrt{2m_t\Delta M_t} \sim m_t$. This also implies that $\Delta M_t \sim m_t$. Within the vNRQCD framework this counting scheme is natural since, due to the pull-up mechanism [33, 51], the ultrasoft scale is directly connected to the hard matching scale via RG evolution without an additional matching at the soft scale. In this counting scheme the phase space constraints are incorporated through the NRQCD Wilson coefficients. On the

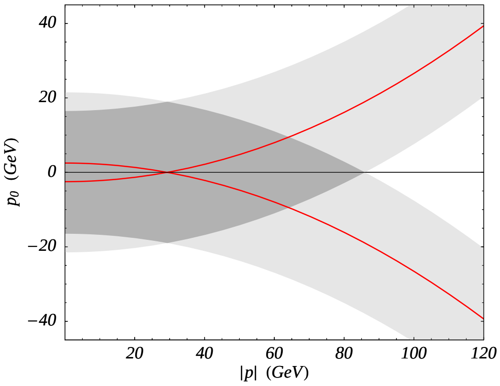

FIG. 2: Phase space integration region spanned in the $p^\mu = (p_0, \mathbf{p})$ variables for $t\bar{t}$ pair production. In terms of p^μ and the external energy $E = \sqrt{s} - 2m_t$ the top and antitop momenta read $p^\mu_{t,\bar{t}} = (m_t + E/2, 0) \pm p^\mu$. The red solid lines correspond to the top and antitop nonrelativistic on-shell conditions; in the limit $\Gamma_t = 0$ the phase-space shrinks to the point where the two on-shell lines intersect, $(p_0, |\mathbf{p}|) = (0, \sqrt{mE})$. Gray, light-gray and white areas correspond to the double-resonant, single-resonant and non-resonant regions, respectively. The gray area represents the phase space region compatible with the invariant mass constraints. We have chosen $E = 5\,\mathrm{GeV}$ and $\Delta M_t = 20\,\mathrm{GeV}$ for this picture.

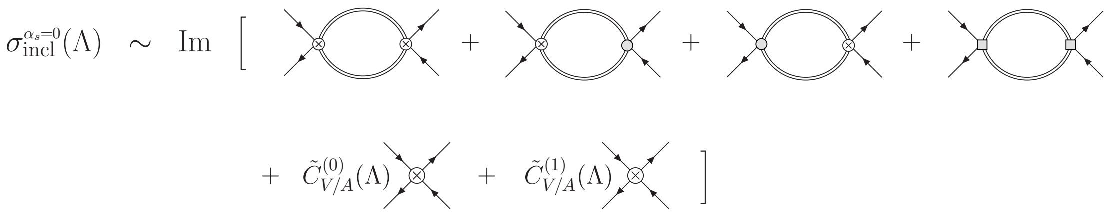

FIG. 3: Graphical illustration of the factorization formula (26) for $\alpha_s = 0$. The $t\bar{t}$ production operators $\mathcal{O}^{(n)}_{V/A,\mathbf{p},\sigma}$ for $\sigma = 1, 2, 3$ are represented by a crossed circle, gray circle and gray box, respectively. Diagrams in the second line correspond to the contributions from the forward scattering operators.

other hand, numerically the scales ΔM_t and $\sqrt{2m_t \Delta M_t}$ are sufficiently below the top mass scale such that all $t\bar{t}$ phase space configurations that pass the invariant mass constraint can still be adequately described by NRQCD. This fact is crucial for the phase space matching method we describe in the following.

When QCD effects are neglected the factorization formula in Eq. (26) can be illustrated graphically as in Fig. 3. For $\alpha_s = 0$ and in the absence of potentials the phase space matching conditions can only contribute to the Wilson coefficients $\tilde{C}^{(n)}_{V/A}$ of the $(e^+e^-)(e^+e^-)$ forward scattering operators $\tilde{\mathcal{O}}^{(n)}_{V/A}$. This is because off-shell (anti)top phase space contributions (corresponding to the light-gray and white areas in Fig. 2) do not match to the operator structure of the $(e^+e^-)(t\bar{t})$ currents. From Eq. (26) and Fig. 2 we see that for the determination of the Wilson coefficients $\tilde{C}^{(n)}_{V/A}$ we need to know the result for the inclusive cross section

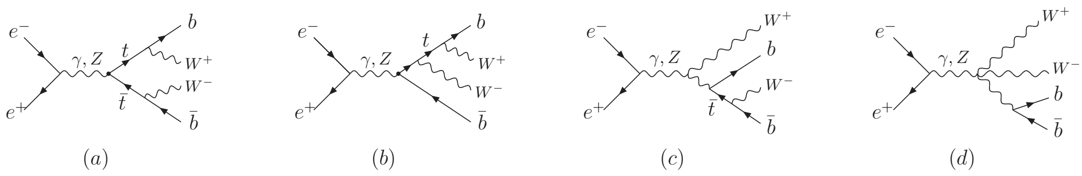

FIG. 4: (a) Full theory diagram for $e^+e^- \to t\bar{t} \to b\bar{b}W^+W^-$. (b,c) Typical single-resonant full theory diagram for $e^+e^- \to t\bar{b}W^- \to b\bar{b}W^+W^-$. (d) Typical full theory diagram for $e^+e^- \to b\bar{b}W^+W^-$ without top or antitop quarks as intermediate states.

$\sigma_{\rm incl}^{\alpha_s=0}(\Lambda)$ with invariant mass constraints. In the common approach to matching computations $\sigma_{\rm incl}^{\alpha_s=0}(\Lambda)$ is computed in the full relativistic theory. After the result is expanded nonrelativistically using the counting of Eq. (1) one can identify the pieces belonging to the Wilson coefficients $\tilde{C}_{V/A}^{(n)}$. On the other hand, as mentioned above, the $t\bar{t}$ phase space regions passing the invariant mass cuts can be determined within the nonrelativistic expansion. We therefore write the expression for the inclusive cross section as a sum of two terms,

$$\sigma_{\rm incl}^{\alpha_s=0}(\Lambda) \,=\, \sigma_{\rm NRQCD}^{\alpha_s=0}(\Lambda) + \sigma_{\rm rem}^{\alpha_s=0}(\Lambda)\,. \tag{37}$$

Here, $\sigma_{\rm NRQCD}^{\alpha_s=0}$ is the cross section computed from NRQCD Feynman rules with the (anti)top invariant mass constraints being applied for the phase space integration. The parameter Λ is related to the invariant mass cut ΔM_t and we use the formal counting $\Lambda \sim m_t$ according to the discussion above. The exact definition of Λ will be discussed below. In this computation the $(e^+e^-)(e^+e^-)$ forward scattering operators do not contribute, and the resulting expressions are just the nonrelativistic expansions of full theory squared matrix elements containing the square of the double resonant diagram $e^+e^- \to t\bar{t} \to b\bar{b}W^+W^-$ (see Fig. 4a) and the interference of the double resonant diagram with the diagrams for $e^+e^- \to b\bar{b}W^+W^-$ having only either the top or the antitop in intermediate stages (see Fig. 4b and c for typical diagrams). As we show in Sec. III B, the contributions to the Wilson coefficients $\tilde{C}_{V/A}^{(n)}$ that result from $\sigma_{\rm NRQCD}^{\alpha_s=0}(\Lambda)$ are local (i.e. energy-independent) and only depend on powers of Γ_t/m_t and Λ/m_t. While $\Gamma_t/m_t \sim v^2$, which obeys the natural NRQCD counting, the Λ/m_t term is of order unity and can - as we show in Sec. III B - lead to power counting breaking contributions for insertions of operators that are higher order in the nonrelativistic expansion. However, we find that the numerical effects of the power-counting breaking contributions are very small and do not spoil the nonrelativistic expansion. This is partly due to the fact that the phase space cutoff Λ is sufficiently smaller than the convergence radius of the nonrelativistic expansion. We refer to this feature as "mild" power-counting breaking.

The remainder contribution of the inclusive cross section, $\sigma_{\rm rem}^{\alpha_s=0}(\Lambda)$ accounts for all other contributions to the full theory matrix element. This includes for example pure background $e^+e^- \to b\bar{b}W^+W^-$ diagrams, see Fig. 4d for a typical diagram, and also the square of the single-top diagrams in Figs. 4b and c. In Sec. III C we determine the remainder contribution from a numerical analysis using MadEvent [30]. We demonstrate that the remainder contribution is very small and can be neglected in view of the experimental precision expected at a future linear collider (see Sec. I). Restricting the MadEvent amplitude to the diagrams with an intermediate $t\bar{t}$ pair we also show the excellent approximation that is provided by the nonrelativistic computations in $\sigma^{\alpha_s=0}_{\rm NRQCD}$.

B. NRQCD Phase Space Matching

In this section we compute $\sigma^{\alpha_s=0}_{\rm NRQCD}$, the NRQCD cross section for $\alpha_s = 0$ with a cut ΔM_t on the invariant masses $M_{t,\bar t}$, see Eq. (34). As explained above, we treat ΔM_t and Λ as a hard scale.

Leading order diagram:

We start with the leading order NRQCD diagram to set up the notation and explain our method of computation. Technically, the least involved method to determine the form of the phase space integral and the proper normalization factors is to use the factorization theorem of Eq. (26) and apply the cutting rules on the (anti)top propagators in the NRQCD current-current correlators. After identifying the top and antitop momenta according to Eq. (33) it is then straightforward to derive the expression for the phase space integral and the phase space boundaries compatible with the invariant mass constraints.

We start from the form of the leading order current correlator

$$
\begin{aligned}
\mathcal{A}_1^{0,\alpha_s=0}(v,m_t,\nu) &= 6N_c G^0(a=0,v,m_t,\nu)\\
&= 6N_c\, i\int\frac{d^4p}{(2\pi)^4}\frac{i}{\left(\frac{E}{2}+p_0-\frac{\mathbf{p}^2}{2m_t}+i\frac{\Gamma_t}{2}\right)}\frac{i}{\left(\frac{E}{2}-p_0-\frac{\mathbf{p}^2}{2m_t}+i\frac{\Gamma_t}{2}\right)}\,. \qquad (38)
\end{aligned}
$$

It is easy to identify $p^\mu_{t,\bar t} = (m_t + E/2, 0) \pm p^\mu$ as the top and antitop four-momenta. Using the cutting rule for the unstable (anti)top propagators

$$
\frac{i}{\frac{E}{2}\pm p_0-\frac{\mathbf{p}^2}{2m_t}+i\frac{\Gamma_t}{2}} \to -2\,\mathrm{Im}\left[\frac{1}{\frac{E}{2}\pm p_0-\frac{\mathbf{p}^2}{2m_t}+i\frac{\Gamma_t}{2}}\right] \qquad (39)
$$

and recalling the form of the invariant mass constraints in the nonrelativistic limit given in Eq. (35) we obtain

$$
\begin{aligned}
\sigma^{0,\alpha_s=0}_{\rm NRQCD}(\Lambda) &= N_c\left((C^{\rm Born}_{V,1})^2+(C^{\rm Born}_{A,1})^2\right)\int_{\Delta(\Lambda)}\frac{d^4p}{(2\pi)^4}\frac{\Gamma_t}{\left(\frac{E}{2}+p_0-\frac{\mathbf{p}^2}{2m_t}+i\frac{\Gamma_t}{2}\right)\left(\frac{E}{2}+p_0-\frac{\mathbf{p}^2}{2m_t}-i\frac{\Gamma_t}{2}\right)}\\
&\quad\times\frac{\Gamma_t}{\left(\frac{E}{2}-p_0-\frac{\mathbf{p}^2}{2m_t}+i\frac{\Gamma_t}{2}\right)\left(\frac{E}{2}-p_0-\frac{\mathbf{p}^2}{2m_t}-i\frac{\Gamma_t}{2}\right)}\,, \qquad (40)
\end{aligned}
$$

where $\Delta(\Lambda)$ stands for the phase space constraint

$$
\Big|\,\frac{E}{2}\pm p_0-\frac{\mathbf{p}^2}{2m_t}\,\Big| \le \Delta M_t \qquad (41)
$$

as derived before in Eq. (35). The form of the allowed region in the $(p_0,\mathbf{p})$-plane is shown in Fig. 2 and a graphical illustration of the computation in Eq. (40) is depicted in Fig. 5. The expression in Eq. (40) agrees with the result of a full theory cross section computation

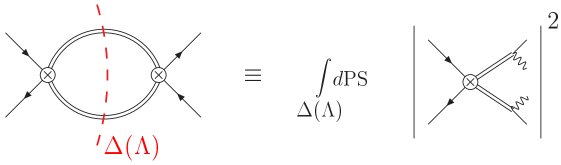

FIG. 5: Leading order diagram for the phase space matching computation. The red dashed line in the diagram on the LHS means that we cut through the (unstable) top lines and integrate over the phase space region defined by $\Delta(\Lambda)$. This is equivalent to the full theory cross section computation from the tree-level matrix element for $e^+e^- \to t\bar{t} \to b\bar{b}W^+W^-$ (shown on the RHS) in the nonrelativistic limit. The average over the electron and positron spin states is implicit.

from the tree-level matrix element for $e^+e^- \to t\bar{t} \to b\bar{b}W^+W^-$ in the nonrelativistic limit. In this computation one has to first carry out the bW^+ and $\bar{b}W^-$ phase space integrals as a function of the top and antitop invariant masses, respectively. The proper nonrelativistic limit is obtained by setting the invariant masses of the bW^+ and $\bar{b}W^-$ systems to m_t (which gives two factors of the on-shell width Γ_t) and by taking the nonrelativistic limit of all other remaining terms. Upon contraction of all indices in Dirac space and resumming the width terms into the top propagators - which is required from the counting in the double resonant kinematic region - one arrives at Eq. (40).

A more compact representation of the $t\bar{t}$ phase space integral in Eq. (40) is obtained by switching variables to the nonrelativistic invariant mass variables t_1 and t_2 defined by

$$t_{1,2} = 2m_t\Big(\frac{E}{2} \pm p_0 - \frac{\mathbf{p}^2}{2m_t}\Big)\,. \tag{42}$$

Inverting the relations gives

$$p_0 \;=\; \frac{t_1 - t_2}{4m_t}\,, \qquad \mathbf{p}^2 \;=\; Em_t - \frac{t_1 + t_2}{2}\,. \tag{43}$$

Using the Jacobian $dp_0 d^3\mathbf{p} = \pi/(2m_t) \times \sqrt{m_t E - \frac{1}{2}(t_1+t_2)}\, dt_1 dt_2$ the expression in Eq. (40) takes the form

$$\sigma^{i,\alpha_s=0}_{\rm NRQCD}(\Lambda) \;= N_c\,\big((C^{\rm Born}_{V,1})^2 + (C^{\rm Born}_{A,1})^2\big)\frac{m_t^3\Gamma_t^2}{2\pi^3}\int\limits_{\tilde{\Delta}(\Lambda)} dt_1 dt_2 \frac{\sqrt{m_t E - \frac{1}{2}(t_1+t_2)}}{(t_1^2 + m_t^2\Gamma_t^2)(t_2^2 + m_t^2\Gamma_t^2)}\,\Delta^i(t_1,t_2)\;, \tag{44}$$

with

$$\Delta^0(t_1,t_2) \;=\; 1 \quad \text{for} \quad \sigma^{0,\alpha_s=0}_{\rm NRQCD}\,. \tag{45}$$

The integration region in (t_1,t_2)-space has the form

$$\tilde{\Delta}(\Lambda) = \Big\{(t_1,t_2) \in \mathbb{R}^2 : \Big(|t_{1,2}| < \Lambda^2\Big) \wedge \Big(0 < m_t E - \frac{1}{2}(t_1+t_2)\Big)\Big\}\,, \tag{46}$$

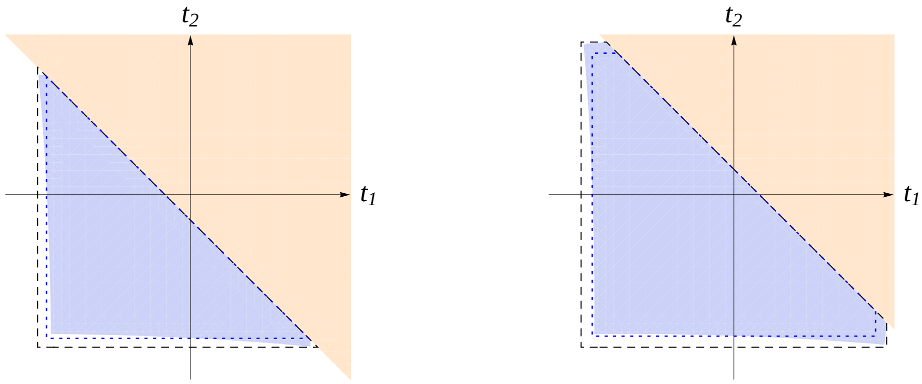

FIG. 6: Allowed phase-space region in the $t_1 - t_2$ plane. The left and right panels show the cases $E < 0$ and $E > 0$, respectively. The triangular-shaped blue shaded regions corresponds to the exact relativistic phase-space region allowed by the kinematics and the invariant mass cuts in Eq. (34). The orange region located on the upper right of each panel is forbidden since $|\mathbf{p}|$ must be real. The area inside the dashed lines corresponds to the points that pass the conditions (46). When the relativistic corrections to the cut Λ are included according to Eq. (52), the allowed region is the one indicated by the dotted lines.

where $\Lambda^2 \equiv 2m_t\Delta M_t$. In Fig. 6 the allowed region in the t_1-t_2 plane is illustrated by the area within the dotted lines for $E < 0$ (left panel) and $E > 0$ (right panel). The second condition in Eq. (46) for $t_{1,2}$ is from kinematics to ensure real values of the momentum $|\mathbf{p}| = \sqrt{m_t E - (t_1 + t_2)/2}$. Beyond the nonrelativistic approximation the relation between Λ^2 and ΔM_t receives additional relativistic corrections which are discussed below. We have to evaluate Eq. (44) in a nonrelativistic expansion for

$$m_t E\,, m_t\Gamma_t \,\sim\, m_t^2 v^2 \ll \Lambda^2\,. \tag{47}$$

To this end, we carry out an asymptotic expansion based on the four regions $(t_1, t_2) \sim (m_t^2 v^2, m_t^2 v^2)$ (double resonant), $(t_1, t_2) \sim (m_t^2 v^2, \Lambda^2)$ and $(t_1, t_2) \sim (\Lambda^2, m_t^2 v^2)$ (single resonant), and $(t_1, t_2) \sim (\Lambda^2, \Lambda^2)$ (hard). We obtain

$$\begin{aligned}\sigma^{0,\alpha_s=0}_{\rm NRQCD}(\Lambda) \,=\, & 2N_c\left((C_{V,1}^{\rm Born})^2 + (C_{A,1}^{\rm Born})^2\right)\frac{m_t^2}{4\pi}\bigg(\mathrm{Im}\,(iv) - \frac{2\sqrt{2}}{\pi}\,\frac{\Gamma_t}{\Lambda} + \frac{4+2\sqrt{2}\sinh^{-1}(1)}{3\,\pi^2}\,\frac{m_t\Gamma_t^2}{\Lambda^3} \\ & - \frac{2\sqrt{2}}{3\,\pi}\,\frac{m_t E\,\Gamma_t}{\Lambda^3} + \mathcal{O}\bigg(v^6\,\frac{m_t^5}{\Lambda^5}\bigg)\bigg)\,,\end{aligned} \tag{48}$$

where $v = \sqrt{(E + i\Gamma_t)/m_t}$. The first term in the parenthesis is the well known NRQCD Born cross section obtained from the unrestricted phase space integration. It constitutes the leading order cross section and is $\mathcal{O}(v)$, see Eq. (8) for $\alpha_s = 0$. The second term in Eq. (48) proportional to Γ_t/Λ is the dominant phase space correction and of order v^2, i.e. it contributes at NLL order. We also see terms proportional to $m_t\Gamma_t^2/\Lambda^3$ and $m_t E\Gamma_t/\Lambda^3$ which contribute at N^{3}LL order. These NLL and N^{3}LL corrections are subtracting the phase space contributions that do not pass the invariant mass constraints, represented by the white regions in Figs. 6. One may wonder why these corrections are polynomial in E and Γ_t and not a non-trivial function of E/Γ_t given that this region also has single resonant

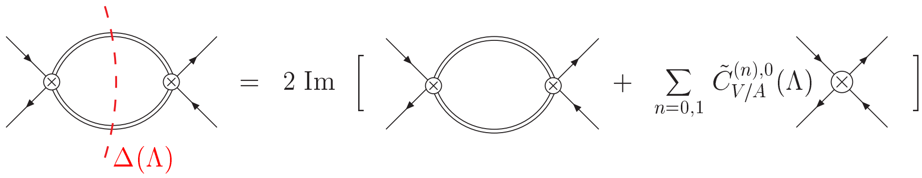

FIG. 7: One-loop renormalization condition for $\tilde{C}^{(n),0}_{V/A}(\Lambda)$.

regions where either t_1 or t_2 are resonant, i.e. of order $m_t^2 v^2$. This can be understood from the form of the integrand in Eq. (44) which shows that it is impossible to generate a nontrivial E/Γ_t dependence if $t_1 \gg t_2 \sim m_t^2 v^2$ or $t_2 \gg t_1 \sim m_t^2 v^2$. Thus the contributions that arise from the invariant mass constraints, and in fact all selection criteria that do not cut into the double resonant phase space region $(t_1, t_2) \sim (m_t^2 v^2, m_t^2 v^2)$ represent hard contributions that can be matched onto the local $(e^+e^-)(e^+e^-)$ forward scattering operators $\tilde{\mathcal{O}}^{(n)}_{V/A}$. Accounting for the form of Eq. (26) it is then straightforward to identify the contributions to the Wilson coefficients $\tilde{C}_{V/A}(\Lambda, 1)$ and $\tilde{C}^{(1)}_{V/A}(\Lambda, 1)$. A graphical illustration of the procedure is shown in Fig. 7. We obtain the results

$$\tilde{C}^{0}_{V/A}(\Lambda, 1) \;=\; 2\,i\,N_c\,\big(C^{\rm Born}_{V/A,1}\big)^2\,\frac{m_t^2}{4\pi}\,\bigg(-\,\frac{2\sqrt{2}}{\pi}\,\frac{\Gamma_t}{\Lambda} + \frac{4+2\sqrt{2}\sinh^{-1}(1)}{3\,\pi^2}\,\frac{m_t\Gamma_t^2}{\Lambda^3}\bigg)\,, \tag{49}$$

and

$$\tilde{C}^{(1),0}_{V/A}(\Lambda, 1) \;=\; -\,2\,i\,N_c\,\big(C^{\rm Born}_{V/A,1}\big)^2\,\frac{m_t^2}{4\pi}\,\frac{2\sqrt{2}}{3\,\pi}\,\frac{m_t^2\,\Gamma_t}{\Lambda^3}\,. \tag{50}$$

The coefficients $\tilde{C}^{0}_{V/A}(\Lambda, 1)$ contribute at NLL order and the $\tilde{C}^{(1),0}_{V/A}(\Lambda, 1)$ at N^{3}LL order. The superscripts "0" are a reminder that QCD corrections are neglected.

Relativistic corrections:

We now determine the phase space matching contributions from $\mathcal{O}(v^2)$ relativistic corrections to the NRQCD cross section. Since they come with one additional factor of $\mathbf{p}^2/m_t^2$, they are suppressed by v^2 according to the counting $\mathbf{p} \sim m_t v$. However, since the imposed invariant mass constraints act like a hard momentum-cutoff for the NRQCD phase space integration, power-like dependences involving the cut parameter Λ appear as a consequence of employing the nonrelativistic expansion. This occurs whenever the nonrelativistic expansion leads to integrals that are divergent for $|\mathbf{p}| \to \infty$. In effective field theory computations where a hard cutoff regularization is used, this means that once power-counting breaking occurs from the insertion of a higher dimensional operator $\mathcal{O}$, Wilson coefficients contributing to a lower order than the operator $\mathcal{O}$ might have to be modified during the matching procedure to the full theory. This happens e.g. in lattice computations and, while it is admittedly not esthetically elegant, it only represents a technical subtlety from the field theoretic point of view. For the method we use for the phase space matching, however, the occurrence of power-counting breaking terms that are numerically large could be disastrous since our method relies on the assumption that the $t\bar{t}$ phase space passing the selection cuts can be computed reliably in the nonrelativistic expansion. This restricts the size of the invariant mass cut ΔM_t we can handle within our method for the phase space matching procedure. We show in Sec. III C that for the invariant mass cuts ΔM_t between 15 and 35 GeV which we consider in this work power-counting breaking effects are very small and do not cause any problems.

There is an important relativistic effect related to the invariant mass constraint given in Eq. (41). These corrections modify the bounds on the $t_{1,2}$ integrations in Eq. (46). To determine these corrections one needs to solve the equations

$$\begin{aligned}
\Big(\frac{E}{2}+m_t\pm p_0\Big)^2-\mathbf{p}^2-\Big(m_t\mp\Delta M_t\Big)^2 &= 0\,,\\
\Big(\frac{E}{2}+m_t\pm p_0\Big)^2-\mathbf{p}^2-\Big(m_t\pm\Delta M_t\Big)^2 &= 0\,,
\end{aligned}\tag{51}$$

where $E=\sqrt{s}-2m_t$. The condition $m_tE-\frac{1}{2}(t_1+t_2)>0$ remains unchanged. The allowed phase space region in the t_1-t_2 plane accounting for all relativistic effects is illustrated by the blue shaded regions in Fig. 6. Since an exact analytic integration within the relativistic phase space boundary is not required for the precision aimed for in this work, we derive the following approximation. The main effect of accounting for the exact boundaries is a change in the lower boundaries of the $t_{1,2}$ integrations. The approximation can be made because the single resonant regions where either t_2 or t_1 are zero (*i.e.* the regions close to the negative x- or y-axes inside the blue shaded areas in Fig. 6) give the largest contributions. For the determination of the new lower boundary for the $t_{1,2}$ integration one can take, for example, the first of the relations in Eqs. (51). Switching to the t-variables and setting for example $t_2=0$, it is straightforward to find the relation

$$|t_{1,2}|\,<\,\Lambda^2\,=\,2m_t\Delta M_t-\frac{3}{4}(\Delta M_t)^2-\frac{1}{2}E\Delta M_t+\,\ldots\tag{52}$$

The associated region in the t_1-t_2 plane is indicated by the dotted lines in Fig. 6. The omitted terms in Eq. (52) indicate: (a) terms involving the energy E, which contribute beyond N^{3}LL order to the cross section and thus can be safely dropped for the range of energies E considered in our analysis, and (b) terms which give power-counting breaking contributions similar to those arising from the N^{4}LL order kinetic energy corrections, that are shown below to be numerically negligible. Apart from the neglected terms in Eq. (52), the difference between the exact relativistic phase space region (with curved boundaries) and the approximation given by the dotted lines in Fig. 6, can also be shown to yield terms beyond N^{3}LL, or terms of type (b).

The other contributions from $\mathcal{O}(v^2)$ relativistic corrections to $\sigma^{\alpha_s=0}_{\rm NRQCD}(\Lambda)$ can be cast into the form of Eq. (44), where the functions $\Delta^i(t_1, t_2)$ read

$$
\begin{aligned}
\Delta^{\mathrm{kin},0} &= -\frac{\mathbf{p}^4}{2m_t^2}\left(\frac{t_1}{t_1^2+m_t^2\Gamma_t^2}+\frac{t_2}{t_2^2+m_t^2\Gamma_t^2}\right)\,,\\
\Delta^{\mathrm{dil},0} &= \frac{\mathbf{p}^2}{m_t^2}\,\frac{m_t^4\Gamma_t^4-t_1^2t_2^2}{(t_1^2+m_t^2\Gamma_t^2)(t_2^2+m_t^2\Gamma_t^2)}\,,\\
\Delta^{v^2,0} &= \frac{2C_{V,1}^{\mathrm{Born}}C_{V,2}^{\mathrm{Born}}+2C_{A,1}^{\mathrm{Born}}C_{A,2}^{\mathrm{Born}}}{(C_{V,1}^{\mathrm{Born}})^2+(C_{A,1}^{\mathrm{Born}})^2}\,\frac{\mathbf{p}^2}{m_t^2}\,,\\
\Delta^{P\text{-wave},0} &= \frac{2}{3}\,\frac{(C_{V,3}^{\mathrm{Born}})^2+(C_{A,3}^{\mathrm{Born}})^2}{(C_{V,1}^{\mathrm{Born}})^2+(C_{A,1}^{\mathrm{Born}})^2}\,\frac{\mathbf{p}^2}{m_t^2}\,,\\
\Delta^{\mathrm{int},0} &= -\frac{C_{V,1}^{\mathrm{Born}}C_{V,1}^{\mathrm{int}}+C_{A,1}^{\mathrm{Born}}C_{A,1}^{\mathrm{int}}}{(C_{V,1}^{\mathrm{Born}})^2+(C_{A,1}^{\mathrm{Born}})^2}\,\frac{t_1+t_2}{m_t\Gamma_t}\,.
\end{aligned}
\tag{53}
$$

Here $\Delta^{\mathrm{kin},0}$ comes from the insertion of the kinetic energy correction $\mathbf{p}^4/(8m_t^3)$ and $\Delta^{\mathrm{dil},0}$ from the time dilation correction $-i\,\Gamma_t\,\mathbf{p}^2/(4m_t^2)$ contained in the quark bilinear Lagrangian Eq. (5). The term $\Delta^{v^2,0}$ comes from the insertions of the v^2-suppressed S-wave current $\mathcal{O}_{\mathbf{p},2}$ and $\Delta^{P\text{-wave},0}$ from the P-wave current $\mathcal{O}_{\mathbf{p},3}$, see Eqs. (10). Finally, the function $\Delta^{\mathrm{int},0}$ arises from interference contributions of the double resonant amplitudes $e^+e^-\to t\bar{t}\to b\bar{b}W^+W^-$ with those where only either the top or the antitop appear at intermediate stages, see Eqs. (22) and (23). Using the methods of the previous subsection to compute the corrections to the cross section with invariant mass cuts we obtain the following expressions for the contributions to the Wilson coefficients $\tilde{C}_{V/A}(\Lambda,1)$ and $\tilde{C}_{V/A}^{(1)}(\Lambda,1)$:

$$
\begin{aligned}
\tilde{C}_{V/A}^{\mathrm{kin},0}(\Lambda,1) &= 2\,i\,N_c\,\big(C_{V/A,1}^{\mathrm{Born}}\big)^2\,\frac{5m_t^2}{32\pi}\Big(\frac{9}{5\sqrt{2}\,\pi}\,\frac{\Gamma_t\Lambda}{m_t^2}+\frac{-86+105\sqrt{2}\sinh^{-1}(1)}{30\pi^2}\,\frac{\Gamma_t^2}{m_t\Lambda}\Big)\,,\\
\tilde{C}_{V/A}^{\mathrm{dil},0}(\Lambda,1) &= 2\,i\,N_c\,\big(C_{V/A,1}^{\mathrm{Born}}\big)^2\,\frac{3m_t^2}{16\pi}\Big(-\frac{2\sqrt{2}}{3\,\pi}\,\frac{\Gamma_t\Lambda}{m_t^2}+\frac{4\,(2-3\sqrt{2}\sinh^{-1}(1))}{3\,\pi^2}\,\frac{\Gamma_t^2}{m_t\Lambda}\Big)\,,\\
\tilde{C}_{V/A}^{v^2,0}(\Lambda,1) &= 2\,i\,N_c\,2\,C_{V/A,1}^{\mathrm{Born}}C_{V/A,2}^{\mathrm{Born}}\,\frac{m_t^2}{4\pi}\Big(\frac{\sqrt{2}}{\pi}\,\frac{\Gamma_t\Lambda}{m_t^2}+\frac{-2+3\sqrt{2}\sinh^{-1}(1)}{\pi^2}\,\frac{\Gamma_t^2}{m_t\Lambda}\Big)\,,\\
\tilde{C}_{V/A}^{P\text{-wave},0}(\Lambda,1) &= \frac{4}{3}\,i\,N_c\,\big(C_{V/A,3}^{\mathrm{Born}}\big)^2\,\frac{m_t^2}{4\pi}\Big(\frac{\sqrt{2}}{\pi}\,\frac{\Gamma_t\Lambda}{m_t^2}+\frac{-2+3\sqrt{2}\sinh^{-1}(1)}{\pi^2}\,\frac{\Gamma_t^2}{m_t\Lambda}\Big)\,,\\
\tilde{C}_{V/A}^{\mathrm{int},0}(\Lambda,1) &= 2\,i\,N_c\,2\,C_{V/A,1}^{\mathrm{Born}}C_{V/A,1}^{\mathrm{int}}\Big(\frac{m_t\Lambda}{2\sqrt{2}\,\pi^2}+\frac{-2+3\sqrt{2}\sinh^{-1}(1)}{4\pi^3}\,\frac{m_t^2\Gamma_t}{\Lambda}\Big)\,,
\end{aligned}
\tag{54}
$$

and

$$\tilde{C}^{(1),\mathrm{kin},0}_{V/A}(\Lambda,1) \;=\; -\,2\,i\,N_c\,\big(C^{\mathrm{Born}}_{V/A,1}\big)^2\,\frac{5m_t^2}{32\pi}\,\frac{7}{\sqrt{2}\,\pi}\,\frac{\Gamma_t}{\Lambda}\,,$$

$$\tilde{C}^{(1),\mathrm{dil},0}_{V/A}(\Lambda,1) \;=\; 2\,i\,N_c\,\big(C^{\mathrm{Born}}_{V/A,1}\big)^2\,\frac{3m_t^2}{16\pi}\,\frac{2\sqrt{2}}{\pi}\,\frac{\Gamma_t}{\Lambda}\,,$$

$$\tilde{C}^{(1),v^2,0}_{V/A}(\Lambda,1) \;=\; -2\,i\,N_c\,2\,C^{\mathrm{Born}}_{V/A,1}C^{\mathrm{Born}}_{V/A,2}\,\frac{m_t^2}{4\pi}\frac{3\sqrt{2}}{\pi}\,\frac{\Gamma_t}{\Lambda}\,,$$

$$\tilde{C}^{(1),P\text{-wave},0}_{V/A}(\Lambda,1) \;=\; -\frac{4}{3}\,i\,N_c\,\big(C^{\mathrm{Born}}_{V/A,3}\big)^2\,\frac{m_t^2}{4\pi}\,\frac{3\sqrt{2}}{\pi}\,\frac{\Gamma_t}{\Lambda}\,,$$

$$\tilde{C}^{(1),\mathrm{int},0}_{V/A}(\Lambda,1) \;=\; -2\,i\,N_c\,2\,C^{\mathrm{Born}}_{V/A,1}C^{\mathrm{int}}_{V/A,1}\frac{1}{2\sqrt{2}\pi^2}\,\frac{m_t^3}{\Lambda}\,, \tag{55}$$

where $C^{\mathrm{Born}}_{V/A,2} = -1/6\,C^{\mathrm{Born}}_{V/A,1}$. As anticipated for the results contributing to $\tilde{C}_{V/A}(\Lambda,1)$, apart from the N^{3}LL terms $\propto \Gamma_t^2/m_t^2$, there are in Eq. (54) terms $\propto \Gamma_t\Lambda/m_t$ that are power-counting breaking since they contribute at NLL order. These contributions feature a relative factor $\Lambda^2/m_t^2 = 2\Delta M_t/m_t = 0.15-0.4$ with respect to the NLL order terms in $\tilde{C}^0_{V/A}$ of Eq. (49) that come from the cross section in the nonrelativistic limit. For the interference contributions this statement also applies because $C^{\mathrm{int}}_{V/A,1} \sim C^{\mathrm{Born}}_{V/A,1}\Gamma_t/m_t$. The small size of this factor is one reason why these power-counting contributions do not spoil the quality of the nonrelativistic expansion.

For visualization we show in Fig. 8, as a function of ΔM_t, the numerical contributions to the inclusive cross section from the NLL phase space matching coefficients $\tilde{C}^0_{V/A}(\Lambda,1) + E/m_t\tilde{C}^{(1),0}_{V/A}(\Lambda,1)$ in Eqs. (49) and Eqs. (50) (red solid line), and those from the different NNLL relativistic corrections, $\tilde{C}^{i,0}_{V/A}(\Lambda,1) + E/m_t\tilde{C}^{(1),i,0}_{V/A}(\Lambda,1)$ ($i = \mathrm{kin}, \mathrm{dil}, v^2, P\text{-wave}, \mathrm{int}$) given in Eqs. (54) and (55) (blue, green, brown, magenta and cyan dashed lines, respectively). The difference of dashed lines between left and right panels illustrates the size of N^{3}LL effects in the $E/m_t\tilde{C}^{(1),i,0}_{V/A}(\Lambda,1)$ terms. Note that the various contributions have different signs and that in Fig. 8 only their absolute value is displayed. For comparison, the solid black line shows the NRQCD cross section without phase space cuts. The sum of all the contributions in Eqs. (54) and (55) is displayed as the dotted black line, which almost overlaps with the interference contributions. We see that except for the interference contributions all phase space matching corrections in Eqs. (54) are an order of magnitude smaller than those obtained from the leading order NRQCD cross section in Eq. (49). This shows that the power-counting breaking terms $\propto \Gamma_t\Lambda/m_t^2$ are small and do not spoil the nonrelativistic expansion. Interestingly, in the sum these phase space matching corrections also cancel to a large extent due to their different signs. In Fig. 8 we also see that the contributions from the interference coefficients, $\tilde{C}^{\mathrm{int},0}_{V/A}(\Lambda,1)$, are the by far largest terms that come from NNLL order relativistic insertions. For $\Delta M_t > 35$ GeV they are comparable to the contributions of $\tilde{C}^0_{V/A}(\Lambda,1)$. Since we have numerically that $2C^{\mathrm{Born}}_{V,1}C^{\mathrm{int}}_{V,1} + 2C^{\mathrm{Born}}_{A,1}C^{\mathrm{int}}_{A,1} = -4.7\,((C^{\mathrm{Born}}_{V,1})^2 + (C^{\mathrm{Born}}_{A,1})^2)\,\Gamma_t/m_t$, we see, however, that the large size of the interference terms comes from the size of the coefficients $C^{\mathrm{int}}_{V/A,1}$ and is not related to power-counting breaking effects. As far as the size of higher order relativistic corrections are concerned we thus also expect a good perturbative behavior for the interference effects.

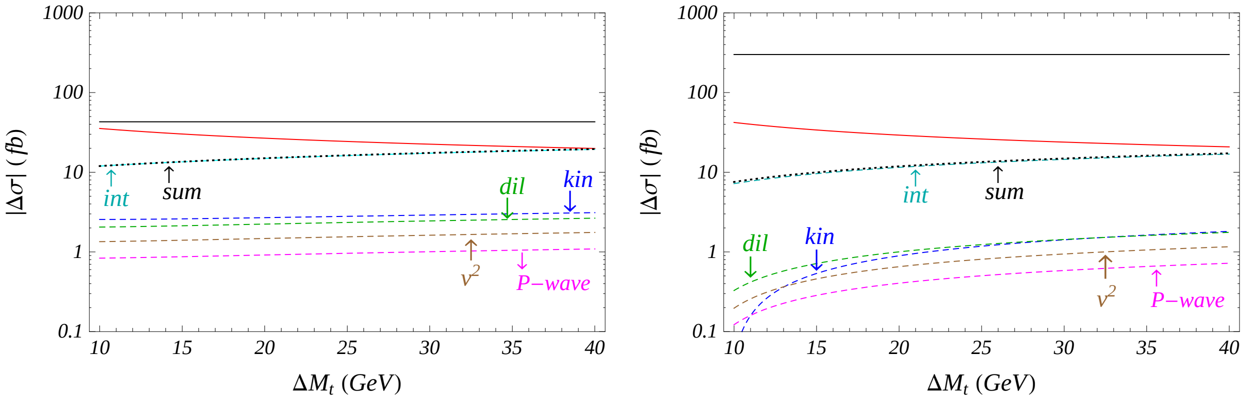

FIG. 8: Absolute values of the contributions to the inclusive cross section from the leading order diagram phase space matching coefficients, $\tilde{C}^{0}_{V/A}(\Lambda,1) + E/m_t\tilde{C}^{(1),0}_{V/A}(\Lambda,1)$, found in Eqs. (49), and (50) (red solid line), and those from the different NNLL relativistic corrections, $\tilde{C}^{i,0}_{V/A}(\Lambda,1) + E/m_t\tilde{C}^{(1),i,0}_{V/A}(\Lambda,1)$ (i = kin, dil, v^2, P-wave, int) given in Eqs. (54) and (55) (blue, green, brown, magenta and cyan dashed lines, respectively). For comparison we also display the corresponding contributions from the tree-level NRQCD cross section without phase space matching contributions, $\sigma^{0,\alpha_s=0}_{\rm NRQCD}(\Lambda=\infty) = 2N_c\,((C^{\rm Born}_{V,1})^2 + (C^{\rm Born}_{A,1})^2)\,m_t^2/(4\pi)\,{\rm Im}(iv)$ (black horizontal lines). The left panel corresponds to $E=-5$ while for the right we have $E=5$ GeV. The values chosen for the input parameters can be found in Eq. (63). We have used the energy-independent form of the coefficients $C^{\rm Born}_{V/A,i}$ and $C^{(1),\rm Born}_{V/A,i}$ ($i=1,2,3$) given by Eqs. (20).

To examine in an example the behavior of power-counting breaking effects from operator insertions beyond NNLL order we now consider the phase space matching contributions arising from the N^{4}LL order kinetic energy corrections. These emerge either from two insertions of the $\mathcal{O}(v^4)$ kinetic energy operator $\mathbf{p}^4/(8m_t)^3$ or from one insertion of the $\mathcal{O}(v^6)$ subleading kinetic energy operator $-\mathbf{p}^6/(16m_t)^5$. The respective expressions for the functions $\Delta^i(t_1,t_2)$ read

$$
\begin{aligned}
\Delta^{\rm kin,0,2\times\mathbf{p}^4/(8m_t^3)} &= \frac{\mathbf{p}^8}{32m_t^4}\left(\frac{3t_1^2-5m_t^2\Gamma_t^2}{(t_1^2+m_t^2\Gamma_t^2)^2}+\frac{3t_2^2-5m_t^2\Gamma_t^2}{(t_2^2+m_t^2\Gamma_t^2)^2}+\frac{3(t_1^2+t_2^2)+8t_1t_2+6m_t^2\Gamma_t^2}{(t_1^2+m_t^2\Gamma_t^2)(t_2^2+m_t^2\Gamma_t^2)}\right)\,,\\
\Delta^{\rm kin,0,1\times\mathbf{p}^6/(16m_t^5)} &= -\frac{\mathbf{p}^2}{2m_t^2}\Delta^{\rm kin,0}\,,
\end{aligned}
\tag{56}
$$

and the corresponding contributions to the Wilson coefficients $\tilde{C}_{V/A}(\Lambda,1)$ and $\tilde{C}^{(1)}_{V/A}(\Lambda,1)$

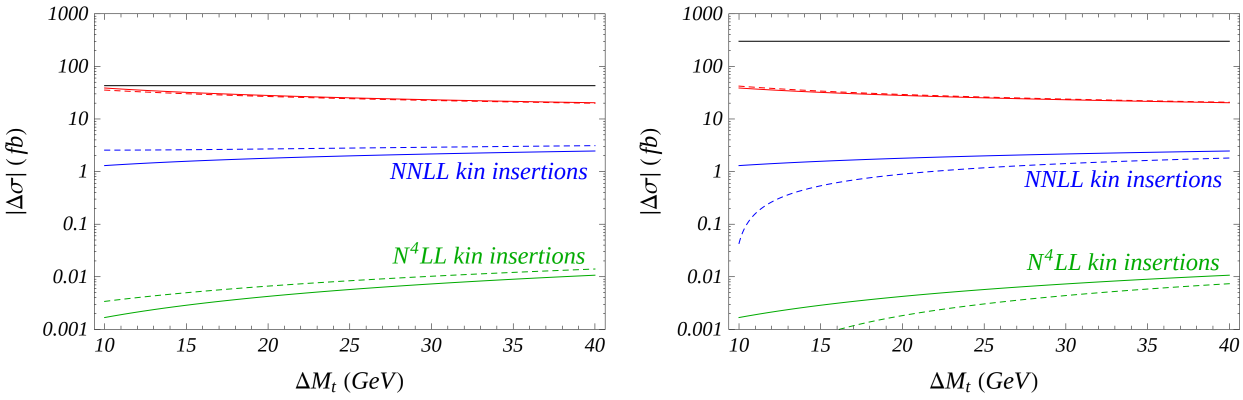

FIG. 9: Absolute values of the phase space matching contributions to the inclusive cross section from the NNLL (from Eqs. (54, 55), blue lines), and N^{4}LL insertions of the kinetic energy operators (Eq. (57, 58), green lines), as a function of ΔM_t for $E = -5$ (left panel) and 5 GeV (right panel). The solid lines show the contributions from $\tilde{C}_{V/A}(\Lambda, 1)$ and the dashed lines show the contributions for $\tilde{C}_{V/A}(\Lambda,1)+E/m_t\tilde{C}^{(1)}_{V/A}(\Lambda,1)$. For comparison we also display the corresponding contributions from the tree-level NRQCD cross section without phase space matching contributions (black horizontal lines), and the dominant phase space matching corrections from Eq. (49) and Eq. (50) (red lines). We have used the energy-independent form of the coefficients $C^{\rm Born}_{V/A,i}$ and $C^{(1),\rm Born}_{V/A,i}$ $(i = 1, 2, 3)$ given by Eqs. (20).

are

$$
\begin{aligned}
\tilde{C}^{\rm kin,[2\times \mathbf{p}^4/(8m_t^3)],0}_{V/A}(\Lambda,1) &= 2\,i\,N_c\left(C^{\rm Born}_{V/A,1}\right)^2\frac{63m_t^2}{512\pi}\bigg(\frac{53}{252\sqrt{2}\,\pi}\frac{\Gamma_t\Lambda^3}{m_t^4} \\
&\quad + \frac{5\,(754-483\sqrt{2}\sinh^{-1}(1))}{1176\pi^2}\frac{\Gamma_t^2\Lambda}{m_t^3}\bigg)\,, \\
\tilde{C}^{\rm kin,[1\times \mathbf{p}^6/(16m_t^5)],0}_{V/A}(\Lambda,1) &= 2\,i\,N_c\left(C^{\rm Born}_{V/A,1}\right)^2\frac{-7m_t^2}{64\pi}\bigg(\frac{11}{42\sqrt{2}\,\pi}\frac{\Gamma_t\Lambda^3}{m_t^4} \\
&\quad + \frac{514-315\sqrt{2}\sinh^{-1}(1)}{140\pi^2}\frac{\Gamma_t^2\Lambda}{m_t^3}\bigg)\,,
\end{aligned} \tag{57}
$$

and

$$
\begin{aligned}
\tilde{C}^{(1),[2\times \mathbf{p}^4/(8m_t^3)],0}_{V/A}(\Lambda,1) &= 2\,i\,N_c\left(C^{\rm Born}_{V/A,1}\right)^2\frac{63m_t^2}{512\pi}\,\frac{115}{28\sqrt{2}\,\pi}\frac{\Gamma_t\Lambda}{m_t^2}\,, \\
\tilde{C}^{(1),[1\times \mathbf{p}^6/(16m_t^5)],0}_{V/A}(\Lambda,1) &= -2\,i\,N_c\left(C^{\rm Born}_{V/A,1}\right)^2\frac{7m_t^2}{64\pi}\,\frac{9}{2\sqrt{2}\,\pi}\frac{\Gamma_t\Lambda}{m_t^2}\,.
\end{aligned} \tag{58}
$$

In Eqs. (57) and (58) we have displayed all terms that contribute at NLL and N^{3}LL order. They all are proportional to powers of Λ/m_t and power-counting breaking. In Fig. 9 the numerical contributions of the kinetic energy corrections to the inclusive cross section from the NNLL (from Eqs. (54, 55), blue lines) and N^{4}LL insertions (Eq. (57, 58), green lines) of the kinetic energy operators are displayed over ΔM_t for $E = -5$ and 5 GeV. The respective solid lines show the contributions to $\tilde{C}_{V/A}(\Lambda, 1)$ and the dashed lines show the contributions to $\tilde{C}_{V/A}(\Lambda, 1) + E/m_t \tilde{C}^{(1)}_{V/A}(\Lambda, 1)$. For comparison we also display the corresponding contributions from the tree-level NRQCD cross section without phase space matching contribution, $\sigma^{0,\alpha_s=0}_{\rm NRQCD}(\Lambda = \infty) = 2N_c\left((C^{\rm Born}_{V,1})^2 + (C^{\rm Born}_{A,1})^2\right) m_t^2/(4\pi)\,{\rm Re}(v)$ (black lines), and the dominant phase space matching corrections $\tilde{C}^0_{V/A}(\Lambda, 1)$ from Eq. (49) (red lines). The red dashed lines account for the energy dependent terms in Eq. (50), that also originate from the leading order diagram. The results show again that despite the existence of contributions that are power-counting breaking the numerical impact of these terms is very small. The phase space matching corrections from the NNLL kinetic energy insertions never exceed the level of a few fb and those from the N^{4}LL insertions, which are purely power-counting breaking at the order we consider, are of order 0.01 fb or smaller. Morever we see that the contributions to $\tilde{C}_{V/A}(\Lambda, 1)$ and to $E/m_t \tilde{C}^{(1)}_{V/A}(\Lambda, 1)$ coming from NNLL kinetic energy insertions are similar in size, as would be expected in the absence of power-counting breaking terms. This confirms that power-counting breaking effects are not of any concern. In particular we see that the quality of the nonrelativistic expansion is excellent and the corrections from insertions of higher dimensional relativistic operators are numerically compatible with the nonrelativistic v-counting.

C. Full Theory Analysis

In this section we analyze results for the inclusive cross section obtained from relativistic amplitudes in the full theory for $\alpha_s = 0$. In the first part we compare the NRQCD prediction using the factorization formula of Eq. (26) at NNLL order with the corresponding inclusive cross section from the full theory accounting only for the amplitude $e^+e^- \to t\bar{t} \to b\bar{b}W^+W^-$. In this case the remainder contribution $\sigma^{\alpha_s=0}_{\rm rem}(\Lambda)$ vanishes since this amplitude is fully accounted for in the usual NRQCD matrix element and matching computations. We show that the NRQCD factorization formula provides an excellent approximation to the full theory prediction for invariant mass cuts $\Delta M_t = 15$–35 GeV. We also demonstrate that the NRQCD prediction in the $\overline{\rm MS}$ scheme without the phase space matching contributions[7] overestimates by far the full theory predictions. This shows the importance of the phase space matching procedure and also explains why the NRQCD contributions turn out to be the dominant terms in the phase space matching corrections. In the second part of this section we compare the full Standard Model prediction for $e^+e^- \to b\bar{b}W^+W^-$ with invariant mass cuts with the NNLL NRQCD prediction including the NRQCD phase space matching contribution. We demonstrate that, as indicated before, the remainder cross section $\sigma^{\alpha_s=0}_{\rm rem}(\Lambda)$ is small and only amounts to at most several femptobarn. For the precision expected for threshold cross section measurements at a future linear collider the remainder contributions can therefore be safely neglected. For the full theory computations carried out in this section we use MadGraph and MadEvent [30]. At this point we note that the amplitudes generated by MadGraph are at the tree-level and use the fixed-width scheme for the top quark propagator, $i(\not{p} + m_t)/(q^2 - m_t^2 + i m_t \Gamma_t)$. This expression for the top propagator is the correct form

[7] All NRQCD predictions for top pair threshold production that can be found in the previous literature were carried out in this approximation.

in the resonance limit and compatible with the nonrelativistic expansion of NRQCD at the order we are working. We note that a discussion on invariant mass cuts for the threshold production of a W^+W^- pair in e^+e^- collisions based on full theory calculations similar to the ones given here was presented in Ref. [52]. We also refer to Refs. [53, 54].

Analysis for $e^+e^- \to t\bar{t} \to b\bar{b}W^+W^-$:

Since the amplitude for $e^+e^- \to \gamma, Z \to t\bar{t} \to b\bar{b}W^+W^-$ contains a $t\bar{t}$ intermediate state, its contribution in the $t\bar{t}$ threshold region is fully described in NRQCD. Thus as long as invariant mass cuts are applied in the region where the nonrelativistic expansion is valid, the phase space matching contributions can be computed entirely within NRQCD and the remainder contribution to the cross section, $\sigma^{\alpha_s=0}_{\rm rem}(\Lambda)$ is zero. Thus the comparison of the NRQCD prediction of the inclusive cross section with invariant mass cuts based on Eq. (26) with a fully relativistic tree-level computation based on the same amplitude serves as an important numerical check of the nonrelativistic expansion and of the NRQCD phase space matching method. In this section we carry out this check for the tree-level full theory cross section (i.e. without accounting for one-loop electroweak corrections) and at NNLL order in the nonrelativistic v-expansion. We note that the amplitude for $e^+e^- \to b\bar{b}W^+W^-$ is not gauge-invariant if one includes only the diagrams with a $t\bar{t}$ intermediate state.[8] To be definite we therefore pick the unitary gauge for all the calculations in this section.

For the relativistic calculations we employ MadGraph for the amplitude generation and MadEvent with 10^4 events to numerically compute the cross section with cuts on the top and antitop invariant masses. For the NRQCD calculation one employs the factorization formula of Eq. (26) neglecting all QCD effects from matching coefficients and potentials and the real one-loop electroweak corrections to the Wilson coefficients $C^{\rm 1loop}_{V/A,1}$ of the $(e^+e^-)(t\bar{t})$ current operators. One also needs to neglect the imaginary interference contributions $iC^{\rm int}_{V/A,1}$ to the Wilson coefficients of the $(e^+e^-)(t\bar{t})$ current operators (see Eqs. (22) and (23)) because we do not account for diagrams with either only a top or an antitop at intermediate stages. However, there are off-shell corrections to the (anti)top decay from the full theory relativistic amplitude which in the matching procedure for $iC^{\rm int}_{V/A,1}$ are related to the imaginary part of the top wave-function renormalization constant in unitary gauge. These imaginary matching contributions have the form [27]

$$
\begin{aligned}
(iC^{\rm int}_{V,1})^{Z_t,{\rm uni}} &= -i\,\frac{\alpha^2\pi|V_{tb}|^2}{32xm_t^2 s_w^4(4c_w^2-x)}\Big[3Q_eQ_ts_w^2(4-x+4x^2-9x^3+2x^4)-4Q_es_w^2(1-x^3)\\
&\qquad +3Q_ts_w^2(1+x^2-2x^3)-1+x^3\Big]\,,\\
(iC^{\rm int}_{A,1})^{Z_t,{\rm uni}} &= i\,\frac{\alpha^2\pi|V_{tb}|^2}{32xm_t^2 s_w^4(4c_w^2-x)}\Big[3Q_ts_w^2(1+x^2-2x^3)-1+x^3\Big]\,,
\end{aligned}
\tag{59}
$$

and need to be included. The resulting expression for the NRQCD cross section at NNLL

[8] In the nonrelativistic expansion the gauge-dependence of the results based only on the amplitude for $e^+e^- \to \gamma, Z \to t\bar{t} \to b\bar{b}W^+W^-$ starts at NNLL order.

order is remarkably simple and has the form

$$\begin{aligned}
\sigma^{\alpha_s=0,\mathrm{NNLL}}_{\mathrm{NRQCD,t\bar{t}}}(\Lambda) \,=\, & N_c\,\bigg(\Big(\big((C_{V,1}^{\mathrm{Born}})^2+(C_{A,1}^{\mathrm{Born}})^2\big)\Big(\frac{m_t^2}{2\pi}\mathrm{Im}(iv)-\frac{\sqrt{2}m_t^2\Gamma_t}{\pi^2\Lambda}-\frac{13\Gamma_t\Lambda}{48\sqrt{2}\pi^2}\\
& -\frac{3m_t\Gamma_t}{8\pi}\mathrm{Re}(iv)+\frac{7m_t^2}{48\pi}\mathrm{Im}(iv^3)\Big)\\
& +\big((C_{V,3}^{\mathrm{Born}})^2+(C_{A,3}^{\mathrm{Born}})^2\big)\Big(\frac{\sqrt{2}\Gamma_t\Lambda}{3\pi^2}+\frac{m_t^2}{3\pi}\mathrm{Im}(iv^3)\Big)\\
& +\big(C_{V,1}^{\mathrm{Born}}(C_{V,1}^{\mathrm{int}})^{Z_t,\mathrm{uni}}+C_{A,1}^{\mathrm{Born}}(C_{A,1}^{\mathrm{int}})^{Z_t,\mathrm{uni}}\big)\Big(\frac{\sqrt{2}m_t\Lambda}{\pi^2}+\frac{m_t^2}{\pi}\mathrm{Re}(iv)\Big)\bigg)\,, \qquad (60)
\end{aligned}$$

where the subscript $t\bar{t}$ is a reminder that for the amplitude only diagrams with a $t\bar{t}$ pair in the intermediate state are considered and where we use the s-dependent convention for the current coefficients $C^{\mathrm{Born}}_{V/A,i}$ given in Eq. (21). The corresponding LL cross section is just the well known nonrelativistic lowest order expression which does not contain phase space matching corrections

$$\sigma^{\alpha_s=0,\mathrm{LL}}_{\mathrm{NRQCD,t\bar{t}}} \,=\, 2N_c\,\big((C_{V,1}^{\mathrm{Born}})^2+(C_{A,1}^{\mathrm{Born}})^2\big)\,\frac{m_t^2}{4\pi}\,\mathrm{Im}\,(iv)\,, \qquad (61)$$

and the NLL cross section reads

$$\begin{aligned}
\sigma^{\alpha_s=0,\mathrm{NLL}}_{\mathrm{NRQCD,t\bar{t}}}(\Lambda) \,=\, & N_c\,\bigg(\big((C_{V,1}^{\mathrm{Born}})^2+(C_{A,1}^{\mathrm{Born}})^2\big)\Big(\frac{m_t^2}{2\pi}\mathrm{Im}(iv)-\frac{\sqrt{2}m_t^2\Gamma_t}{\pi^2\Lambda}-\frac{13\Gamma_t\Lambda}{48\sqrt{2}\pi^2}\Big)\\
& +\big((C_{V,3}^{\mathrm{Born}})^2+(C_{A,3}^{\mathrm{Born}})^2\big)\frac{\sqrt{2}\Gamma_t\Lambda}{3\pi^2}\\
& +\big(C_{V,1}^{\mathrm{Born}}(C_{V,1}^{\mathrm{int}})^{Z_t,\mathrm{uni}}+C_{A,1}^{\mathrm{Born}}(C_{A,1}^{\mathrm{int}})^{Z_t,\mathrm{uni}}\big)\frac{\sqrt{2}m_t\Lambda}{\pi^2}\bigg)\,. \qquad (62)
\end{aligned}$$

In the upper panels of Fig. 10 the full relativistic cross section $\sigma^{\alpha_s=0}_{t\bar{t}}(\Lambda)$ obtained from MadEvent (red lines) and the LL (lower green dotted line), NLL (blue dash-dotted lines) and NNLL order (blue dashed lines) NRQCD cross sections of Eqs. (61), (62) and (60), are shown for $\Delta M_t = 15$ (left panels) and 35 GeV (right panels). We use the following set of parameters for the computations:

$$\begin{aligned}
m_t &= 172.00\,\mathrm{GeV}\,, & \Gamma_t &= 1.4614\,\mathrm{GeV}\,,\\
M_W &= 80.419\,\mathrm{GeV}\,, & M_Z &= 91.188\,\mathrm{GeV}\,,\\
c_w &= M_W/M_Z\,, & \alpha &= 1/132.51\,. \qquad (63)
\end{aligned}$$

We see that the quality of the nonrelativistic expansion is excellent. Moreover, at the scale of the figures no differences between the full relativistic and the NNLL order NRQCD cross section are visible. The corresponding lower panels show the difference of the relativistic and the NNLL NRQCD cross section, $\Delta\sigma_{t\bar{t}}(\Lambda)=\sigma^{\alpha_s=0}_{t\bar{t}}(\Lambda)-\sigma^{\alpha_s=0,\mathrm{NNLL}}_{\mathrm{NRQCD,t\bar{t}}}(\Lambda)$, which illustrates the small size of corrections coming from beyond NNLL order in the NRQCD computation. Here the shaded bands represent the statistical uncertainty of the MadEvent integrations. (The statistical error is proportional to the cross section value and is therefore increasing for $\sqrt{s}>2m_t$.) We see that $\Delta\sigma_{t\bar{t}}(\Lambda)$ is at the level of $1-2$ fb for $\sqrt{s}<2m_t$ and compatible

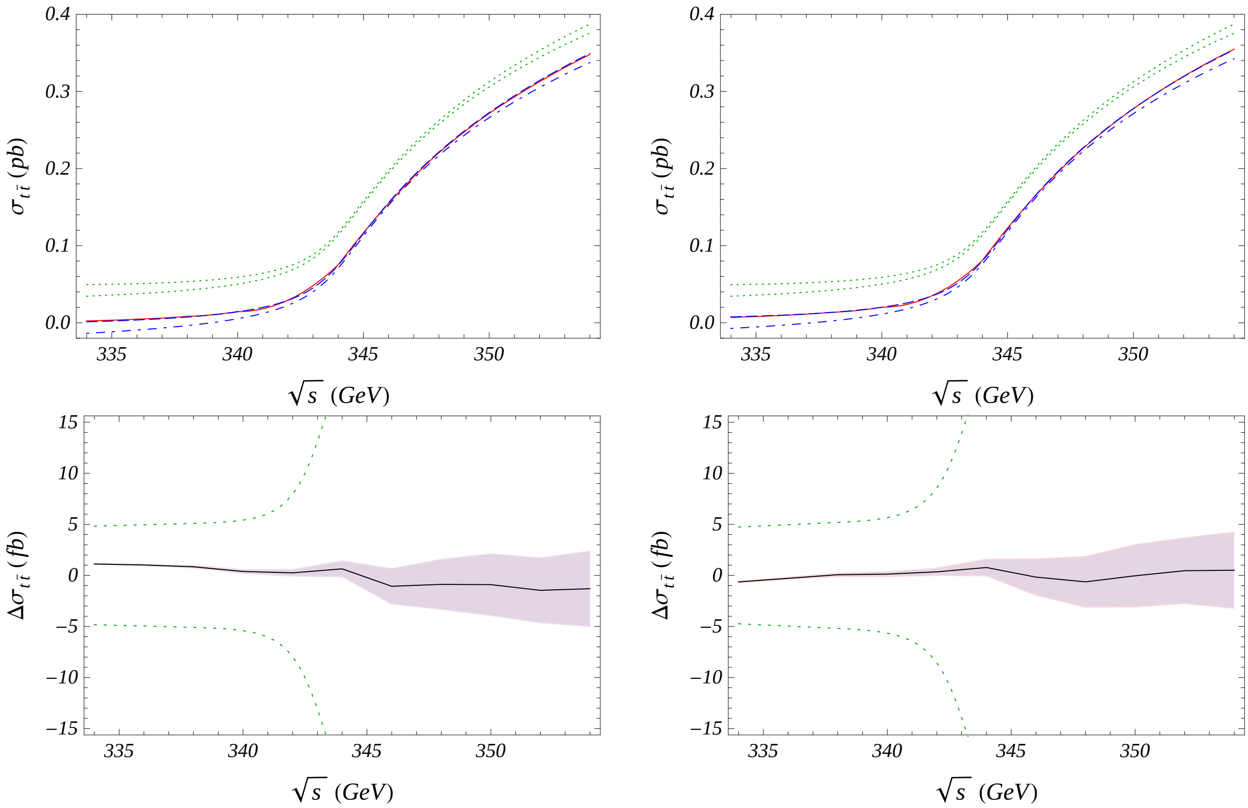

FIG. 10: Upper panels: the full relativistic cross section $\sigma_{t\bar{t}}^{\alpha_s=0}(\Lambda)$ obtained from MadEvent (red lines) and the LL (lower green dotted line), NLL (blue dash-dotted lines) and NNLL order (blue dashed lines) NRQCD cross sections. The uncut NNLL NRQCD cross section is also shown (upper green-dotted lines). Lower panels: difference of the relativistic and the NNLL NRQCD cross section (solid line), shaded bands represent the statistical uncertainty of the MadEvent integrations while the green dotted lines delimit the theoretical precision goal. We have chosen $\Delta M_t = 15$ for all panels on the left, and $\Delta M_t = 35$ GeV for those on the right.

with zero within the statistical uncertainty of the MadEvent results for $\sqrt{s} > 2m_t$. The greed dotted lines show the theoretical precision goal we have formulated in view of the experimental uncertainties expected at a future linear collider. The lines are determined from the quadratic sum of an energy-independent error of 5 fb and a 2% relative uncertainty with respect to the full NRQCD inclusive cross section prediction (including QCD effects) presented in Sec. V. Overall, we find that $\Delta\sigma_{t\bar{t}}(\Lambda)$ is much smaller than the theoretical precision goal indicated by the green dotted lines and compatible with the size of $\mathcal{O}(v^3)$ relativistic corrections. This demonstrates the excellent quality of the NRQCD phase space matching procedure we propose in this work and it should be adequate for the expected precision achievable at a future linear collider.

In the upper panels of Fig. 10 we have also shown the NNLL NRQCD cross section without the phase space matching contributions[9] (upper green dotted lines). Except for the wave

[9] For $\alpha_s = 0$ and without phase space constraints there are no NLL order corrections, and the LL and NLL

function contribution in $i(C^{\rm int}_{V/A,1})^{Z_t,\rm uni}$, which contributes less than 15 fb for the displayed energy range, this represents the approximation which has been used in all previous literature on the top pair threshold cross section where the top quark instability was accounted for by the replacement rule $E \to E + i\,\Gamma_t$. We see that without phase space matching contributions the cross section is overestimated by about $30-50$ fb at all energies. The relative discrepancy to the correct answer is particularly large for $\sqrt{s} < 2m_t$ where the predictions that only account for the complex shift $E \to E + i\Gamma_t$ do not vanish sufficiently fast. This unphysical feature is related to the fact that the top propagator of Eq. (3) leads to an overestimate of the contributions from NRQCD phase space regions with large top and antitop invariant masses. Thus the phase space matching corrections are essential to reach the intended precision goal for the theoretical predictions.

Analysis for the full amplitude $e^+e^- \to b\bar{b}W^+W^-$:

We now consider the fully relativistic Standard Model amplitude for $e^+e^- \to b\bar{b}W^+W^-$ at tree-level, $\sigma^{\alpha_s=0}(\Lambda)$. The results allow us to determine the remainder parts of the cross section, $\sigma^{\alpha_s=0}_{\rm rem}(\Lambda)$. In the upper panel of Fig. 11 the fully relativistic cross section $\sigma^{\alpha_s=0}(\Lambda)$ obtained from MadEvent (red line) and the NNLL order NRQCD cross section $\sigma^{\alpha_s=0,\rm NNLL}_{\rm NRQCD,t\bar{t}}(\Lambda)$ (blue dashed lines) are shown for $\Delta M_t = 15$ (left panels) and 35 GeV (right panels), where the parameter set of Eq. (63) has been employed and 10^4 events have been used for integrations. The analytic formula for $\sigma^{\alpha_s=0,\rm NNLL}_{\rm NRQCD,t\bar{t}}(\Lambda)$ is just Eq. (60) with the electroweak top wave function contributions $(iC^{\rm int}_{V/A,1})^{Z_t,\rm uni}$ being replaced by the full interference coefficients $iC^{\rm int}_{V/A,1}$ from Eqs. (22) and (23). Up to relativistic corrections beyond NNLL order, which we neglect in the following discussion, the difference between the relativistic and the NNLL order NRQCD results is just $\sigma^{\alpha_s=0}_{\rm rem}(\Lambda)$, which we use to determine the remainder contributions to the phase space matching coefficients $\tilde{C}^0_{V/A}(\Lambda)$ and $\tilde{C}^{(1),0}_{V/A}(\Lambda)$. For the invariant mass cuts $\Delta M_t = 15$ and 35 GeV $\sigma^{\alpha_s=0}_{\rm rem}(\Lambda)$ is displayed in fb units in the middle panel of Fig. 11. The shaded region represents the statistical uncertainties of the MadEvent computation. For $\Delta M_t = 35$ GeV $\sigma^{\alpha_s=0}_{\rm rem}(\Lambda)$ ranges from 0 to 5 fb and increases with the c.m. energy. For $\Delta M_t = 15$ GeV it is almost energy-independent and below 1 fb for $\sqrt{s} < 2m_t$ and compatible with zero within the statistical MadEvent errors for $\sqrt{s} > 2m_t$. The results are fully consistent with a linear dependence in E, which confirms the structure and NRQCD counting of the $(e^+e^-)(e^+e^-)$ forward scattering operators. Overall, the size of the remainder contributions is much smaller than the theoretical precision goal explained above and indicated by the green dotted lines. So the remainder part can be neglected for the theoretical predictions. With Eq. (26) it is straightforward to fit for the remainder contributions to the phase space matching coefficients $\tilde{C}^0_{V/A}$ and $\tilde{C}^{(1),0}_{V/A}$. We use an analysis for $\Delta M_t = 15, 20, 25, 30$ and 35 GeV, and assuming a linear dependence on ΔM_t the result of this fit reads

$$\begin{aligned}
\Big(\tilde{C}^0_V(\Lambda) + \tilde{C}^0_A(\Lambda)\Big)^{\rm rem} &= i\left[(-1.2 \pm 0.9)\,\text{fb} \,+\, (28 \pm 6)\frac{\Delta M_t}{m_t}\,\text{fb}\right], \\
\Big(\tilde{C}^{(1),0}_V(\Lambda) + \tilde{C}^{(1),0}_A(\Lambda)\Big)^{\rm rem} &= i\left[(-14 \pm 25)\,\text{fb} \,+\, (260 \pm 170)\,\frac{\Delta M_t}{m_t}\,\text{fb}\right]. \qquad (64)
\end{aligned}$$

NRQCD cross sections agree.

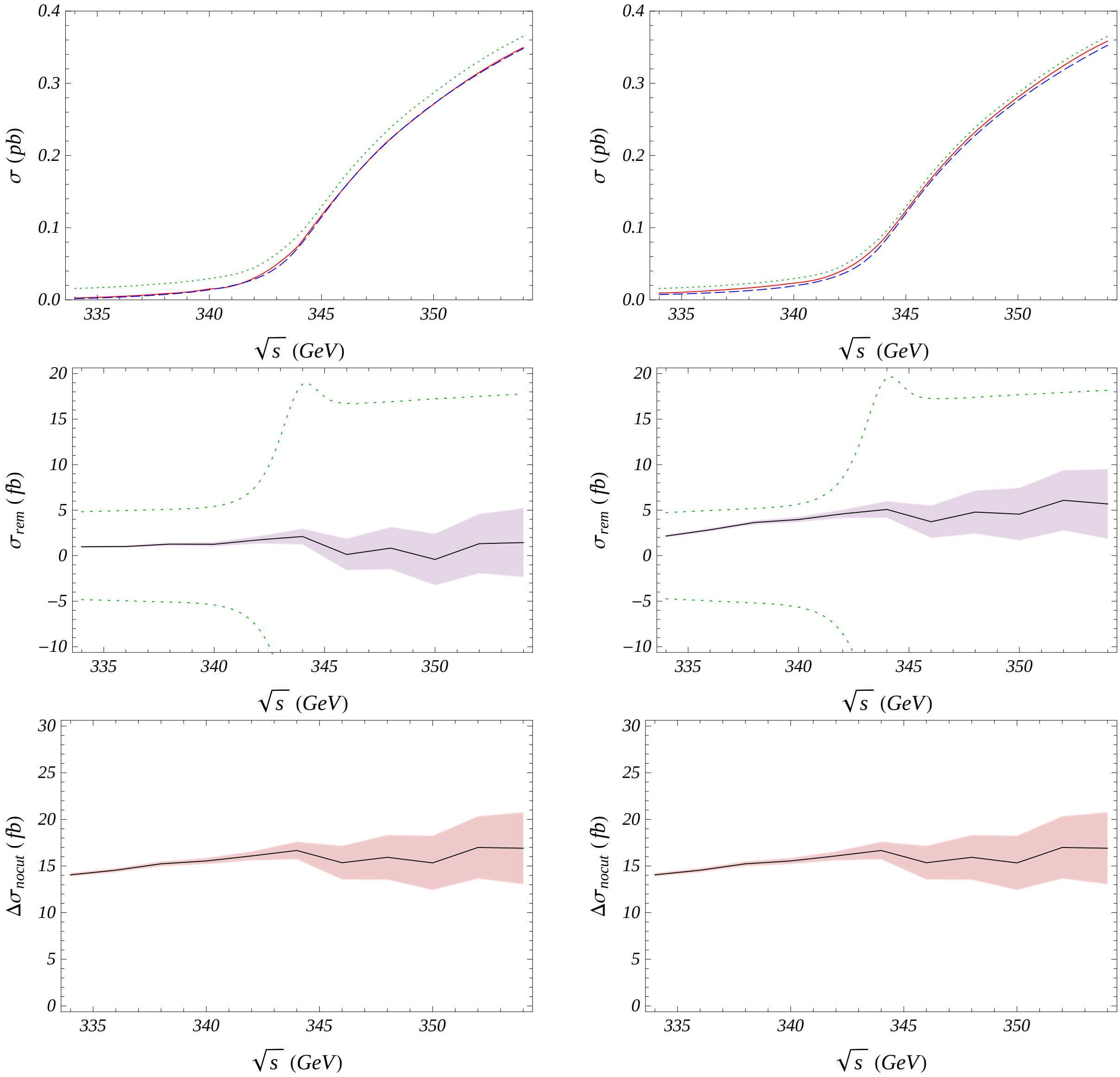

FIG. 11: Upper panel: fully relativistic $b\bar{b}W^+W^-$ cross section $\sigma^{\alpha_s=0}(\Lambda)$ obtained from MadEvent with cut (red line) and without cut (green dotted lines), and NNLL order NRQCD cross section $\sigma^{\alpha_s=0,\mathrm{NNLL}}_{\mathrm{NRQCD,t\bar{t}}}(\Lambda)$ (blue dashed lines). Middle panel: $\sigma^{\alpha_s=0}_{\mathrm{rem}}(\Lambda)$ in fb units with the statistical uncertainties of the MadEvent computation (shaded region), and the theoretical precision goal (green dotted lines). Lower panel: $\Delta\sigma_{\mathrm{nocut}}(\Lambda) = \sigma^{\alpha_s=0}_{\mathrm{nocut}} - \sigma^{\alpha_s=0,\mathrm{NNLL}}_{\mathrm{NRQCD}}(\Lambda)$ (black solid lines), and the statistical uncertainties from MadEvent (shaded regions). We have chosen $\Delta M_t = 15$ for all panels on the left, and $\Delta M_t = 35$ GeV for those on the right.

For the fit we added an energy-independent error of 1 fb to $\sigma^{\alpha_s=0}_{\mathrm{rem}}(\Lambda)$ to account for higher order relativistic corrections $\propto (E/m_t)^n$ with $n > 1$.

Total cross section without cuts:

Rather than predicting the inclusive cross section with cuts on the (anti)top invariant masses it is also natural to ask about the total cross section for the case that no such cuts are applied on the $b\bar{b}W^+W^-$ final state. The phase space matching concept can be also applied in this case since the difference between the full theory phase space for the cases with and without invariant mass cuts constitutes again a hard NRQCD effect, much like the difference between applying cuts of different sizes. This can be easily understood because even without invariant mass cuts the phase space is constrained by kinematic bounds that in the $t\bar{t}$ threshold region ($\sqrt{s} \approx 2m_t$) also represent hard scales of order m_t. In the upper panels of Fig. 11 the green dotted lines represent the full theory $b\bar{b}W^+W^-$ cross section without any cuts from MadEvent. The difference $\Delta\sigma_{\rm nocut}(\Lambda) = \sigma^{\alpha=0}_{\rm nocut} - \sigma^{\alpha_s=0,{\rm NNLL}}_{\rm NRQCD}(\Lambda)$ is displayed by the black solid lines in the lowest panels of Fig. 11 for $\Delta M_t = 15$ (left) and 35 GeV (right). In the figure the statistical uncertainties from MadEvent are again represented by the gray shaded regions. In contrast to predictions for the cross section with invariant mass cuts, here, Λ acts simply as a UV cutoff for the NRQCD phase space integration. Since the cross section is independent of the cutoff Λ, $\Delta\sigma_{\rm nocut}(\Lambda)$ just compensates the Λ-dependence of the NRQCD cross section. Applying the same fitting procedure as for Eq. (64) we obtain the following results for the remainder contributions to the phase space matching coefficients $\tilde{C}^0_{V/A}$ and $\tilde{C}^{(1),0}_{V/A}$:

$$\begin{aligned}
\Big(\tilde{C}^0_V(\infty) + \tilde{C}^0_A(\infty)\Big)^{\rm rem} &= i\left[(-18.9 \pm 0.9)\,{\rm fb} + (-42 \pm 6)\frac{\Delta M_t}{m_t}\,{\rm fb}\right], \\
\Big(\tilde{C}^{(1),0}_V(\infty) + \tilde{C}^{(1),0}_A(\infty)\Big)^{\rm rem} &= i\left[(21 \pm 26)\,{\rm fb} + (90 \pm 170)\,\frac{\Delta M_t}{m_t}\,{\rm fb}\right]. \qquad (65)
\end{aligned}$$

Although we do not need the phase space matching coefficients $\tilde{C}^0_{V/A}(\infty)$ and $\tilde{C}^{(1),0}_{V/A}(\infty)$ for the predictions intended in this work, we give the results for future reference.

IV. PHASE SPACE MATCHING WITH QCD EFFECTS

In the previous sections we have discussed the concepts of the phase space matching procedure and computed the phase space matching coefficients neglecting QCD effects. We have demonstrated that the phase space matching coefficients can be reliably computed within NRQCD and that the remainder contributions which contain all effects that need the evaluation of full theory diagrams are small. For the precision goal we need to achieve, these remainder contributions can be neglected. We have also shown that for invariant mass cuts $\Delta M_t = 15$–35 GeV, power-counting breaking terms that arise from insertions of higher order relativistic operators do not spoil the nonrelativistic expansion.

In this section we extend the phase space matching procedure to account for QCD corrections. Due to the additional QCD-induced interactions the required operator structure is more complicated. Up to NNLL order only the $(e^+e^-)(e^+e^-)$ forward scattering operators already discussed in the previous sections are required. At N^{3}LL order we also need to account for imaginary phase space matching contributions to the Wilson coefficients of the $(e^+e^-)(t\bar{t})$ top pair production operators to account for non-analytic energy-dependent terms in the matching relations. As for the previous sections we compute the phase space matching coefficients within NRQCD. Since for $\alpha_s = 0$ we found the remainder contributions to the coefficients to be negligible and since no kinematic or dynamical enhancement is expected for the QCD corrections, we ignore the QCD corrections to the remainder contributions in our analysis. For the determination of the QCD corrections we have to account

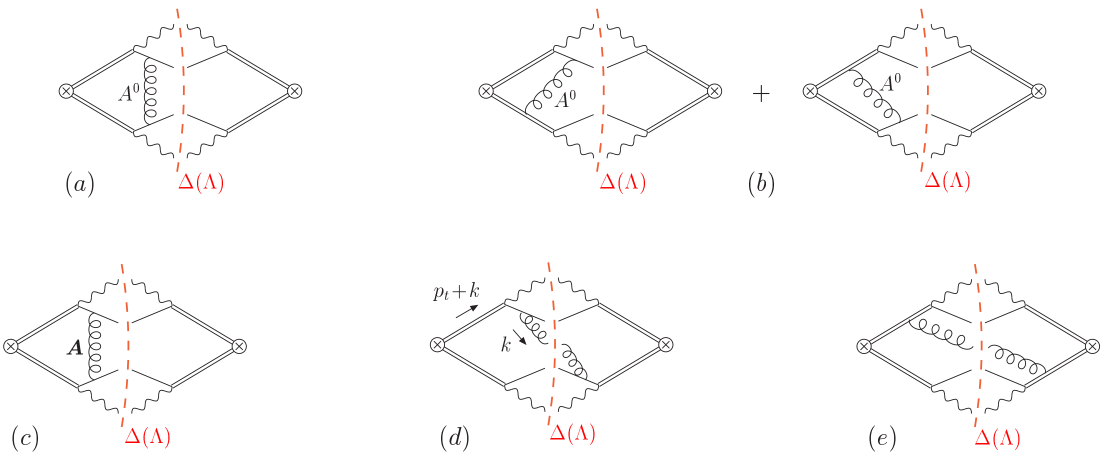

FIG. 12: $\mathcal{O}(\alpha_s)$ QCD radiative corrections to $e^+e^- \to \bar{t}t \to bW^-\bar{b}W^+$ originating from (a) time-like gluon exchange between $b\bar{b}$-quarks, (b) time-like gluon exchange between $t\bar{b}$ and $\bar{t}b$-quarks, (c) space-like gluon exchange between $b\bar{b}$, and (d) interference between gluon radiation from b and $\bar{b}$. Contribution (e) involving gluon radiation off the nonrelativistic top/antitop lines is suppressed with respect to the previous ones. The conjugated diagrams have to be added for each case. The definition of the top momenta p_t in terms of the nonrelativistic momenta can be found in Fig. 2.

for the QCD potentials and for the exchange of ultrasoft gluons among the top and antitop quarks and their decay products. Both types of corrections are analyzed in the following subsections.

A. Ultrasoft Gluon Exchange and Nonperturbative Effects

In the threshold region ultrasoft gluons, which carry momenta of order $m_t v^2 \sim \Gamma_t$, can propagate and lead to interactions among the top and the antitop quark and their decay products. These ultrasoft interactions are sometimes called "QCD interference effects" since the corresponding Feynman diagrams and their interference contributions all have comparable numerical size. The exchange of ultrasoft gluons starts to contribute at NLL order; the relevant diagrams at $\mathcal{O}(\alpha_s)$ in Coulomb gauge are displayed in Fig. 12. It is known that the QCD interference effects cancel in the total cross section at NLL [55, 56] and NNLL order [27] if no cuts are imposed on the NRQCD phase space. Some of the interference effects have shown to cancel at NLL also for other inclusive observables where the top energy is integrated out, for example for the top quark three-momentum distribution [57]. For the top and antitop invariant masses M_t and $M_{\bar{t}}$, on the other hand, the effects of ultrasoft gluon exchange are essential because they directly affect the form of the distribution. The invariant mass distribution is further affected - at leading order - by nonperturbative effects. The precise way how both effects enter the distribution depends on the details of the reconstruction prescription, see Refs. [49, 50] for a detailed treatment at large c.m. energies $\sqrt{s} \gg 2m_t$. The situation is, however, considerably simpler for the predictions of the inclusive cross section with the invariant mass cuts of Eq. (4) for $\Delta M_t \gg \Gamma_t$. Because the inclusive cross section is an integral over M_t and $M_{\bar{t}}$ in the resonance region, the main effects of the ultrasoft gluon exchange and of the nonperturbative contributions effectively correspond to a shift in ΔM_t

of order Γ_t and $\Lambda_{\rm QCD}$, respectively. This allows us to estimate that the size of the ultrasoft and the nonperturbative corrections to the phase space matching coefficients are of order $\alpha_s m_t\Gamma_t\Lambda^2$ and $m_t\Lambda_{\rm QCD}/\Lambda^2$, respectively, with respect to the dominant NLL contributions of Eq. (49), which are proportional to Γ_t/Λ. The form of the nonperturbative corrections can also be understood from the point of view that there is an operator product expansion for the inclusive cross section. For the estimate for the ultrasoft gluons we have included a factor of α_s from the coupling of the gluon to the quarks. With $\Lambda_{\rm QCD}\approx\alpha_s\Gamma_t$ and $\Lambda\sim m_t$ both effects represent N^{4}LL corrections and are beyond the N^{3}LL order level we consider in this work. Numerically they are suppressed by two orders of magnitude with respect to the NLL order phase space matching contributions. To confirm our argumentation for the ultrasoft corrections we explicitly compute in the appendix the phase space matching corrections to the $(e^+e^-)(e^+e^-)$ forward scattering operators that arise from the diagrams in Fig. 12. We use the invariant mass definition of Eq. (33) and assume that the ultrasoft gluon can be resolved. While being not entirely realistic from the experimental point of view, this prescriptions should nevertheless give the typical size of the ultrasoft corrections. As shown in the appendix, we find that the ultrasoft phase space matching corrections indeed have the scaling behavior estimated above. In addition, they have a strong numerical suppression that make them irrelevant. For the rest of this paper we therefore ignore ultrasoft and nonperturbative phase space matching corrections.

B. Potential Interactions

We now consider the phase space matching corrections originating from the potential interactions. Since the phase space matching procedure shares the properties of common loop graph matching computations, we find that once loop diagrams are involved, we also have to carry out phase space matching for subdiagrams in order to obtain local results for the matching coefficients.

We start with the $\mathcal{O}(\alpha_s)$ contribution to the NRQCD cross section that arises from the insertion of one Coulomb potential. The diagrams to be considered are depicted on the LHS of the equality shown in Fig. 13. Following the approach of Sec. III B, the result can be cast into the form

$$\sigma^{i,\mathcal{O}(\alpha_s)}_{\rm NRQCD} = N_c\left((C^{\rm Born}_{V,1})^2+(C^{\rm Born}_{A,1})^2\right)\frac{m_t^3\Gamma_t^2}{2\pi^3}\int\limits_{\tilde\Delta(\Lambda)} dt_1dt_2\frac{\sqrt{m_tE-\frac{1}{2}(t_1+t_2)}}{(t_1^2+m_t^2\Gamma_t^2)(t_2^2+m_t^2\Gamma_t^2)}\,\Delta^i(t_1,t_2)\,+\,\text{c.c.}\,, \tag{66}$$

where in comparison to Eq. (44) we have to add the complex conjugate expressions because the computation involves a loop subgraph either to the left or to the right of the cut. For the Coulomb potential it is straightforward to derive

$$\Delta^1(t_1,t_2)\,=\,\mathcal{D}\bigg(\sqrt{m_tE-\frac{t_1+t_2}{2}}\bigg)\,, \tag{67}$$

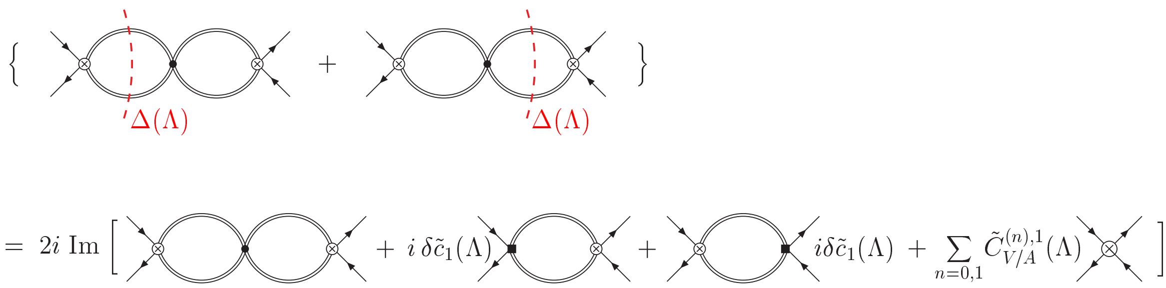

FIG. 13: $\mathcal{O}(\alpha_s)$ matching condition for the Wilson coefficients of e^+e^- forward scattering operators.

where ($q = |\mathbf{q}|$, $\mathcal{V}_c^{(s)} = -4\pi C_F \alpha_s \equiv -4\pi a$)

$$\begin{aligned}\mathcal{D}(q) &= \tilde{\mu}^{2\epsilon} \int \frac{d^d\mathbf{r}}{(2\pi)^d} \frac{i}{\frac{E}{2} + r_0 - \frac{\mathbf{r}^2}{2m_t} + i\frac{\Gamma_t}{2}} \frac{i}{\frac{E}{2} - r_0 - \frac{\mathbf{r}^2}{2m_t} + i\frac{\Gamma_t}{2}} \frac{-i\,\mathcal{V}_c^{(s)}}{(\mathbf{r}-\mathbf{q})^2} \\ &= i\,a\,\frac{m_t}{2q}\,\ln\frac{m_t v + q}{m_t v - q}\,. \end{aligned} \tag{68}$$

The term $\mathcal{D}$ is just the vertex diagram for $t\bar{t}$ production with one insertion of the Coulomb potential. Using Eq. (46) for the boundaries of the phase space integration we obtain the result

$$\begin{aligned}\sigma^{i,\mathcal{O}(\alpha_s)}_{\rm NRQCD} =& \,2\,N_c\left((C^{\rm Born}_{V,1})^2 + (C^{\rm Born}_{A,1})^2\right)\frac{m_t^2}{4\pi}\,a\,\bigg[-\,{\rm Im}\big[\ln(-i\,v)\big] - 2\frac{m_t\Gamma_t}{\Lambda^2} \\ & - \frac{8\sqrt{2}}{3\pi}\,\frac{m_t^2\Gamma_t}{\Lambda^3}\,{\rm Re}\big[\,i\,v\,\big] + \mathcal{O}\left(v^4\frac{m_t^4}{\Lambda^4}\right)\bigg]\,. \end{aligned} \tag{69}$$

$\mathcal{O}(\alpha_s)$ Matching for the forward scattering operators:

The first Λ-independent and non-analytic term in the brackets in Eq. (69) is from the well known $\mathcal{O}(\alpha_s)$ contribution of the nonrelativistic Coulomb Green function, which contributes to the LL NRQCD cross section without cuts, see Eq. (8). The second term $\propto \alpha_s m_t\Gamma_t/\Lambda^2$ is local and contributes at NNLL order. Through the phase space matching procedure using Eq. (26), the second term contributes to the imaginary Wilson coefficient $\tilde{C}_{V/A}$ of the $(e^+e^-)(e^+e^-)$ forward scattering operators $\tilde{\mathcal{O}}_{V/A}$. The result reads

$$\tilde{C}^1_{V/A}(\Lambda) = 2\,i\,N_c\left(C^{\rm Born}_{V/A,1}\right)^2\frac{m_t^2}{4\pi}\left[-\,2\,a\,\frac{m_t\Gamma_t}{\Lambda^2}\right], \tag{70}$$

and constitutes an $\mathcal{O}(\alpha_s)$ correction to the NLL matching contributions of Eq. (49). The determination of the $\mathcal{O}(\alpha_s)$ contributions to $\tilde{C}^1_{V/A}$ arising from insertions of higher-dimension operators and potentials describing relativistic v^2-corrections is carried out in analogy. Here we just quote the final results and refer to Ref. [29] for details:

$$
\begin{aligned}
\tilde{C}^{r,1}_{V/A}(\Lambda) &= 2\,i\,N_c\left(C^{\rm Born}_{V/A,1}\right)^2\frac{m_t^2}{4\pi}\left[-a\left(\ln\frac{m_t}{\Lambda}+\frac{1}{2}+\frac{1}{2}\ln 2\right)\frac{\Gamma_t}{m_t}\right]\,,\\
\tilde{C}^{s,1}_{V/A}(\Lambda) &= 0\,,\\
\tilde{C}^{\rm kin,1}_{V/A}(\Lambda) &= 2\,i\,N_c\left(C^{\rm Born}_{V/A,1}\right)^2\frac{m_t^2}{4\pi}\left[-a\left(\ln\frac{m_t}{\Lambda}+\frac{3}{8}+\frac{1}{2}\ln 2\right)\frac{\Gamma_t}{m_t}\right]\,,\\
\tilde{C}^{\rm dil,1}_{V/A}(\Lambda) &= 2\,i\,N_c\left(C^{\rm Born}_{V/A,1}\right)^2\frac{m_t^2}{4\pi}\left[a\left(\ln\frac{m_t}{\Lambda}+\frac{1}{2}+\frac{1}{2}\ln 2\right)\frac{\Gamma_t}{m_t}\right]\,,\\
\tilde{C}^{v^2,1}_{V/A}(\Lambda) &= 2\,i\,N_c\,2C^{\rm Born}_{V/A,1}C^{\rm Born}_{V/A,2}\,\frac{m_t^2}{4\pi}\left[-a\left(\ln\frac{m_t}{\Lambda}+\frac{1}{2}+\frac{1}{2}\ln 2\right)\frac{\Gamma_t}{m_t}\right]\,,\\
\tilde{C}^{P\text{-wave},1}_{V/A}(\Lambda) &= \frac{4}{3}\,i\,N_c\,\left(C^{\rm Born}_{V/A,3}\right)^2\frac{m_t^2}{4\pi}\left[-a\left(\ln\frac{m_t}{\Lambda}+\frac{2}{3}+\frac{1}{2}\ln 2\right)\frac{\Gamma_t}{m_t}\right]\,,\\
\tilde{C}^{\rm int,1}_{V/A}(\Lambda) &= 2\,i\,N_c\,2\,C^{\rm Born}_{V/A,1}C^{\rm int}_{V/A,1}\,\frac{m_t^2}{4\pi}\left[-a\left(\ln\frac{m_t}{\Lambda}+\frac{1}{2}+\frac{1}{2}\ln 2\right)\right]\,,
\end{aligned}
\tag{71}
$$

where the definitions of the coefficients $C^{\rm Born}_{V/A,i}$ are given in Eqs. (20) and (21). The coefficients $\tilde{C}^{r,1}_{V/A}$ and $\tilde{C}^{s,1}_{V/A}$ come from one insertion of the potentials ($\mathbf{k}=\mathbf{p}-\mathbf{p}'$)

$$
\frac{\mathcal{V}_r^{(s)}(\mathbf{p}^2+\mathbf{p}'^2)}{2m_t^2\mathbf{k}^2}\quad\text{and}\quad\frac{\mathcal{V}_s^{(s)}}{m_t^2}\,,
\tag{72}
$$

where we used $\mathcal{V}_r^{(s)}(\nu=1)=-4\pi a$ and $\mathcal{V}_s^{(s)}(\nu=1)=4\pi a/3$, respectively. The origin of the other coefficients arises from insertions of the kinetic energy correction (kin), the time dilation correction (dil), the v^2-suppressed S-wave current $\mathcal{O}_{\mathbf{p},2}$ (v^2), the P-wave current $\mathcal{O}_{\mathbf{p},3}$ (P-wave) and the interference coefficient (int), as explained already after Eq. (53). The spin-dependent, momentum-independent potential $\mathcal{V}_s^{(s)}/m_t^2$ does not lead to a contribution at the order we consider.[10] In analogy to our examinations for $\alpha_s=0$ we find that the phase space matching contributions originating from the relativistic insertions also contribute at NNLL order and are power-counting breaking. They also feature a relative factor Λ^2/m_t^2 with respect to the terms in $\tilde{C}^{1}_{V/A}(\Lambda)$ of Eq. (70). Through the numerical analysis of the $\tilde{C}^{i,1}_{V/A}(\Lambda)$ coefficients which we carry out in Fig. 14, we find a similar situation as for the case of the corresponding tree-level matching coefficients $\tilde{C}^{i,0}_{V/A}(\Lambda)$ studied in Sec. III B: The phase space matching contributions in $\tilde{C}^{1}_{V/A}(\Lambda)$ of Eq. (70) are about an order of magnitude larger than the ones from the relativistic corrections in Eqs. (71), which also cancel each other

[10] Since the potential $\mathcal{V}_s^{(s)}/m_t^2$ is momentum-independent, its insertion leads to a factorized expression for the correction to the Green function that can only contribute to the phase space matching coefficient $\delta\tilde{c}_1^{s,1}$ of the S-wave $t\bar{t}$ current discussed in the following subsection.

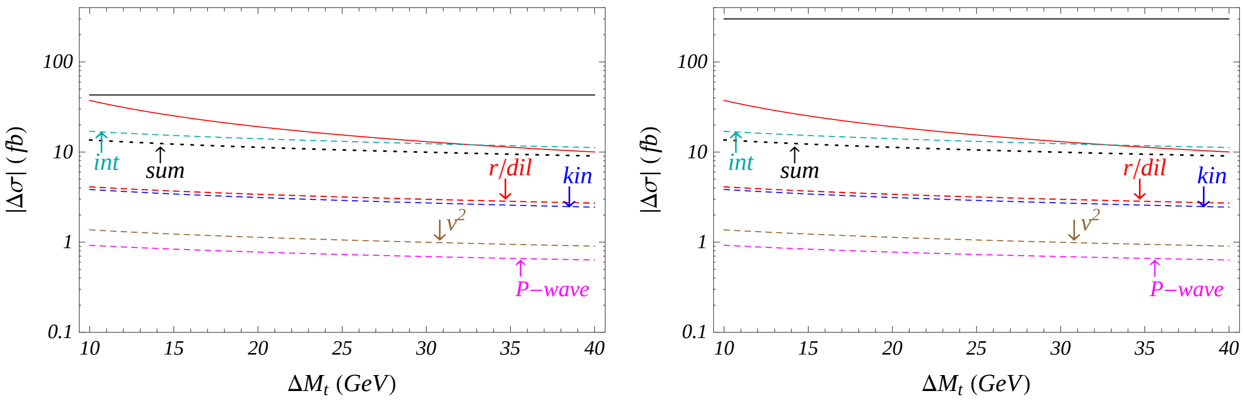

FIG. 14: Absolute values of the contributions to the inclusive cross section from the $\mathcal{O}(\alpha_s)$ phase space matching corrections $\tilde{C}^{1}_{V/A}(\Lambda)$ of Eq. (70) (red lines) and $\tilde{C}^{i,1}_{V/A}(\Lambda)$, $i = \mathrm{r/dil}, \mathrm{kin}, v^2, P\text{-wave}, \mathrm{int}$ (red,blue, brown, magenta and cyan dashed lines, respectively), listed in Eq. (71). The sum of the $\tilde{C}^{i,1}_{V/A}(\Lambda)$ contributions is shown as the dotted black line. For comparison we also display the tree-level NRQCD cross section without phase space matching contributions (black lines). The left panel corresponds to $E = -5$ while for the right $E = 5$ GeV. The values chosen for the input parameters can be found in Eq. (63), and $\alpha_s = 0.1077$. We have used the energy-independent form of the coefficients $C^{\mathrm{Born}}_{V/A,i}$ and $C^{(1),\mathrm{Born}}_{V/A,i}$ ($i = 1, 2, 3$) given by Eqs. (20).

partly due to their different signs. The cancellation is, however, less effective as for $\alpha_s = 0$ due to the additional contribution coming from the $\mathcal{V}_r$ potential. Again, this does not apply to the contributions from the interference corrections in $\tilde{C}^{\mathrm{int},1}_{V/A}(\Lambda)$, which are comparable to $\tilde{C}^{1}_{V/A}(\Lambda)$ for $\Delta M_t \gtrsim 25$ GeV. As explained in Sec. III B before, this behavior is related to the large size of the interference coefficients $C^{\mathrm{int}}_{V/A,1}$ and not to power-counting breaking effects. As far as the size of higher order relativistic corrections are concerned we thus also find a good perturbative behavior for the $\mathcal{O}(\alpha_s)$ corrections to the phase space matching coefficients $\tilde{C}_{V/A}(\Lambda)$.

$\mathcal{O}(\alpha_s)$ Matching for the $t\bar{t}$ currents:

Let us now discuss the third term in the brackets on the RHS of Eq. (69) which is $\propto \mathrm{Re}[iv]$. It is non-analytic in the energy and can therefore not contribute to the phase space matching coefficients of the $(e^+e^-)(e^+e^-)$ forward scattering operators $\tilde{\mathcal{O}}^{(n)}_{V/A}$. This term contributes at N^{3}LL order and is also of theoretical interest as it illustrates how the phase space matching procedure is carried out at higher orders. We recall that the phase space matching follows the common rules of matching computations, where the matching involving diagrams with a higher number of loops first requires the matching of operators relevant for subdiagrams in order to deal with all terms that are non-analytic in the external momenta. To deal with the non-analytic term $\propto \mathrm{Re}[iv]$ in Eq. (69) we need to determine the imaginary phase space matching term $i\,\delta\tilde{c}_1(\Lambda)$ contained in the Wilson coefficient $C_{V/A,1}$ of the dominant S-wave $t\bar{t}$ current operators $\mathcal{O}_{V/A,\mathbf{p},1}$, see Eqs. (17).

In the following we compute the contribution to the phase space matching term $i\,\delta\tilde{c}_1(\Lambda)$ generated by an insertion of one Coulomb potential, as illustrated in Fig 15. Suppressing the

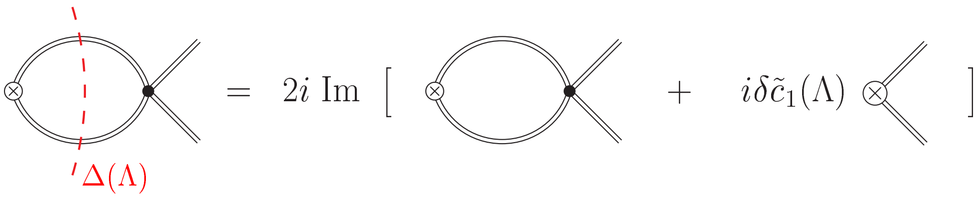

FIG. 15: $\mathcal{O}(\alpha_s)$ matching condition for the Wilson coefficient of a $t\bar{t}$ production current. The black dot represents an insertion of a potential operator.

external (anti)top quark spinors and the lepton current the amplitude for the cut diagram reads

$$\mathcal{A}^{\rm cur}(\Lambda) \,=\, \int\limits_{\Delta(\Lambda)}\frac{d^4p}{(2\pi)^4}\frac{\Gamma_t}{\left(\frac{E}{2}+p_0-\frac{\mathbf{p}^2}{2m_t}+i\frac{\Gamma_t}{2}\right)\left(\frac{E}{2}+p_0-\frac{\mathbf{p}^2}{2m_t}-i\frac{\Gamma_t}{2}\right)}$$
$$\times\,\frac{\Gamma_t}{\left(\frac{E}{2}-p_0-\frac{\mathbf{p}^2}{2m_t}+i\frac{\Gamma_t}{2}\right)\left(\frac{E}{2}-p_0-\frac{\mathbf{p}^2}{2m_t}-i\frac{\Gamma_t}{2}\right)}\,\frac{-i\,\mathcal{V}_c^{(s)}}{(\mathbf{p}-\mathbf{p}')^2}\,, \tag{73}$$

where $\pm\mathbf{p}'$ is the 3-momentum of the top and the antitop quark in the c. m. frame, respectively, and $\mathcal{V}_c^{(s)} = -4\pi C_F\alpha_s \equiv -4\pi a$. For the determination of the matching condition for the $t\bar{t}$ current it is sufficient to consider on-shell external top quarks, and we therefore set $\mathbf{p}'^2 = m_tE$, $E>0$. By carrying out the angular integration and changing variables we obtain an intermediate result of the form (44) with ($|\mathbf{p}| = (m_tE-\frac{1}{2}(t_1+t_2))^{1/2}$)

$$\Delta^{\rm cur}(t_1,t_2) = -i\,\mathcal{V}_c\,\frac{2\pi}{|\mathbf{p}|\sqrt{m_tE}}\,\ln\left|\frac{\sqrt{m_tE}+|\mathbf{p}|}{\sqrt{m_tE}-|\mathbf{p}|}\right|\,. \tag{74}$$

The evaluation of the remaining integral with the invariant mass restrictions (46) yields

$$\mathcal{A}^{\rm cur}(\Lambda) \,=\, i\,a\left[\sqrt{\frac{m_t}{E}}\,\mathrm{Re}\left[\ln\frac{m_tv+\sqrt{m_tE}}{m_tv-\sqrt{m_tE}}\right]-\frac{8\sqrt{2}}{3\pi}\frac{m_t^2\Gamma_t}{\Lambda^3}+\mathcal{O}\left(v^4\frac{m_t^5}{\Lambda^5}\right)\right]. \tag{75}$$

The first term in the brackets is just twice the imaginary part of the vertex diagram $\mathcal{D}$ defined in Eq. (68) without phase space restrictions

$$\mathcal{A}^{\rm cur}(\infty) \,=\, 2\,i\,\mathrm{Im}\left[\mathcal{D}\left(\sqrt{m_tE}\right)\right], \tag{76}$$

and corresponds to the first term on the RHS of the matching relation in Fig. 15. The second term, on the other hand, gives a contribution to the matching term $i\delta\tilde{c}_1(\Lambda)$, and we obtain

$$i\,\delta\tilde{c}_1^1(\Lambda) = \frac{1}{2}\left(\mathcal{A}^{\rm cur}(\Lambda)-\mathcal{A}^{\rm cur}(\infty)\right) \,=\, -i\,a\frac{4\sqrt{2}}{3\pi}\frac{m_t^2\Gamma_t}{\Lambda^3}\,, \tag{77}$$

where the factor $1/2$ is to compensate the factor 2 that appears in the optical theorem, see Fig. 15. It is now straightforward to check that using the matching relation of Fig. 13

the phase space matching term $i\,\delta\tilde{c}_1^1(\Lambda)$ in the Wilson coefficient of the $t\bar{t}$ current operators $\mathcal{O}_{V/A,\mathbf{p},1}$ indeed accounts for the non-analytic term $\propto \mathrm{Re}[iv]$ in Eq. (69). This demonstrates the consistency of the phase space matching procedure at the loop level. We note that the same coefficient is obtained for the respective annihilation currents. Thus the imaginary phase space matching coefficients are not affected by the hermitian conjugation of the current operators in Eq. (16).

The determination of the $\mathcal{O}(\alpha_s)$ contributions to $i\,\delta\tilde{c}_1(\Lambda)$ arising from insertions of higher-dimension operators and potentials describing relativistic v^2-corrections is carried out in analogy. Here we just quote the final results and refer again to Ref. [29] for details:

$$i\,\delta\tilde{c}_1^{r,1}(\Lambda) = -i\,a\frac{\sqrt{2}}{\pi}\frac{\Gamma_t}{\Lambda}\,, \qquad i\,\delta\tilde{c}_1^{s,1}(\Lambda) = i\,a\frac{4\sqrt{2}}{3\pi}\frac{\Gamma_t}{\Lambda}\,, \qquad i\,\delta\tilde{c}_1^{\mathrm{kin},1}(\Lambda) = -i\,a\frac{7}{4\sqrt{2}\,\pi}\frac{\Gamma_t}{\Lambda}$$

$$i\,\delta\tilde{c}_1^{\mathrm{dil},1}(\Lambda) = i\,a\frac{\sqrt{2}}{\pi}\frac{\Gamma_t}{\Lambda}\,, \qquad i\,\delta\tilde{c}_1^{v^2,1}(\Lambda) = i\,a\frac{\sqrt{2}}{3\pi}\frac{\Gamma_t}{\Lambda}\,, \qquad i\,\delta\tilde{c}_1^{\mathrm{int},1}(\Lambda) = -i\,a\frac{2\sqrt{2}}{\pi}\frac{m_t}{\Lambda}\,. \tag{78}$$

Note that the insertion of the current operators $\mathcal{O}_{V/A,\mathbf{p},2}$ gives the mixing term $i\delta\tilde{c}_1^{v^2,1}$ contributing to the matching condition of $\mathcal{O}_{V/A,\mathbf{p},1}$. An analogous mixing does not arise from insertions of the P-wave current $\mathcal{O}_{V/A,\mathbf{p},3}$ due to angular momentum conservation. All terms shown in Eq. (78) are of relative order Λ^2/m_t^2 with respect to the one for the dominant S-wave current in Eq. (77). In the case of the interference correction this is also true because $C_{V/A,1}^{\mathrm{int}} \sim C_{V/A,1}^{\mathrm{Born}}\Gamma_t/m_t$.

C. Perturbative Expansion and Higher Order Corrections

In Secs. III B and IV B we have computed the $\mathcal{O}(\alpha_s^0)$ and $\mathcal{O}(\alpha_s)$ phase space matching contributions to the $(e^+e^-)(e^+e^-)$ forward scattering operators. We have completed all contributions at NNLL order, and we have demonstrated that power-counting breaking terms do not spoil the nonrelativistic expansion. For the $\mathcal{O}(\alpha_s)$ contributions we have also shown that the Wilson coefficients of the $(e^+e^-)(t\bar{t})$ current operators receive phase space matching terms, which contribute at N^{3}LL order. In this section we examine the α_s-series of the phase space matching contributions. To render the analysis more transparent it is useful to distinguish the phase space matching contributions according to where they originate in the computation of the NRQCD cross section $\sigma_{\mathrm{NRQCD}}(\Lambda)$.

Contributions related to the imaginary part of the Coulomb Green function

We first analyze the phase space matching contributions originating from the imaginary part of the Coulomb Green function $\mathrm{Im}[G^c]$ determined in Eqs. (49), (50), (70) and (77). Since the imaginary part of the Coulomb Green function constitutes the leading order contribution of the factorization formula (26), these phase space matching terms represent the numerically dominant contributions. We define the NRQCD cross section associated to the imaginary part of the Coulomb Green function as

$$\sigma_{\mathrm{NRQCD}}^{\mathrm{Im}[G^c]}(\Lambda,\nu) = N_c\left((C_{V,1}^{\mathrm{Born}})^2 + (C_{A,1}^{\mathrm{Born}})^2\right)\Gamma_t^2\int\limits_{\Delta(\Lambda)}\frac{d^4p}{(2\pi)^4}\,\frac{(2m_t)^4}{(t_1^2+m_t^2\Gamma_t^2)(t_2^2+m_t^2\Gamma_t^2)}\left|f_{v,m_t,\nu}(|\mathbf{p}|)\right|^2, \tag{79}$$

where t_1 and t_2 are the invariant mass variables of Eq. (42) and $f_{v,m_t,\nu}$ is the Coulomb vertex factor. The Coulomb vertex factor can be written in the form

$$f_{v,m_t,\nu}(|\mathbf{p}|) \,=\, \left[\frac{|\mathbf{p}|^2}{m_t} - (E + i\Gamma_t)\right] \tilde{G}^0_{v,m_t,\nu}(0, |\mathbf{p}|)\,. \tag{80}$$

Here $\tilde{G}^0_{v,m_t,\nu}(0, |\mathbf{p}|)$ is the partially Fourier transformed Coulomb Green function with the first argument in position space at $\mathbf{x} = 0$ and the second in momentum space with the momentum $\mathbf{p}$. Because of $\mathbf{x} = 0$ there is no dependence on the direction of $\mathbf{p}$. At LL order, i.e. accounting only for iterations of the LL Coulomb potential of Eq. (6), $\tilde{G}^0_{v,m_t,\nu}(0, |\mathbf{p}|)$ is known analytically:

$$\begin{aligned}\tilde{G}^0_{v,m_t,\nu}(0, |\mathbf{p}|) \,=\, -\frac{i\,m_t}{4k|\mathbf{p}|}\frac{1}{1-\lambda}\bigg[\,{}_2F_1\left(2, 1; 2-\lambda; \frac{1}{2}\left(1 + \frac{i\,|\mathbf{p}|}{k}\right)\right) \\ -\,{}_2F_1\left(2, 1; 2-\lambda; \frac{1}{2}\left(1 - \frac{i\,|\mathbf{p}|}{k}\right)\right)\bigg]\,,\end{aligned} \tag{81}$$

where $k \equiv \sqrt{-m_t(E + i\Gamma_t)}$ and $\lambda \equiv C_F\alpha_s(m_t\nu)\, m_t/2k$, and ${}_2F_1(a, b; c; z)$ is the hypergeometric function. At NLL and NNLL order we use numerical results for the form factor $f_{v,m_t,\nu}$ using the computational techniques we also employ for the determination of the Coulomb Green function at the respective orders, see Refs. [47, 48]. These numerical methods have been applied and thoroughly tested before for predictions of the top three-momentum distribution, see e.g. Refs. [28, 48]. Without phase space restrictions, i.e. for $\Lambda = \infty$, Eq. (79) reduces to the form

$$\sigma^{\mathrm{Im}[G^c]}_{\mathrm{NRQCD}}(\infty) = \,2N_c\left((C^{\mathrm{Born}}_{V,1})^2 + (C^{\mathrm{Born}}_{A,1})^2\right)\mathrm{Im}\Big[G^c(a, v, m_t, \nu)\Big]\,. \tag{82}$$

In Fig. 16 we display $\Delta\sigma^{\mathrm{Im}[G^c]} = \sigma^{\mathrm{Im}[G^c]}_{\mathrm{NRQCD}}(\Lambda) - \sigma^{\mathrm{Im}[G^c]}_{\mathrm{NRQCD}}(\infty)$ for $\Delta M_t = 15$ GeV (left panel) and $\Delta M_t = 35$ GeV (right panel) using the LL (black solid line), NLL (red solid line) and NNLL (blue solid line) Coulomb Green functions, and the 1S top mass scheme [28, 58] with $m_t = 172$ GeV. The strong coupling is evaluated at the hard scale $\nu = 1$, $\alpha_s(m_t) = 0.1077$ and the other input parameters are given in Eq. (63), except for the electromagnetic coupling constant, which is also taken at the hard scale $\alpha_{\mathrm{qed}}(m_t) = 1/125.9$. For simplicity we neglect here and in the following examinations of Sec. IV C the hard QCD corrections to the $t\bar{t}$ current matching coefficient, i.e. we set $c_1(\nu = 1) = 1$. The lines for $\Delta\sigma^{\mathrm{Im}[G^c]}$ represent the effects of the invariant mass cuts including iterations of the Coulomb potential to all orders. From our examinations in Sec. IV B we know that $\Delta\sigma^{\mathrm{Im}[G^c]}$ exhibits hard and soft contributions that can only be separated by the phase space matching procedure. Thus $\Delta\sigma^{\mathrm{Im}[G^c]}$ unavoidably contains large logarithmic terms for any choice of the renormalization scale. The size of the higher order corrections discussed in the following should therefore be interpreted with some care as they might not reflect the quality of the α_s-expansion when all logarithms are properly summed up. Despite this fact we see that the effects of including the $\mathcal{O}(\alpha_s)$ and $\mathcal{O}(\alpha_s^2)$ corrections to the Coulomb potential in $\Delta\sigma^{\mathrm{Im}[G^c]}$ show good convergence. For $\Delta M_t = 15$ GeV (35 GeV) the $\mathcal{O}(\alpha_s^2)$ corrections to the Coulomb potential (difference between the red and blue solid lines) lead to a shift between -10 fb (-4 fb) and -5 fb (-2 fb). For $\Delta M_t = 15$ GeV this exceeds our theoretical precision aim (green dashed lines in the lower panel of Fig. 10) for $\sqrt{s} - 2m_t \lesssim -2$ GeV. The shift caused by the $\mathcal{O}(\alpha_s^2)$ corrections to the Coulomb potential, however, quickly drops below the precision aim for

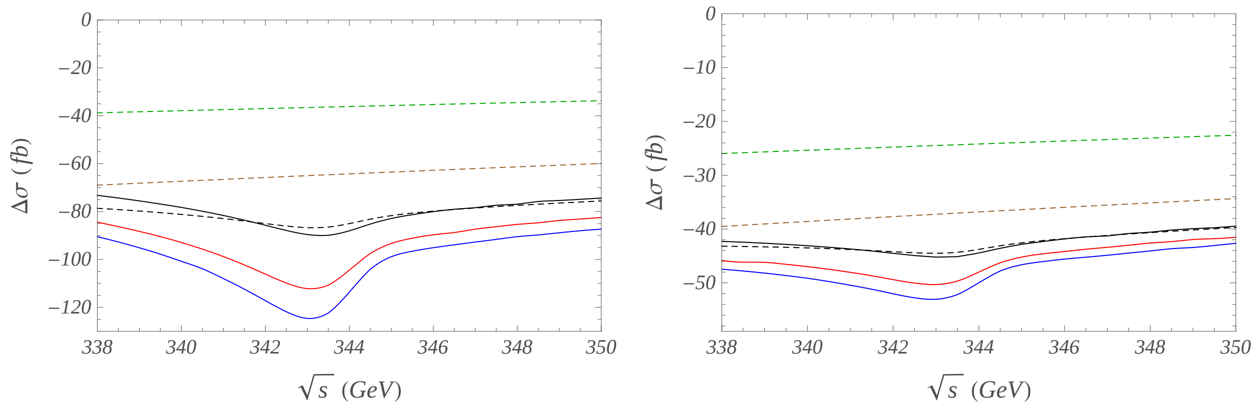

FIG. 16: Contributions to the inclusive cross section from the NLL, NNLL and N^{3}LL order phase space matching corrections in $\Delta\sigma_{\rm psm}^{{\rm Im}[G^c]}$ (green, brown and black dashed lines, respectively) as a function of the total center of mass energy for $\Delta M_t = 15$ (left) and $\Delta M_t = 35$ GeV (right). The solid lines correspond to the phase space matching contributions $\Delta\sigma^{{\rm Im}[G^c]}$ obtained from the imaginary part of the exact cut Coulomb Green function at LL, NLL and NNLL (black, red and blue, respectively).

$\Delta M_t > 15$ GeV for all values of E, and we conclude that phase space matching corrections related to insertions of the $\mathcal{O}(\alpha_s^2)$ corrections to the Coulomb potential, which contribute at N^{4}LL order and higher, do not have to be considered.

We now examine $\Delta\sigma^{{\rm Im}[G^c]}$ computed from the phase space matching procedure carried out in the previous sections. Up to the N^{3}LL order it has the form

$$\begin{aligned}\Delta\sigma_{\rm psm}^{{\rm Im}[G^c]} =& \,{\rm Im}\Big[\tilde{C}_V^0(\Lambda)+\tilde{C}_A^0(\Lambda)\Big]_{\rm NLL} + {\rm Im}\Big[\tilde{C}_V^1(\Lambda)+\tilde{C}_A^1(\Lambda)\Big]_{\rm NNLL} \\ &+ {\rm Im}\bigg[\tilde{C}_V^2(\Lambda)+\tilde{C}_A^2(\Lambda) + \frac{E}{m_t}\Big(\tilde{C}_V^{(1),0}(\Lambda)+\tilde{C}_A^{(1),0}(\Lambda)\Big) \\ &\qquad + 4\,N_c\left((C_{V,1}^{\rm Born})^2+(C_{A,1}^{\rm Born})^2\right) i\,\delta\tilde{c}_1(\Lambda)\,G^c(a,v,m_t,\nu)\bigg]_{\rm N^3LL},\end{aligned} \tag{83}$$

where we have indicated the NLL, NNLL and N^{3}LL order corrections. The results for $\tilde{C}_{V/A}^0$, $\tilde{C}_{V/A}^1$, $\tilde{C}_{V/A}^{(1),0}$ and $\delta\tilde{c}_1$ have been given in Eqs. (49), (70), (50), and (77), respectively. The N^{3}LL corrections depend on the ($\overline{\rm MS}$ renormalized) real part of the Coulomb Green function which at this order can be replaced by its LL expression G^0, see Eq. (8). Note that for actual NRQCD predictions the Green function $G^c(a,v,m_t,\nu)$ in Eq. (83) has to be evaluated with $\nu\sim\alpha_s$ to properly sum large logarithms. As mentioned above, we set $\nu=1$ for the following examinations. In Fig. 16 the NLL and the NNLL approximations for $\Delta\sigma_{\rm psm}^{{\rm Im}[G^c]}$ are displayed as the green and brown dashed lines, respectively. For $\Delta M_t = 35$ GeV (right panel) we find that the NNLL corrections are about half the size of the NLL contributions. For $\Delta M_t = 15$ GeV (left panel), where we expect a worse α_s-expansion due to the Λ-dependence of $\tilde{C}_{V/A}^0\sim\Gamma_t/\Lambda$ and $\tilde{C}_{V/A}^1\sim a\,m_t\Gamma_t/\Lambda^2$, the NNLL corrections are only about 15% smaller than the NLL contributions. The difference of $\Delta\sigma_{\rm psm}^{{\rm Im}[G^c]}$ at NNLL order and

$\Delta\sigma^{\mathrm{Im}[G^c]}$ accounting for the LL Coulomb potential (black solid lines) is between 3 and 7 fb for $\Delta M_t = 35$ GeV and between 7 and 25 fb for $\Delta M_t = 15$ GeV. For $\Delta M_t = 15$ GeV this exceeds our theoretical precision aim, visualized by the green dashed line in the lower panel of Fig. 10. The difference is even larger with respect to $\Delta\sigma^{\mathrm{Im}[G^c]}$ accounting for the NLL Coulomb potential (red solid lines). It is therefore required to also account for the full set of N^{3}LL phase space matching contributions displayed in Eq. (83). Unfortunately, at this time the full expressions for $\tilde{C}^2_{V/A}$ are unknown. They get contributions from two insertions of the leading Coulomb potential (contained in the LL Coulomb Green function) and from one insertion of the $\mathcal{O}(\alpha_s)$ correction to the Coulomb Green function (contained in the NLL Coulomb Green function). We have computed the contribution from two insertions of the Coulomb potential using the methods described in Sec. IV B. The result reads

$$\tilde{C}^{2,V_cV_c}_{V/A}(\Lambda) = 2\,i\,N_c\,(C^{\mathrm{Born}}_{V/A,1})^2\,\frac{m_t^2}{4\pi}\left[a^2\,\frac{4\sqrt{2}}{3\pi}\left(\ln\left(\frac{\mu^2}{\Lambda^2}\right) - \frac{7}{3} - \frac{\pi^2}{4} + \frac{2}{3}\ln 2\right)\frac{m_t^2\Gamma_t}{\Lambda^3}\right]. \tag{84}$$

The logarithmic term is related to a NNLL order contribution to the imaginary anomalous dimension of $\tilde{C}_{V/A}(\Lambda,\nu)$. The fact that the logarithm vanishes for $\mu = \Lambda \sim m_t$ reconfirms that the phase space matching contributions are hard effects. Although we do not have the complete result for $\tilde{C}^2_{V/A}(\Lambda)$, using instead the result of Eq. (84) allows us to compare $\Delta\sigma^{\mathrm{Im}[G^c]}_{\mathrm{psm}}$ at N^{3}LL order (black dashed lines) with the numerical results for $\Delta\sigma^{\mathrm{Im}[G^c]}$ accounting for the LL Coulomb Green function (black solid lines). We see that including the N^{3}LL phase space matching contributions leads to a considerably improved agreement with the Coulomb resummed numerical results. For $\Delta M_t = 15$ GeV and 35 GeV the difference is always smaller than 5 fb, except when $E < -5$ GeV for $\Delta M_t = 15$ GeV. Since this is acceptable for our precision aim, we believe that the full set of N^{3}LL phase space matching corrections should be adequate for the precision expected at a future linear collider. Since the full result for $\tilde{C}^2_{V/A}(\Lambda)$ is unknown, we use for the time being as a substitute for the N^{3}LL order terms in $\Delta\sigma^{\mathrm{Im}[G^c]}_{\mathrm{psm}}$ the numerical Coulomb-resummed expression of Eq. (79), evaluated with the NLL Coulomb vertex factor at the hard scale for α_s minus the NLL and NNLL order terms of Eq. (83):

$$(\Delta\sigma^{\mathrm{Im}[G^c]}_{\mathrm{psm}})_{\mathrm{N^3LL}} = \sigma^{\mathrm{Im}[G^c]}_{\mathrm{NRQCD}}(\Lambda,1) - \mathrm{Im}\Big[\tilde{C}^0_V(\Lambda) + \tilde{C}^0_A(\Lambda)\Big]_{\mathrm{NLL}} - \mathrm{Im}\Big[\tilde{C}^1_V(\Lambda) + \tilde{C}^1_A(\Lambda)\Big]_{\mathrm{NNLL}}. \tag{85}$$

Contributions related to the real part of the Coulomb Green function

We now analyze the phase space matching contributions related to the real part of the Coulomb Green function. These phase space matching contributions are proportional to the type-1 imaginary Wilson coefficients $iC^{\mathrm{int}}_{V/A,1}$ in Eqs. (22) and (23), which describe the interference of the $e^+e^- \to t\bar{t} \to b\bar{b}W^+W^-$ diagram with diagrams for $e^+e^- \to b\bar{b}W^+W^-$ with only either t or $\bar{t}$ at intermediate stages. As we have shown in Sec. III B, the interference effects cause the largest phase space matching contributions among the $\mathcal{O}(v^2)$ relativistic corrections in the factorization formula (26), and we therefore examine them separately. In analogy to the previous section we first define the Coulomb-resummed NRQCD cross section

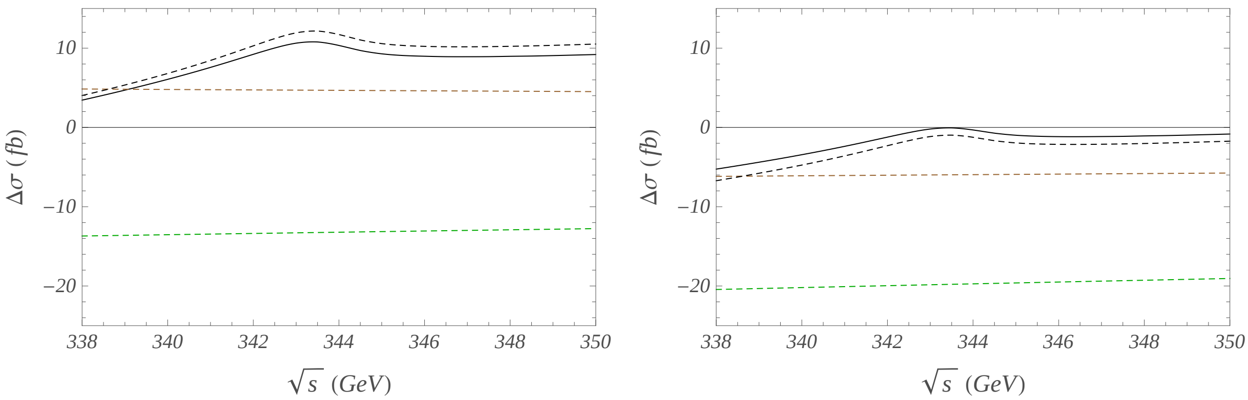

FIG. 17: Contributions to the inclusive cross section from the NLL, NNLL and N^{3}LL order phase space matching corrections in $\Delta\sigma_{\rm psm}^{{\rm Re}[G^c]}$ (green, brown and black dashed lines, respectively) as a function of the total center of mass energy for $\Delta M_t = 15$ (left) and $\Delta M_t = 35$ GeV (right). The black solid lines correspond to the phase space matching contributions $\Delta\sigma^{{\rm Re}[G^c]}$ obtained from the real part of the exact cut Coulomb Green function at LL.

with invariant mass restrictions arising from the real part of the Coulomb Green function:

$$\sigma_{\rm NRQCD}^{{\rm Re}[G^c]}(\Lambda) = 2N_c\left(C_{V,1}^{\rm Born}C_{V,1}^{\rm int}+C_{A,1}^{\rm Born}C_{A,1}^{\rm int}\right)\Gamma_t^2\int\limits_{\Delta(\Lambda)}\frac{d^4p}{(2\pi)^4}\,\frac{(2m_t)^4}{(t_1^2+m_t^2\Gamma_t^2)(t_2^2+m_t^2\Gamma_t^2)}$$
$$\times\left[-\frac{t_1+t_2}{2m_t\Gamma_t}\,{\rm Re}\left[f_{v,m_t,\nu}(|\mathbf{p}|)\right]-{\rm Im}\left[f_{v,m_t,\nu}(|\mathbf{p}|)\right]\right]. \tag{86}$$

Since the interference contributions are related to $\mathcal{O}(v^2)$ operator insertions in the factorization theorem (26), we only consider the vertex factor in the LL approximation as given in Eq. (80). The expression in the brackets involves the Coulomb-resummed generalization of the function $\Delta^{\rm int,0}$ given in Eqs. (53). The corresponding phase space matching contributions at N^{3}LL order can be derived from Eq. (26) and read

$$\begin{aligned}\Delta\sigma_{\rm psm}^{{\rm Re}[G^c]} = {}& {\rm Im}\Big[\tilde C_V^{\rm int,0}(\Lambda)+\tilde C_A^{\rm int,0}(\Lambda)\Big]_{\rm NLL}+{\rm Im}\Big[\tilde C_V^{\rm int,1}(\Lambda)+\tilde C_A^{\rm int,1}(\Lambda)\Big]_{\rm NNLL}\\ &+{\rm Im}\Big[\tilde C_V^{\rm int,2}(\Lambda)+\tilde C_A^{\rm int,2}(\Lambda)+\frac{E}{m_t}\Big(\tilde C_V^{(1),\rm int,0}(\Lambda)+\tilde C_A^{(1),\rm int,0}(\Lambda)\Big)\\ &\qquad+4\,N_c\left(C_{V,1}^{\rm Born}C_{V,1}^{\rm int}+C_{A,1}^{\rm Born}C_{A,1}^{\rm int}\right)i\,\delta\tilde c_1^{\rm int,1}(\Lambda)\,G^c(a,v,m_t,\nu)\Big]_{\rm N^3LL},\end{aligned} \tag{87}$$

where we have again indicated the NLL, NNLL and N^{3}LL order corrections. The results for the $\tilde C_{V/A}^{\rm int,0}$, $\tilde C_{V/A}^{\rm int,1}$, $\tilde C_{V/A}^{(1),\rm int,0}$ and $\delta\tilde c_1^{\rm int,1}$ have been given in Eqs. (54), (71), (55) and (78), respectively. The results for $\tilde C_{V/A}^{\rm int,2}$ are currently unknown. In the following analyses we neglect them, i.e. we set them to zero.

In Fig. 17 the numerical LL Coulomb-resummed phase space effects $\Delta\sigma^{{\rm Re}[G^c]}\equiv\sigma_{\rm NRQCD}^{{\rm Re}[G^c]}(\Lambda)-\sigma_{\rm NRQCD}^{{\rm Re}[G^c]}(\infty)$ (solid black lines) and the corresponding NLL (green dashed lines), NNLL (brown dashed lines) and N^{3}LL (black dashed lines) approximations from the phase space matching procedure are shown. The left panel refers to $\Delta M_t = 15$ GeV and the right panel to $\Delta M_t = 35$ GeV. The strong and QED couplings are again evaluated at the hard scale $\nu = 1$, i.e. $\alpha_s(m_t) = 0.1077$ and $\alpha_{\rm qed}(m_t) = 1/125.9$, and the other input parameters are given in Eq. (63). As in the previous subsection we again neglect the hard QCD corrections to the $t\bar{t}$ current matching coefficient, i.e. we set $c_1(\nu = 1) = 1$. The situation we find is quite similar to the one discussed before for the imaginary part of the Coulomb Green function. The NLL order phase space matching contributions amount to around -13 (-20) fb, and the NNLL order contributions to about $+18$ ($+15$) fb for $\Delta M_t = 15$ (35) GeV. The NNLL corrections are quite sizeable and even exceed the NLL contributions for $\Delta M_t = 15$ GeV. It is conspicuous that the NLL and NNLL phase space matching corrections have opposite signs and cancel each other to a large extent. The sum of the NLL and NNLL phase space matching corrections differ from $\Delta\sigma^{{\rm Re}[G^c]}$ by at most 5 fb. The N^{3}LL order phase space matching corrections, on the other hand, are much smaller than the NLL and NNLL order ones. Although we have neglected the $\tilde{C}^{\rm int,2}_{V/A}$, which arise from diagrams with two insertions of the Coulomb potential, the difference of the phase space matching contributions up to N^{3}LL order and the exact LL Coulomb-resummed result amounts to less than 2 fb for all ΔM_t between 15 and 35 GeV. We conclude that the $\tilde{C}^{\rm int,2}_{V/A}$ are numerically small and that the N^{3}LL phase space matching contributions are more than adequate for our theoretical precision aim.

Contributions related to the other $\mathcal{O}(v^2)$ relativistic corrections

As the third class of phase space matching contributions we now examine the corrections that arise from insertions of $\mathcal{O}(v^2)$ suppressed operators other than the interference corrections just discussed above. Up to N^{3}LL order the contributions of these matching corrections to the inclusive NRQCD cross section have the form ($i = \{{\rm kin}, {\rm dil}, v^2, P\text{-wave}\}$, $j = \{r, s, {\rm kin}, {\rm dil}, v^2, P\text{-wave}\}$, $k = \{r, s, {\rm kin}, {\rm dil}, v^2\}$)

$$\begin{aligned}
\Delta\sigma^{\mathcal{O}(v^2)}_{\rm psm} \;=\; & {\rm Im}\Big[\sum_i \Big(\tilde{C}^{i,0}_V(\Lambda) + \tilde{C}^{i,0}_A(\Lambda)\Big)\Big]_{\rm NLL} + {\rm Im}\Big[\sum_j \Big(\tilde{C}^{j,1}_V(\Lambda) + \tilde{C}^{j,1}_A(\Lambda)\Big)\Big]_{\rm NNLL} \\
& + {\rm Im}\Big[\sum_j \Big(\tilde{C}^{j,2}_V(\Lambda) + \tilde{C}^{j,2}_A(\Lambda)\Big) + \frac{E}{m_t}\sum_i \Big(\tilde{C}^{(1),i,0}_V(\Lambda) + \tilde{C}^{(1),i,0}_A(\Lambda)\Big) \\
& \qquad + 4\,N_c\Big((C^{\rm Born}_{V,1})^2 + (C^{\rm Born}_{A,1})^2\Big)\sum_k\; i\,\delta\tilde{c}^{k,1}_1(\Lambda)\,G^c(a,v,m_t,\nu)\Big]_{\rm N^3LL}\,, \qquad (88)
\end{aligned}$$

where we have again indicated the NLL, NNLL and N^{3}LL order corrections. The results for the $\tilde{C}^{i,0}_{V/A}$, $\tilde{C}^{j,1}_{V/A}$, $\tilde{C}^{(1),i,0}_{V/A}$ and $\delta\tilde{c}^{k,1}_1$ have been given in Eqs. (54), (71), (55) and (78), respectively. As for the interference coefficients the results for the $\tilde{C}^{j,2}_{V/A}$ are currently unknown and are neglected in the following analyses.

In Fig. 18 $\Delta\sigma^{\mathcal{O}(v^2)}_{\rm psm}$ is displayed at NLL (green dashed lines), NNLL (brown dashed line) and N^{3}LL (black dashed lines). It is striking that the NLL contributions are at the sub-fb level and an order of magnitude smaller than the NNLL terms. The small size of the NLL terms is, however, due to an almost complete cancellation in the sum of the individual $\tilde{C}^{i,0}_{V/A}$ coefficients (see Fig. 8). The size of the individual coefficients is at the level of $1-3$ fb

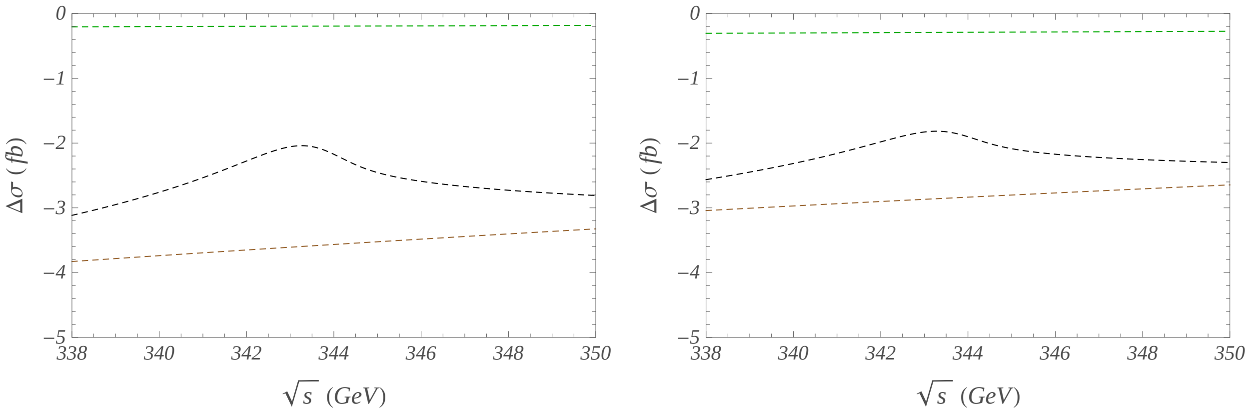

FIG. 18: Contributions to the inclusive cross section from the sum of the phase space matching arising from insertions of $\mathcal{O}(v^2)$ relativistic corrections other than the interference contributions at NLL (green), NNLL (brown) and N^{3}LL (black) order, as a function of the total center of mass energy for $\Delta M_t = 15$ (left) and $\Delta M_t = 35$ GeV (right).

and comparable in size to the individual NNLL coefficients $\tilde{C}^{j,1}_{V/A}$ (see Fig. 14). The NNLL coefficients, on the other hand, do not cancel to the same extent due to the additional contribution from the potential $\mathcal{V}_r^{(s)}$, see Eq (71). Thus the situation concerning the α_s-expansion for the third class of the phase space matching contributions is similar to the other classes of phase space matching contributions discussed above. This is also confirmed by the size of the N^{3}LL corrections which amount to at most 1 to 2 fb. Although we do not have a numerical Coulomb-resummed expression for a more thorough comparison, the results indicate that the α_s-expansion is also well under control for the third class of phase space matching contributions. Due to the overall small size of these contributions we conclude again that keeping the phase space matching contributions up to N^{3}LL order is more than adequate to reach our theoretical precision goal.

V. NUMERICAL ANALYSIS

In Sec. III C we have demonstrated for the case $\alpha_s = 0$ that the phase space matching contributions are essential in order to compensate for the fact that the previous NRQCD predictions for top threshold production overestimate the full theory cross section by a substantial amount. The problem of the previous NRQCD predictions is related to the fact that upon shifting the energy by $E \to E + i\Gamma_t$, in order to account for the top quark finite lifetime, the NRQCD $t\bar{t}$ phase space becomes unrestricted and extends to unphysical regions as a consequence of the nonrelativistic expansion. The phase space matching procedure removes these unphysical phase space contributions and implements the information on possible experimental cuts into the NRQCD predictions. These phase space matching contributions are represented by imaginary contributions to the Wilson coefficients of NRQCD, see Sec. II.

In this section we analyze the complete set of N^{3}LL phase space matching contributions determined in the previous sections for predictions of the inclusive NRQCD top pair threshold cross section with cuts on the invariant masses of the top and the antitop quark defined in Eq. (34). We also compare the size of the phase space matching contributions to the other and previously known types of electroweak effects relevant for the top pair threshold cross section: the NNLL QED corrections, the hard electroweak corrections [22] and the (type-1) finite lifetime corrections, which are not related to phase space restrictions [27]. Together with the phase space matching contributions, which we call type-2 finite lifetime corrections, these three classes of contributions constitute all effects of the electroweak interactions on the threshold cross section.[11]

To start we collect all phase space matching contributions to the inclusive NRQCD cross section up to N^{3}LL order. In the previous sections we have for simplicity neglected the hard QCD and QED matching corrections contained in the Wilson coefficient $c_1(\nu = 1)$ of the leading $(e^+e^-)(t\bar{t})$ top pair production operator. Accounting for these matching corrections the complete set of N^{3}LL phase space matching contributions can be derived from the factorization formula in Eq. (26) and takes the form

$$\begin{aligned}\Delta\sigma_{\rm PSM}(\Lambda,\nu=1) \,=\, & \Delta\sigma^{\rm NLL}(\Lambda,1) + \Big[\Delta\sigma^{\rm NNLL}(\Lambda,1) + 2\,h_1^{(1)}\,\Delta\sigma^{\rm NLL}(\Lambda,1)\Big]_{\rm NNLL} \\ & + \Big[\Delta\sigma^{\rm N^3LL}(\Lambda,1) + 2\,h_1^{(1)}\,\Delta\sigma^{\rm NNLL}(\Lambda,1) + \Big(2\,h_1^{(2)} + (h_1^{(1)})^2\Big)\,\Delta\sigma^{\rm NLL}(\Lambda,1)\Big]_{\rm N^3LL}\,, \qquad (89)\end{aligned}$$

where we have specifically indicated by brackets the NNLL and N^{3}LL order contributions. Explicit expressions for the NLL and NNLL hard QCD/QED matching conditions $h_1^{(1)}$ and $h_1^{(2)}$ are given in Eq. (19). The terms $\Delta\sigma^{\rm N^kLL}(\Lambda,1)$ are the N^{k}LL phase space matching contributions to the inclusive cross section with the $h_1^{(1,2)}$ set to zero. The result for $\Delta\sigma^{\rm NLL}$ reads ($i = {\rm int}, {\rm dil}, {\rm kin}, v^2, \text{P-wave}$)

$$\Delta\sigma^{\rm NLL}(\Lambda,1) \,=\, {\rm Im}\Big[\tilde{C}_V^0(\Lambda) + \tilde{C}_A^0(\Lambda) + \sum_i \Big(\tilde{C}_V^{i,0}(\Lambda) + \tilde{C}_A^{i,0}(\Lambda)\Big)\Big]\,, \qquad (90)$$

where expressions for $\tilde{C}^0_{V/A}$ and the $\tilde{C}^{i,0}_{V/A}$ have been given in Eqs. (49) and (54), respectively. The term $\Delta\sigma^{\rm NNLL}$ has the form ($j = r, s, {\rm int}, {\rm dil}, {\rm kin}, v^2, P\text{-wave}$)

$$\begin{aligned}\Delta\sigma^{\rm NNLL}(\Lambda,1) \,=\, {\rm Im}\Big[& \tilde{C}_V^1(\Lambda) + \tilde{C}_A^1(\Lambda) + \sum_j \Big(\tilde{C}_V^{j,1}(\Lambda) + \tilde{C}_A^{j,1}(\Lambda)\Big) \\ & - h_1^{(1)}\Big(\tilde{C}_V^{v^2,0}(\Lambda) + \tilde{C}_A^{v^2,0}(\Lambda)\Big)\Big]\,, \qquad (91)\end{aligned}$$

where expressions for $\tilde{C}^1_{V/A}$ and the $\tilde{C}^{j,1}_{V/A}$ have been given in Eqs. (70) and (71), respectively. Finally, $\Delta\sigma^{\rm N^3LL}$ reads ($i = \{{\rm int}, {\rm dil}, {\rm kin}, v^2, \text{P-wave}\}, j = \{r, s, {\rm int}, {\rm dil}, {\rm kin}, v^2, \text{P-wave}\}, k =$

[11] We do not discuss here the effects of the e^+e^- luminosity spectrum since it is determined for the most part from experimental measurements and simulations.

$\{r, s, \mathrm{dil}, \mathrm{kin}, v^2\})$

$$\begin{aligned}
\Delta\sigma^{\mathrm{N^3LL}}(\Lambda,1) \,=\, & (\Delta\sigma_{\mathrm{psm}}^{\mathrm{Im}[G^c]})_{\mathrm{N^3LL}} \,+\, \mathrm{Im}\bigg[\frac{E}{m_t}\sum_i \Big(\tilde{C}_V^{(1),i,0}(\Lambda)+\tilde{C}_A^{(1),i,0}(\Lambda)\Big)\bigg] \\
& + \,\mathrm{Im}\bigg[\sum_j \Big(\tilde{C}_V^{j,2}(\Lambda)+\tilde{C}_A^{j,2}(\Lambda)\Big)\bigg] \\
& + \,\mathrm{Im}\bigg[4\,N_c\,\Big((C_{V,1}^{\mathrm{Born}})^2+(C_{A,1}^{\mathrm{Born}})^2\Big)\sum_k \,i\,\delta\tilde{c}_1^{k,1}(\Lambda)\,G^c(a,v,m_t,\nu)\bigg] \\
& + \,\mathrm{Im}\bigg[4\,N_c\,\Big(C_{V,1}^{\mathrm{Born}}C_{V,1}^{\mathrm{int}}+C_{A,1}^{\mathrm{Born}}C_{A,1}^{\mathrm{int}}\Big)\,i\,\delta\tilde{c}_1^{\mathrm{int},1}(\Lambda)\,G^c(a,v,m_t,\nu)\bigg] \\
& + \,\mathrm{Im}\bigg[\Big((h_1^{(1)})^2-h_1^{(2)}\Big)\Big(\tilde{C}_V^{v^2,0}(\Lambda)+\tilde{C}_A^{v^2,0}(\Lambda)\Big) \,-\, h_1^{(1)}\Big(\tilde{C}_V^{v^2,1}(\Lambda)+\tilde{C}_A^{v^2,1}(\Lambda)\Big)\bigg]\,,
\end{aligned} \tag{92}$$

where $(\Delta\sigma_{\mathrm{psm}}^{\mathrm{Im}[G^c]})_{\mathrm{N^3LL}}$ is a numerical expression defined in Eq. (85), and the results for $\tilde{C}_{V/A}^{(1),k,0}$ and $i\delta\tilde{c}^{k,1}$ have been given in Eqs. (55) and (78), respectively. The results for the $\tilde{C}_{V/A}^{j,2}$ are currently unknown. For the analysis we carry out in the following we set them to zero. Together with an analytic determination of $(\Delta\sigma_{\mathrm{psm}}^{\mathrm{Im}[G^c]})_{\mathrm{N^3LL}}$ we plan to compute them in a separate publication.

In the following analysis we use $m_t = 172$ GeV for the top mass in the 1S mass scheme [28, 58], and all matching coefficients are evaluated at the scale m_t ($\nu = 1$). For the QCD coupling we use $\alpha_s(m_t) = 0.1077$ and for the QED ($\overline{\mathrm{MS}}$) coupling $\alpha_{\mathrm{qed}}(m_t) = 1/125.9$. All soft matrix element contributions are evaluated for the QCD and QED couplings at the velocity renormalization parameter $\nu = 0.2$ which corresponds to $\mu_{\mathrm{soft}} = 34.4$ GeV for the soft and to $\mu_{\mathrm{usoft}} = 6.88$ GeV for the ultrasoft scales. For the evaluation of the hard one-loop electroweak corrections we choose $m_{\mathrm{Higgs}} = 130$ GeV. All other parameters are given in Eqs. (63).

In Fig. 19 we show the phase space matching corrections to the inclusive $t\bar{t}$ threshold cross section at NLL (black dotted lines), NNLL (black dashed lines) and N^{3}LL order (black solid lines), the NNLL QED corrections (blue lines), the NNLL hard one-loop electroweak corrections (green lines) and the type-1 finite lifetime corrections (red lines) as a function of the c.m. energy $\sqrt{s}$. The left panel shows the results for an invariant mass $\Delta M_t = 15$ GeV and the right panel for $\Delta M_t = 35$ GeV. The QED effects arise from the electromagnetic correction to the QCD Coulomb potential (see text after Eq. (7)) and the one-loop QED matching correction to the Wilson coefficient c_1 of the $t\bar{t}$ current, see Eq. (17). The hard one-loop electroweak corrections are encoded in the coefficients $C_{V/A,1}^{\mathrm{1loop}}$ also shown in Eq. (17). The result for $C_{V/A,1}^{\mathrm{1loop}}$ has been obtained in Ref. [22]. The type-1 finite lifetime corrections represent all finite lifetime corrections which are not related to phase space constraints. They consist of the corrections generated by the imaginary interference matching coefficient $iC_{V/A,1}^{\mathrm{int}}$, see Eq. (17), the time dilation corrections to the Green function shown in Eq. (30) and the contributions from the renormalization group summation of phase space logarithms contained in the coefficients $\tilde{C}_{V/A}$ of the $(e^+e^-)(e^+e^-)$ forward scattering operators given in Eq. (31). The matching and time dilation corrections are known at NNLL order and the

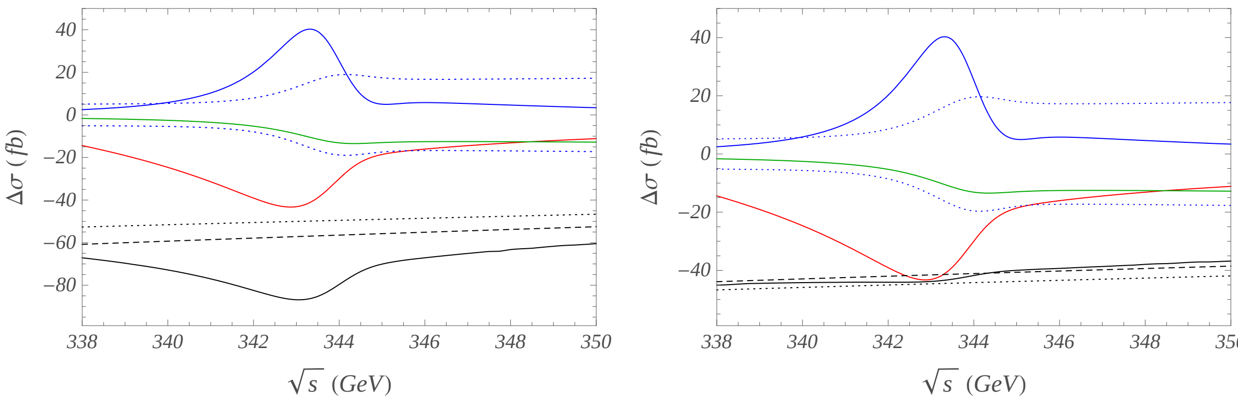

FIG. 19: Sizes of the different contributions to the inclusive cross section arising from electroweak interactions as a function of the total center of mass energy for $\Delta M_t = 15$ GeV (left) and $\Delta M_t = 35$ GeV (right): (green line) NNLL hard one-loop electroweak effects from Ref. [22], (red line) NNLL finite lifetime corrections from Ref. [27], (blue line) NNLL QED effects, and phase space matching corrections at NLL, NNLL and N^{3}LL (dotted, dashed and solid black lines, respectively). The blue dotted lines correspond to the expected experimental uncertainties at the LC.

summation of phase space logarithms at NLL order [27]. The QED, hard electroweak and type-1 finite lifetime corrections do not depend on phase space restrictions and are therefore identical in both panels. In Fig. 19 the blue dotted lines represent a rough (and likely optimistic) estimation of the expected experimental uncertainties at a future linear collider consisting of an energy-independent error of 5 fb and a 2% relative uncertainty with respect to the full prediction, both being added quadratically.

We see that the QED (blue lines) and the type-1 finite lifetime corrections (red lines) are sizeable (at the level of 40 fb) only in the peak region just below $\sqrt{s} = 2m_t$. Above and below the peak region the QED corrections are quite small and do not exceed 5 fb. Above and below the peak the type-1 finite lifetime corrections amount to -15 to -10 fb. Due to their different signs the QED corrections and the type-1 finite lifetime corrections cancel each other to a large extent in the peak region. The hard electroweak corrections (green lines) represent a multiplicative factor of -1.2% to the total cross section and are therefore very small below the peak and at the level of 12-13 fb above the peak region.[12] We see that the phase space matching contributions represent the largest of the four classes of electroweak effects. In contrast to the other classes of electroweak effects they do not decrease strongly for energies below the peak region. For $\Delta M_t = 15$ GeV the N^{3}LL phase space matching contributions amount between -85 and -65 fb and for $\Delta M_t = 35$ GeV they are between -45 and -35 fb. The overall size of the phase space matching corrections decreases for larger values of the top invariant mass cut ΔM_t. We emphasize, however, that the results obtained in this work are valid only for moderate values of ΔM_t in the region between 15 and 35 GeV. For invariant mass cuts below 15 GeV the phase space constraints are not related anymore to hard effects and for invariant mass cuts substantially above 35 GeV matching contributions that need to be computed from full theory diagrams have to be included. The

[12] The small size of the hard electroweak corrections displayed in Fig. 19 is obtained for the QED coupling defined at the scale of the top mass m_t.

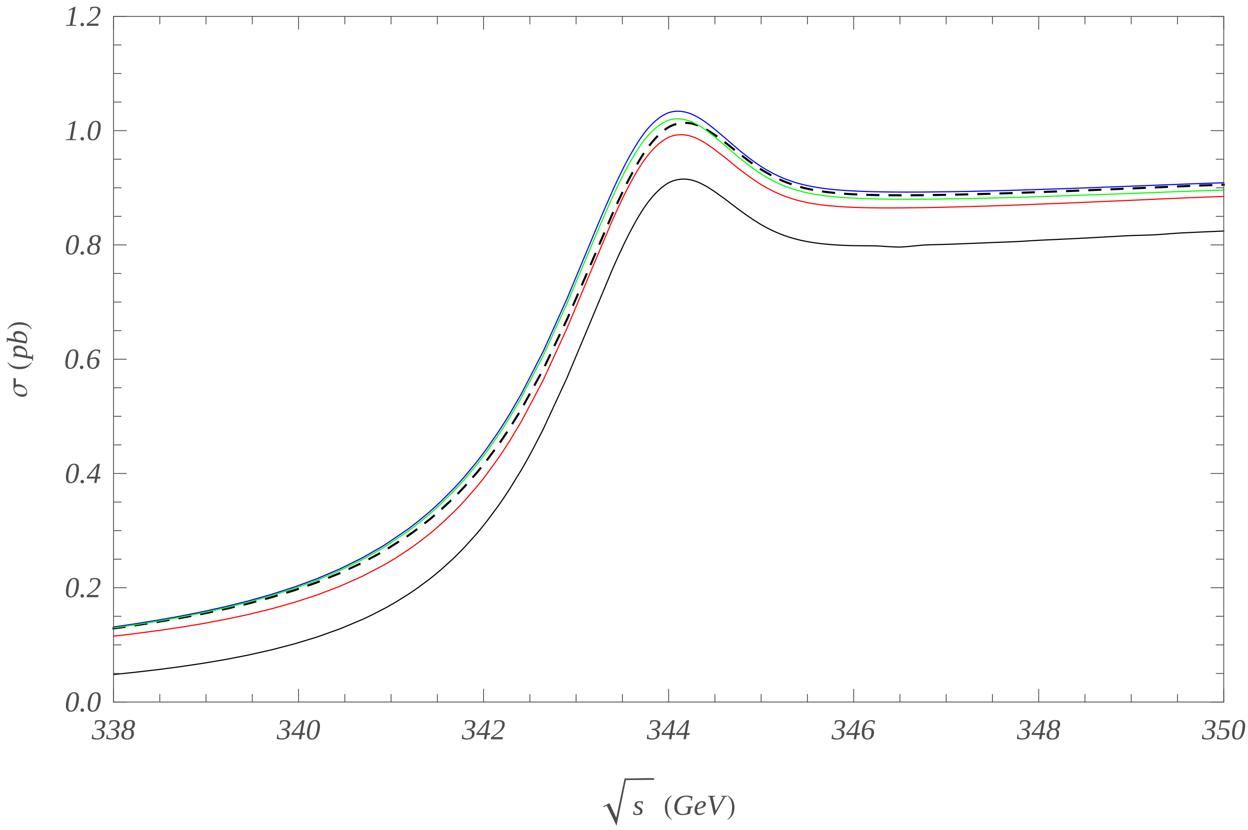

FIG. 20: Total inclusive top pair production cross section from NRQCD: starting from the pure QCD NNLL prediction (black dashed line), we add step-by-step the QED corrections (blue line), the hard electroweak corrections (green line), the type-1 finite lifetime corrections (red line) and the N^{3}LL phase space corrections (black solid line) for $\Delta M_t = 15$ GeV.

relatively flat behavior of the phase space matching contributions is related to the fact that the dominant phase space matching contributions are energy-independent. The small linear dependence on $\sqrt{s}$ is related to the $\sqrt{s}$ dependence of the virtual γ and Z propagators of the basic $e^+e^- \to t\bar{t}$ process and the peak-like structure comes from an imaginary phase space matching contribution to the $(e^+e^-)(t\bar{t})$ top pair production operator which enters the N^{3}LL inclusive cross section in terms of a time-ordered product. This time-ordered product leads to a non-analytic dependence on the energy, see Eqs. (26) and (92). In Fig. 19 we have also displayed the phase space matching contribution to the inclusive cross section at NLL (black dotted lines), NNLL (black dashed lines) and N^{3}LL order (black solid lines) in order to show the convergence of the phase space matching procedure. The results show that the expansion related to the phase space matching procedure is particularly good for larger values of ΔM_t and still well under control for $\Delta M_t = 15$ GeV. We note that the rather small size of the NNLL corrections (difference of black dotted and dashed lines) for $\Delta M_t = 15$ GeV arises from a cancellation between different independent NNLL corrections, see Sec. IV C.

In Figs. 20 and 21 the size of the four different types of electroweak corrections is shown for predictions of the total inclusive cross section. Starting from the pure QCD NNLL

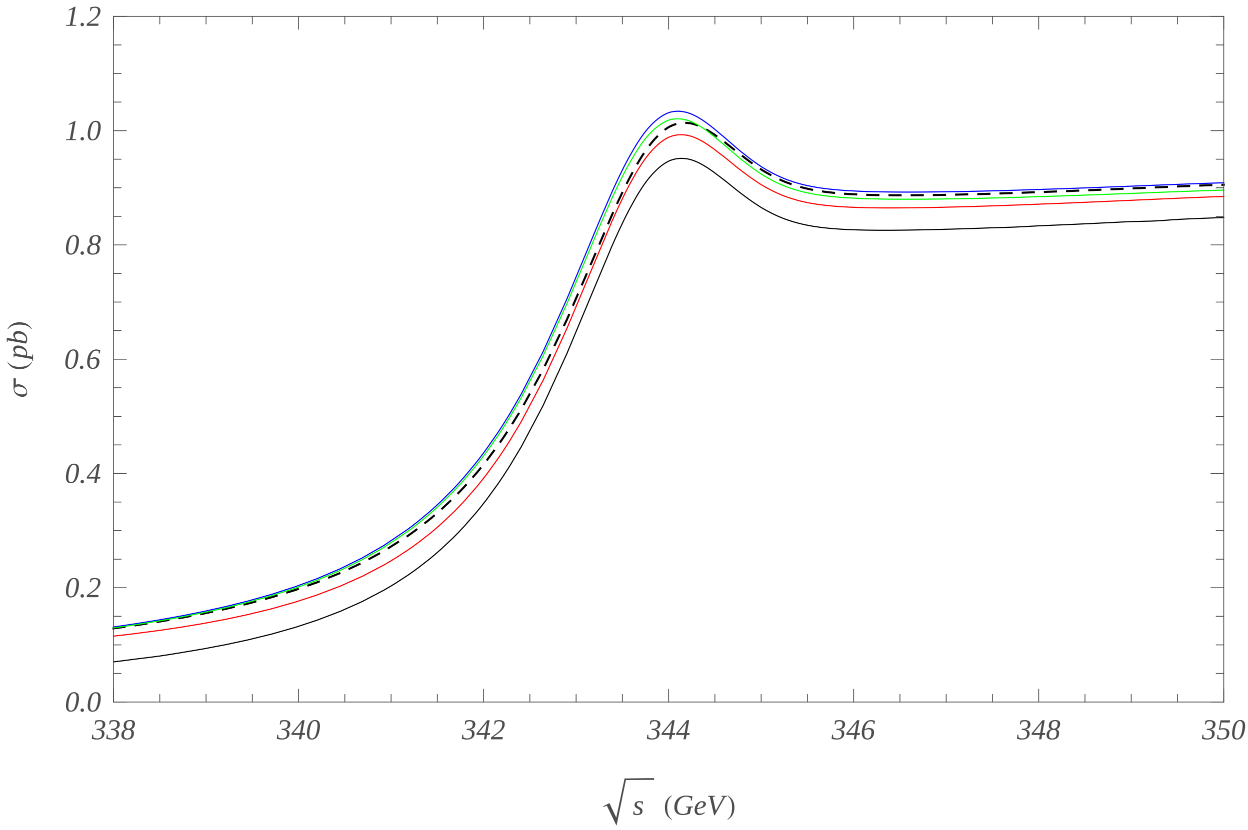

FIG. 21: Total inclusive top pair production cross section from NRQCD: starting from the pure QCD NNLL prediction (black dashed line), we add step-by-step the QED corrections (blue line), the hard electroweak corrections (green line), the type-1 finite lifetime corrections (red line) and the N^{3}LL phase space corrections (black solid line) for $\Delta M_t = 35$ GeV.

cross section (black dashed lines), which accounts only for the electroweak effects from the basic $e^+e^- \to \gamma, Z \to t\bar{t}$ process and the LL finite lifetime effects through the energy replacement rule $E \to E + i\Gamma_t$), we add step-by-step the QED corrections (blue lines), the hard electroweak corrections (green lines), the type-1 finite lifetime corrections (red lines) and the N^{3}LL phase space corrections (black solid lines). In Fig. 20 we have $\Delta M_t = 15$ GeV and in Fig. 21 we have $\Delta M_t = 35$ GeV. Only the phase space matching corrections depend on ΔM_t. We again see that the phase space matching contributions exceed by far the other electroweak corrections. Since we have already discussed the size of the individual types of electroweak corrections in our analysis of Fig. 19, we concentrate here only on the behavior of the predictions for energies below the peak region where the cross section is small. Here the phase space matching corrections are very large and amount to changes of more than 50% percent for $\Delta M_t = 15$. These large corrections are related to the unphysical phase space contributions contained in the pure QCD prediction which are a consequence of the nonrelativistic expansion and the energy replacement rule $E \to E + i\Gamma_t$. We stress that these unphysical effects cannot be cured by adding more of the higher order QCD corrections because they originate from modifications to the nonrelativistic $t\bar{t}$ phase space products caused by the top width. Thus in order to obtain realistic predictions for the top threshold cross section it is essential to account for the phase space matching corrections.

VI. CONCLUSION

The effects of the finite top quark lifetime are an essential ingredient for predictions of the top pair production rate close to threshold $\sqrt{s} \approx 2m_t$, where m_t is the top quark mass. Because the top width Γ_t has approximately the same size as the typical top quark kinetic energies, finite lifetime effects already enter the leading-order predictions and cannot be treated as corrections. An important consequence is that the top pair cross section is only well-defined with a given set of prescriptions how the observed top decay final states are accounted for in the cross section. This entails that the cross section also accounts for non-$t\bar{t}$ processes which lead to the same observed final state, and that the cross section can depend on experimental cuts on kinematic variables such as the reconstructed invariant masses. When matching to the NRQCD effective theory these finite lifetime effects can be integrated out for observables that are inclusive on the top and antitop decays, and lead to imaginary matching contributions to the Wilson coefficients of NRQCD operators. These imaginary matching coefficients are much like the complex indices of refraction in the Maxwell theory of light propagation in an absorptive medium. The cross section including the finite lifetime effects can then be obtained from the absorptive part of the $e^+e^- \to e^+e^-$ forward scattering amplitude using the optical theorem.

One can distinguish two types of imaginary NRQCD matching coefficients. The type-1 contributions [27] account for the (Cutkosky) cuts through the top decay final states in full theory diagrams. They lead e.g. to the well known quark bilinear top width term and also account for the interference effects mentioned above. Insertions of the associated operators also cause UV divergences in the nonrelativistic $t\bar{t}$ phase space integrations since the resulting unstable top propagator $i/(p_0 - \mathbf{p}^2/2m_t + i\Gamma_t/2)$ lifts the stable particle dispersion relation $p_0 = \mathbf{p}^2/2m_t$ and allows for arbitrarily large final state top invariant masses. These UV divergences require the introduction of $(e^+e^-)(e^+e^-)$ forward scattering operators, which acquire an imaginary anomalous dimension and sum large logarithms of the top velocity in the $t\bar{t}$ final state phase space. The type-2 imaginary matching contributions are the matching conditions of the Wilson coefficients of these $(e^+e^-)(e^+e^-)$ forward scattering operators. They encode the information on the experimental cuts used for the cross section measurement. Since the type-2 matching contributions are not related to hard virtual fluctuations, but to real final state configurations with large top quark off-shellness, we call them *phase space matching contributions*.

In this work we have determined and analyzed the type-2 phase space matching conditions up to N^{3}LL order in the nonrelativistic expansion for cuts on the reconstructed top and antitop invariant masses M_t, $M_{\bar{t}}$ of the form $|M_{t,\bar{t}} - m_t| \le \Delta M_t$, with ΔM_t between 15 and 35 GeV and neglecting the W boson width. We have demonstrated that the numerically dominant effect of the phase space matching is to remove the unphysical NRQCD phase space contributions that do not pass the cut. This is because the nonrelativistic unstable top propagator $i/(p_0 - \mathbf{p}^2/2m_t + i\Gamma_t/2)$ overestimates by far top and antitop fluctuations with large off-shellness. The remaining numerical contributions to the phase space matching conditions coming from calculations of relativistic full theory diagrams were found to be well below 5 fb for the cross section, which is negligible for the experimental precision one can expect at a future linear collider. From the field theoretic point of view, the procedure of carrying out the phase space matching agrees with the common matching and renormalization methods for stable particle theories. Thus at higher orders in the nonrelativistic expansion it is required to account for the phase space matching contributions of subdiagrams to remove non-analytic matrix element terms from the matching equations and to achieve that the matching coefficients are analytic in the external energy. In the phase space matching procedure at N^{3}LL order for top pair production at threshold one has to also include the phase space matching for $(e^+e^-)(t\bar{t})$ top production operators.

Since the phase space matching procedure we have carried out involves the computation of NRQCD phase space integrations with a hard cutoff related to ΔM_t, our results contain power-counting breaking contributions. This means that phase space matching contributions coming from insertions of higher order operators can give contributions that are formally lower order. We have shown that such power-counting breaking contributions do not spoil the nonrelativistic expansion and that power-counting breaking can be ignored from the practical point of view. As far as the α_s expansion is concerned, we have found that the N^{3}LL ($\mathcal{O}(\alpha_s^2)$) corrections to the phase space matching contributions need to be determined to meet the experimental precision expected at a future linear collider. At this time these N^{3}LL corrections are not yet fully known analytically, and their determination shall be addressed in subsequent work.

Our final numerical results have been given in Sec. V. Leaving aside the effects from the e^+e^- luminosity spectrum, which are known to distort the cross section shape and normalization in a quite substantial way, we find that the phase space matching contributions to the cross section exceed by far the other types of electroweak corrections, which are known from previous work. The phase space matching contributions are between -85 and -35 fb for invariant mass cuts ΔM_t between 15 and 35 GeV and are essential for realistic theoretical predictions. In the peak and the continuum region ($\sqrt{s} \gtrsim 2m_t$) they amount to 6 to 10%. They are particularly important in the region below the peak ($\sqrt{s} \lesssim 2m_t$) where the cross section decreases and the unphysical off-shell contributions of the NRQCD $t\bar{t}$ phase space become dominant. Here the phase space matching contributions can amount to more than 50%, and they ensure that the cross section has the correct physical behavior.

Phase space matching is also important for predictions of the top pair threshold cross section if no kinematic cuts are imposed, since the NRQCD phase space contributions involving off-shell top and antitop quarks still lead to large unphysical contributions. Here the phase space matching contributions from relativistic full theory diagrams are numerically important and cannot be neglected (Sec. III C). In this work we have determined these full theory contributions for $\alpha_s = 0$, i.e. at NLL order. We finally note that the phase space matching procedure can also be carried out using exclusively full theory computations with kinematic cuts to determine the imaginary type-2 matching coefficients. This approach does not involve any power-counting breaking contributions and allows to determine the phase space matching contributions more easily for $\Delta M_t > 35$ GeV. At this time these full theory computations are only known for $\alpha_s = 0$, which allows to carry out this phase space matching approach at NLL order. To go beyond the NLL level the results for the $\mathcal{O}(\alpha_s)$ and $\mathcal{O}(\alpha_s^2)$ corrections to the e^+e^- cross section are required for the final states that arise in top pair production. Such results are not available at this time.

Acknowledgments

This work was supported in part by the DFG Sonderforschungsbereich/Transregio 9 “Computergestützte Theoretische Teilchenphysik” and the EU network contract MRTN-

CT-2006-035482 (FLAVIAnet). P.R. thanks M. Beneke for useful discussions. Feynman diagrams have been drawn with the packages AXODRAW [59] and JAXODRAW [60].

Appendix A: QCD interference effects

In this appendix we compute the $\mathcal{O}(\alpha_s)$ ultrasoft corrections to the imaginary phase space matching coefficients $\tilde{C}_{V/A}$ of the $(e^+e^-)(e^+e^-)$ forward scattering operators $\tilde{\mathcal{O}}_{V/A}$ for the invariant mass prescription explained in Sec. IV A. The corresponding diagrams in Coulomb gauge are shown in Fig. 12. For the interference diagram 12d we need to define the top and antitop invariant masses in the presence of an additional ultrasoft gluon in the final state. As a toy prescription that can be easily implemented analytically we assume that we can resolve the gluon down to an infrared scale λ. For gluon energies larger than λ we define the top and antitop 4-momentum as the sum of 4-momenta of their decay products, bW^+ and $\bar{b}W^-$, respectively. The top and antitop invariant masses are then defined exactly as in Eq. (33). The result for the ultrasoft phase space matching corrections obtained from this prescription should also be generic for the typical size of corrections for other, more realistic invariant mass prescriptions. We can write the $\mathcal{O}(\alpha_s)$ contributions to the imaginary phase space matching coefficients $\tilde{C}_{V/A}$ from each of the diagrams in Fig. 12a–d as $(i = a, b, c, d)$

$$\tilde{C}^{\rm us}_{V/A,(i)} \;=\; iN_c(C^{\rm Born}_{V/A,1})^2\, c^{\rm us}_{(i)}\,. \tag{A1}$$

The resulting contributions to the inclusive cross section read

$$\Delta\sigma^{\rm us}_{(i)} = N_c\left[(C^{\rm Born}_{V,1})^2 + (C^{\rm Born}_{A,1})^2\right] c^{\rm us}_{(i)}\,. \tag{A2}$$

The computation of the ultrasoft corrections for energies close to threshold is performed using NRQCD Feynman rules for the top/antitop propagators and ultrasoft gluon couplings. The gluon momentum k is neglected when appropriate according to the scaling $k \sim m_t v^2$. In Coulomb gauge the time-like gluon propagator has the form $i/\mathbf{k}^2$ and the transverse propagator is $i(\delta^{ij} - \mathrm{k}^i\mathrm{k}^j/\mathbf{k}^2)/(k^2 + i\epsilon)$. We cut the diagrams as indicated by the red dashed lines in Fig. 12 using the well-known Cutkosky rules for the transverse gluon propagator and Eq. (39) for the top and antitop propagators. We note that our computation is quite similar to the one presented some time ago in Ref. [56], where, however, no phase space cuts were considered. The main conclusion in the work of Ref. [56] was that for the total cross section (i.e. without phase space restrictions) the contributions from the ultrasoft diagrams in Fig. 12 cancel. This serves as an important cross check of the computations we carry out here.

The contribution from the time-like gluon exchange between the $b\bar{b}$ pair (Fig. 12a plus the conjugated diagram) reads:[13]

$$\begin{aligned} c^{\rm us}_{(a)} \;=\; & \frac{4}{3} i\, C_F m_t^4 \int \frac{d^4p}{(2\pi)^4} \int \frac{d^4k}{(2\pi)^4} \frac{\left(3|A(k^0,\mathbf{k})|^2 - |\mathbf{B}(k^0,\mathbf{k})|^2\right)}{\mathbf{k}^2} \\ & \times \frac{1}{(t_1 - im_t\Gamma_t)(t_2 - im_t\Gamma_t)(t_1 - 2m_tk^0 + im_t\Gamma_t)(t_2 + 2m_tk^0 + im_t\Gamma_t)} + \text{c.c.}, \end{aligned} \tag{A3}$$

[13] We disagree with the corresponding result given in Ref. [56] with respect to the sign of the term $|\mathbf{B}(k^0,\mathbf{k})|^2$. However, this does not alter the conclusion that the contribution cancels in the absence of phase space restrictions.

where the invariant mass variables t_1, t_2, are defined in Eq. (42). The same variables are employed for the computation of the diagrams in Figs. 12b and c. In Eq. (A3) we have already performed the integrations over the bW^+ and $\bar{b}W^-$ phase space variables, which yields the functions

$$
\begin{aligned}
A(k^0,\mathbf{k}) &= -\frac{g_s\Gamma_t}{|\mathbf{k}|}\ln\left(\frac{k^0-|\mathbf{k}|-i\epsilon}{k^0+|\mathbf{k}|-i\epsilon}\right), \\
\mathbf{B}(k^0,\mathbf{k}) &= 2\,\frac{g_s\Gamma_t}{|\mathbf{k}|}\,\frac{2x-1}{2x+1}\left[1+\frac{k^0}{2|\mathbf{k}|}\ln\left(\frac{k^0-|\mathbf{k}|-i\epsilon}{k^0+|\mathbf{k}|-i\epsilon}\right)\right]\frac{\mathbf{k}}{|\mathbf{k}|}, \qquad \text{(A4)}
\end{aligned}
$$

where $x = M_W^2/m_t^2$. It is straightforward to check that Eq. (A3) vanishes if no bounds are imposed on the integration over the top energy: carrying out the p^0 integration by residues one obtains a purely imaginary number, which cancels out when adding the conjugate diagram. This confirms that the diagram vanishes if there are no cuts on the phase space integration. For the invariant mass cuts of Eq. (46) we proceed by performing the integration over the 3-momentum and the energy of the virtual gluon. After the trivial integration over the $\mathbf{p}$ angles we obtain a representation of the time-like gluon exchange diagram of the form

$$
c^{\rm us}_{(i)} = \frac{m_t^3\Gamma_t^2}{2\pi^3}\int_{\tilde{\Delta}(\Lambda)} dt_1 dt_2\, \frac{\sqrt{m_tE-(t_1+t_2)/2}}{(t_1^2+(m_t\Gamma_t)^2)\,(t_2^2+(m_t\Gamma_t)^2)}\,\Delta_{(i)}(t_1,t_2)\,. \qquad \text{(A5)}
$$

We use this generic form for all the QCD interference diagrams, $i = a, b, c, d$. Note that expression (A5) is compatible with Eq. (44), i.e. the $\Delta(t_1, t_2)$ functions in both expressions have the same normalization. For the time-like gluon exchange from diagram 12a we obtain

$$
\begin{aligned}
\Delta_{(a)}(t_1,t_2) &= 2C_F\alpha_s\left(1-\frac{1}{9}\left(\frac{2x-1}{2x+1}\right)^2\right)\frac{1}{(t_1+t_2)^2+4(m_t\Gamma_t)^2} \\
&\times\Bigg\{\Big(2(m_t\Gamma_t)^2+t_2(t_1+t_2)\Big)\arctan\frac{t_1}{m_t\Gamma_t}+\frac{m_t\Gamma_t}{4}(t_1-t_2)\ln\left(\frac{t_2^2+(m_t\Gamma_t)^2}{t_1^2+(m_t\Gamma_t)^2}\right) \\
&+\{t_1\leftrightarrow t_2\}\Bigg\}. \qquad \text{(A6)}
\end{aligned}
$$

The time-like gluon exchange between $t\bar{b}$ and $\bar{t}b$, Fig. 12b, is computed analogously:

$$
\begin{aligned}
c^{\rm us}_{(b)} &= 16\,i\,C_F g_s m_t^5\int\frac{d^4p}{(2\pi)^4}\int\frac{d^4k}{(2\pi)^4}\frac{A(k^0,\mathbf{k})}{\mathbf{k}^2}\frac{1}{(t_1-im_t\Gamma_t)(t_2^2+(m_t\Gamma_t)^2)} \\
&\times\frac{1}{(t_1-2m_tk^0+im_t\Gamma_t)(t_2+2m_tk^0+im_t\Gamma_t)}+\left\{\begin{array}{c} t_1\leftrightarrow t_2 \\ k^0\to -k^0\end{array}\right\}+\text{c.c.}\,. \qquad \text{(A7)}
\end{aligned}
$$

The terms shown explicitly in Eq. (A7) represent the contribution from the $t\bar{b}$ gluon exchange (first diagram in Fig. 12b). The contribution from the $\bar{t}b$ gluon exchange is obtained with the replacements $t_1 \leftrightarrow t_2$, and $k^0 \to -k^0$, as indicated in Eq. (A7). For this contribution we find it more convenient to perform first the k^0-integral. Again, it is easy to check that if the p^0-integration is done by residues, one obtains a result which is purely imaginary, so this contribution vanishes for the total cross section without phase space restrictions. The expression can be cast into the form of Eq. (A5) with

$$\Delta_{(b)}(t_1,t_2) \;=\; -\bigg(1-\frac{1}{9}\bigg(\frac{2x-1}{2x+1}\bigg)^2\bigg)^{-1}\,\Delta_{(a)}(t_1,t_2)\,. \tag{A8}$$

Let us now turn to the space-like gluon exchange between the final state $b\bar{b}$ pair in Fig. 12c. The result reads

$$\begin{aligned} c^{\rm us}_{(c)} \;=&\; -\frac{8}{3}i\,C_F m_t^4\int\frac{d^4p}{(2\pi)^4}\int\frac{d^4k}{(2\pi)^4}\,\frac{|C(k^0,\mathbf{k})|^2}{k^2+i\epsilon}\,\frac{1}{(t_1-im_t\Gamma_t)(t_2-im_t\Gamma_t)}\\ &\times\frac{1}{(t_1-2m_tk^0+im_t\Gamma_t)(t_2+2m_tk^0+im_t\Gamma_t)}+\text{c.c.}\,, \end{aligned} \tag{A9}$$

where

$$C(k^0,\mathbf{k}) \;=\; -\frac{g_s\Gamma_t}{|\mathbf{k}|}\,\frac{2x-1}{2x+1}\left[\frac{k^0}{|\mathbf{k}|}+\frac{(k^0)^2-\mathbf{k}^2}{2\mathbf{k}^2}\ln\bigg(\frac{k^0-|\mathbf{k}|-i\epsilon}{k^0+|\mathbf{k}|-i\epsilon}\bigg)\right]. \tag{A10}$$

The expression can be cast into the form of Eq. (A5) with

$$\begin{aligned} \Delta_{(c)}(t_1,t_2) \;=&\; -\frac{C_F\alpha_s}{12\pi}\bigg(\frac{2x-1}{2x+1}\bigg)^2\bigg\{\bigg(\ln\bigg(\frac{t_1^2+(m_t\Gamma_t)^2}{(2m_t)^4}\bigg)-\frac{4\pi}{3}\arctan\frac{t_1}{m_t\Gamma_t}+\{t_1\leftrightarrow t_2\}\bigg)\\ &+\frac{(t_1-t_2)(4m_t\Gamma_t+\frac{4\pi}{3}(t_1+t_2))}{(t_1+t_2)^2+4(m_t\Gamma_t)^2}\bigg(\arctan\frac{t_1}{m_t\Gamma_t}-\arctan\frac{t_2}{m_t\Gamma_t}\bigg)\\ &+\frac{(t_1-t_2)(t_1+t_2-\frac{4\pi}{3}m_t\Gamma_t)}{(t_1+t_2)^2+4(m_t\Gamma_t)^2}\ln\bigg(\frac{t_2^2+(m_t\Gamma_t)^2}{t_1^2+(m_t\Gamma_t)^2}\bigg)-2\ln\frac{\lambda^2}{(2m_t)^2}\bigg\}\,. \end{aligned} \tag{A11}$$

The $|\mathbf{k}|$ integration in $c^{\rm us}_{(c)}$ yields an infrared divergence, which we have regularized with the cutoff λ mentioned at the beginning of this appendix. This IR divergence is cancelled by a corresponding IR divergence in the real gluon emission diagram in Fig. 12d, as shown below. Attaching a space-like ultrasoft gluon to the top or antitop lines such as in diagram 12e yields an additional v factor, so the corresponding contributions are suppressed in the nonrelativistic expansion with respect to those in Figs. 12a-d. This way we only need to consider real gluon emission from the bottom quark lines. Due to the additional gluon in the final state the relation between the variables $t_{1,2}$ and the nonrelativistic loop momenta $(p^0,\mathbf{p}^2)$ has to be modified. For the momentum routing displayed in Fig. 12d, t_1 and t_2 are defined as

$$\begin{aligned} t_1 &= 2m_t\Big(\frac{E}{2}+p^0-\frac{\mathbf{p}^2}{2m_t}-k^0\Big)\,,\\ t_2 &= 2m_t\Big(\frac{E}{2}-p^0-\frac{\mathbf{p}^2}{2m_t}\Big)\,. \end{aligned} \tag{A12}$$

The result from diagram 12d then reads

$$c^{\rm us}_{(d)} \;=\; \frac{4}{3}\,C_F m_t^4 \int \frac{d^4p}{(2\pi)^4} \int \frac{d^3\mathbf{k}}{(2\pi)^4} \frac{C(|\mathbf{k}|,\mathbf{k})^2}{|\mathbf{k}|} \frac{1}{(t_1 - im_t\Gamma_t)(t_2 + im_t\Gamma_t)}$$
$$\times \frac{1}{(t_1 + 2m_t|\mathbf{k}| + im_t\Gamma_t)(t_2 + 2m_t|\mathbf{k}| - im_t\Gamma_t)} + \text{c.c.}\,. \tag{A13}$$

For this contribution the $|\mathbf{k}|$-integration extends to values such that the phase space factor $|\mathbf{p}| = \sqrt{m_tE - m_t|\mathbf{k}| - (t_1+t_2)/2}$ remains a real number. As anticipated above, the $|\mathbf{k}|$-integration is IR-divergent and we introduce the cutoff λ as in the case of diagram 12c. The expression can be cast into the form of Eq. (A5) with

$$\Delta_{(d)}(t_1,t_2) = \frac{C_F\alpha_s}{12\pi}\bigg(\frac{2x-1}{2x+1}\bigg)^2 \bigg\{ 4\ln\bigg(\frac{2m_tE - (t_1+t_2)}{m_t^2}\bigg) - 2\ln\frac{\lambda^2}{(2m_t)^2}$$
$$+ \bigg(\bigg[\frac{2\,(t_2 - i\,m_t\Gamma_t)}{t_1 - t_2 + 2im_t\Gamma_t}\,\frac{h(t_2)}{\widetilde{h}(t_1+t_2)}\,\ln\bigg(\frac{h(t_2) + \widetilde{h}(t_1+t_2)}{h(t_2) - \widetilde{h}(t_1+t_2)}\bigg) + \{t_1 \leftrightarrow t_2\} \bigg] + \text{c.c.} \bigg) \bigg\}\,, \tag{A14}$$

where

$$h(y) = \sqrt{m_tE - (y - im_t\Gamma_t)/2}\,,$$
$$\widetilde{h}(y) = \sqrt{m_tE - y/2}\,. \tag{A15}$$

We explicitly see the cancellation of the infrared divergent terms in the sum of $c^{\rm us}_{(c)}$ and $c^{\rm us}_{(d)}$. Again it is easy to check that after integrating over the top energy p^0 without restrictions, both contributions cancel completely.

Expanding the ultrasoft phase space matching contributions $m_tE, m_t\Gamma_t \ll \Lambda^2$ up to terms of order $1/\Lambda^3$, we obtain

$$c^{\rm us}_{(a)} \;=\; \frac{\sqrt{2}m_t^2}{3\pi^2} C_F\alpha_s \bigg(1 - \frac{1}{9}\bigg(\frac{2x-1}{2x+1}\bigg)^2\bigg) \frac{m_t\Gamma_t^2}{\Lambda^3} \bigg\{ 3\ln\frac{m_t\Gamma_t}{\Lambda^2} + \ln 2 - 1 - \sqrt{2} - \sinh^{-1}(1) \bigg\}\,,$$

$$c^{\rm us}_{(b)} \;=\; -\frac{\sqrt{2}m_t^2}{3\pi^2} C_F\alpha_s \frac{m_t\Gamma_t^2}{\Lambda^3} \bigg\{ 3\ln\frac{m_t\Gamma_t}{\Lambda^2} + \ln 2 - 1 - \sqrt{2} - \sinh^{-1}(1) \bigg\}\,,$$

$$c^{\rm us}_{(c)} \;=\; \frac{\sqrt{2}m_t^2}{3\pi^3} C_F\alpha_s \bigg(\frac{2x-1}{2x+1}\bigg)^2 \frac{\Gamma_t}{\Lambda} \bigg\{ \ln\frac{\Gamma_t}{\lambda}\bigg(1 + \frac{m_tE}{3\Lambda^2}\bigg) + \frac{1}{3\pi}\frac{m_t\Gamma_t}{\Lambda^2}\Big(\sqrt{2} + \sinh^{-1}(1)\Big)\ln\frac{\lambda m_t}{2\Lambda^2}$$
$$+ \frac{m_t\Gamma_t}{\Lambda^2}\bigg(\frac{\pi}{3}\ln\frac{m_t\Gamma_t}{\Lambda^2} - \frac{k_1}{9\pi}\bigg) \bigg\}\,,$$

$$c^{\rm us}_{(d)} \;=\; -\frac{\sqrt{2}m_t^2}{3\pi^3} C_F\alpha_s \bigg(\frac{2x-1}{2x+1}\bigg)^2 \frac{\Gamma_t}{\Lambda} \bigg\{ \ln\frac{\Gamma_t}{\lambda}\bigg(1 + \frac{m_tE}{3\Lambda^2}\bigg) + \frac{1}{3\pi}\frac{m_t\Gamma_t}{\Lambda^2}\Big(\sqrt{2} + \sinh^{-1}(1)\Big)\ln\frac{\lambda m_t}{2\Lambda^2}$$
$$+ \frac{m_t\Gamma_t}{\Lambda^2}\frac{k_2}{9\pi} \bigg\} \tag{A16}$$

with

$$
\begin{aligned}
k_1 \; &= \; d_1 + 5\sqrt{2} - 6\sqrt{2}\ln 2 - \frac{3\ln^2 2}{2} + \pi(3\ln 2 - \frac{1}{2}) + \pi^2(\sqrt{2} + \frac{5}{12} - 2\ln 2) \\
&\quad +(5 - \pi^2 - 9\ln 2)\sinh^{-1}(1) + \frac{3}{2}\big[\sinh^{-1}(1)\big]^2 - 3\mathrm{Li}_2\Big(\frac{1-\sqrt{2}}{2}\Big)\,, \\
k_2 \; &= \; d_2 + \frac{\pi}{2}(5 - 12\ln 2) + \frac{3\pi^2}{4}\,.
\end{aligned}
\tag{A17}
$$

The constants d_1 and d_2 have been evaluated numerically and read

$$
d_1 = -4.961 \quad , \quad d_2 = -17.75\,. \tag{A18}
$$

Adding up the results of all diagrams we are - as anticipated from the general arguments discussed in Sec. IV A - left with a correction to the cross section of order $m_t\Gamma_t/\Lambda^2$ with respect to the NLL phase space correction:

$$
\sum_{i=a,b,c,d} c^{\rm us}_{(i)} = \frac{m_t^2}{4\pi}\frac{4\sqrt{2}}{\pi}\frac{\Gamma_t}{\Lambda}\Delta^{\rm us}\,, \tag{A19}
$$

where

$$
\Delta^{\rm us} \; = \; \frac{C_F\alpha_s}{27\pi^2}\Big(\frac{2x-1}{2x+1}\Big)^2\frac{m_t\Gamma_t}{\Lambda^2}\Big\{\pi^2\Big(1+\sqrt{2}-\ln 2+\sinh^{-1}(1)\Big) - k_1 - k_2\Big\}\,. \tag{A20}
$$

Apart from the cancellation of the $\ln\lambda$ infrared divergences already pointed out above, we also find that all logarithms of Γ_t cancel in the sum of all diagrams. This is expected because the phase space matching contributions represent hard effects. A proper evaluation of the ultrasoft phase space matching corrections therefore also requires to employ the strong coupling in Eq. (A20) at the hard scale. For $m_t = 172$ GeV, $M_W = 80.425$ GeV and $C_F\alpha_s(m_t) = 0.1436$ we find that $\Delta^{\rm us} = 0.004\, m_t\Gamma_t/\Lambda^2$. We thus find that the ultrasoft corrections based on our invariant mass prescription have an additional strong numerical suppression factor. Although this result might not be generalized to other invariant mass definitions, it nevertheless supports the conclusion that ultrasoft effects are in general irrelevant at the level of precision we aim for in this work.

---

[1] A. H. Hoang et al., Eur. Phys. J. direct **C2**, 1 (2000), hep-ph/0001286.
[2] M. Martinez and R. Miquel, Eur. Phys. J. **C27**, 49 (2003), hep-ph/0207315.
[3] A. H. Hoang, PoS **TOP2006**, 032 (2006), hep-ph/0604185.
[4] A. H. Hoang, Phys. Rev. **D69**, 034009 (2004), hep-ph/0307376.
[5] M. Beneke, Y. Kiyo, and K. Schuller, Nucl. Phys. **B714**, 67 (2005), hep-ph/0501289.
[6] D. Eiras and M. Steinhauser, Nucl. Phys. **B757**, 197 (2006), hep-ph/0605227.
[7] M. Beneke, Y. Kiyo, and K. Schuller, PoS **RADCOR2007**, 051 (2007), 0801.3464.
[8] M. Beneke and Y. Kiyo, Phys. Lett. **B668**, 143 (2008), 0804.4004.
[9] Y. Kiyo, D. Seidel, and M. Steinhauser, JHEP **01**, 038 (2009), 0810.1597.

[10] C. Anzai, Y. Kiyo, and Y. Sumino (2009), 0911.4335.
[11] A. V. Smirnov, V. A. Smirnov, and M. Steinhauser (2009), 0911.4742.
[12] A. V. Smirnov, V. A. Smirnov, and M. Steinhauser (2010), 1001.2668.
[13] A. H. Hoang, M. C. Smith, T. Stelzer, and S. Willenbrock, Phys. Rev. **D59**, 114014 (1999), hep-ph/9804227.
[14] M. Beneke, Phys. Lett. **B434**, 115 (1998), hep-ph/9804241.
[15] A. H. Hoang, A. Jain, I. Scimemi, and I. W. Stewart, Phys. Rev. Lett. **101**, 151602 (2008), 0803.4214.
[16] A. H. Hoang, A. Jain, I. Scimemi, and I. W. Stewart (2009), 0908.3189.
[17] A. H. Hoang, A. V. Manohar, I. W. Stewart, and T. Teubner, Phys. Rev. Lett. **86**, 1951 (2001), hep-ph/0011254.
[18] A. H. Hoang, A. V. Manohar, I. W. Stewart, and T. Teubner, Phys. Rev. **D65**, 014014 (2002), hep-ph/0107144.
[19] A. Pineda and A. Signer, Nucl. Phys. **B762**, 67 (2007), hep-ph/0607239.
[20] A. H. Hoang and M. Stahlhofen, Phys. Rev. **D75**, 054025 (2007), hep-ph/0611292.
[21] A. H. Hoang, Acta Phys. Polon. **B34**, 4491 (2003), hep-ph/0310301.
[22] A. H. Hoang and C. J. Reisser, Phys. Rev. **D74**, 034002 (2006), hep-ph/0604104.
[23] R. J. Guth and J. H. Kuhn, Nucl. Phys. **B368**, 38 (1992).
[24] B. Grzadkowski, J. H. Kuhn, P. Krawczyk, and R. G. Stuart, Nucl. Phys. **B281**, 18 (1987).
[25] V. S. Fadin and V. A. Khoze, JETP Lett. **46**, 525 (1987).
[26] V. S. Fadin and V. A. Khoze, Sov. J. Nucl. Phys. **48**, 309 (1988).
[27] A. H. Hoang and C. J. Reisser, Phys. Rev. **D71**, 074022 (2005), hep-ph/0412258.
[28] A. H. Hoang and T. Teubner, Phys. Rev. **D60**, 114027 (1999), hep-ph/9904468.
[29] C. J. Reißer, Ph.D. thesis, Technical University Munich (2008).
[30] J. Alwall et al., JHEP **09**, 028 (2007), 0706.2334.
[31] M. E. Luke, A. V. Manohar, and I. Z. Rothstein, Phys. Rev. **D61**, 074025 (2000), hep-ph/9910209.
[32] A. V. Manohar and I. W. Stewart, Phys. Rev. **D62**, 074015 (2000), hep-ph/0003032.
[33] A. H. Hoang and I. W. Stewart, Phys. Rev. **D67**, 114020 (2003), hep-ph/0209340.
[34] N. Brambilla, A. Pineda, J. Soto, and A. Vairo, Nucl. Phys. **B566**, 275 (2000), hep-ph/9907240.
[35] M. E. Luke and A. V. Manohar, Phys. Lett. **B286**, 348 (1992), hep-ph/9205228.
[36] W. Fischler, Nucl. Phys. **B129**, 157 (1977).
[37] Y. Schroder, Phys. Lett. **B447**, 321 (1999), hep-ph/9812205.
[38] M. Peter, Phys. Rev. Lett. **78**, 602 (1997), hep-ph/9610209.
[39] M. Peter, Nucl. Phys. **B501**, 471 (1997), hep-ph/9702245.
[40] M. Jezabek and J. H. Kuhn, Phys. Lett. **B316**, 360 (1993).
[41] R. Harlander, M. Jezabek, and J. H. Kuhn, Acta Phys. Polon. **B27**, 1781 (1996), hep-ph/9506292.
[42] A. V. Manohar and I. W. Stewart, Phys. Rev. **D63**, 054004 (2001), hep-ph/0003107.
[43] A. Pineda, Phys. Rev. **D66**, 054022 (2002), hep-ph/0110216.
[44] M. Stahlhofen, Ph.D. thesis, Technical University Munich (2009).
[45] A. H. Hoang and T. Teubner, Phys. Rev. **D58**, 114023 (1998), hep-ph/9801397.
[46] A. H. Hoang, Phys. Rev. **D59**, 014039 (1999), hep-ph/9803454.
[47] M. J. Strassler and M. E. Peskin, Phys. Rev. **D43**, 1500 (1991).
[48] M. Jezabek, J. H. Kuhn, and T. Teubner, Z. Phys. **C56**, 653 (1992).

[49] S. Fleming, A. H. Hoang, S. Mantry, and I. W. Stewart, Phys. Rev. **D77**, 114003 (2008), 0711.2079.
[50] S. Fleming, A. H. Hoang, S. Mantry, and I. W. Stewart, Phys. Rev. **D77**, 074010 (2008), hep-ph/0703207.
[51] A. V. Manohar and I. W. Stewart, Phys. Rev. **D76**, 074002 (2007), hep-ph/0605001.
[52] S. Actis, M. Beneke, P. Falgari, and C. Schwinn, Nucl. Phys. **B807**, 1 (2009), 0807.0102.
[53] M. Beneke, A. P. Chapovsky, A. Signer, and G. Zanderighi, Phys. Rev. Lett. **93**, 011602 (2004), hep-ph/0312331.
[54] M. Beneke, A. P. Chapovsky, A. Signer, and G. Zanderighi, Nucl. Phys. **B686**, 205 (2004), hep-ph/0401002.
[55] V. S. Fadin, V. A. Khoze, and A. D. Martin, Phys. Rev. **D49**, 2247 (1994).
[56] K. Melnikov and O. I. Yakovlev, Phys. Lett. **B324**, 217 (1994), hep-ph/9302311.
[57] M. Peter and Y. Sumino, Phys. Rev. **D57**, 6912 (1998), hep-ph/9708223.
[58] A. H. Hoang, A. V. Manohar, and I. W. Stewart, Phys. Rev. **D64**, 014033 (2001), hep-ph/0102257.
[59] J. A. M. Vermaseren, Comput. Phys. Commun. **83**, 45 (1994).
[60] D. Binosi and L. Theussl, Comput. Phys. Commun. **161**, 76 (2004), hep-ph/0309015.